EFFICIENCY OPTIMISATION IN A DC-DC CHOPPER MOTOR DRIVE

RORY BRUCE PREST

Thesis submitted to the
Department of Electrical Engineering
at the
University of Cape Town
in fulfilment of the requirements
for the degree of
Master of Science in Engineering

September 1983

ABSTRACT

A complete DC-DC motor drive (battery, chopper and motor) is investigated with a view to optimising efficiency. The losses at each stage are analysed in detail and proposals are made to minimise them. The overall system is also modelled for the purpose of computer simulation.

The computer model is used to investigate the possible efficiency saving if both field and armature current are controlled. An optimum control system is developed and compared with other control systems.

ACKNOWLEDGEMENTS

The author wishes to thank Dr M.J. Case for his advice and supervision and Heather for her support during the writing of this thesis.

CONTENTS

SUMMARY

When investigating the efficiency of a dc to dc motor drive it is important to consider the system as a whole, including the dc source, the chopper converter, the motor and the method of control.

In this thesis the lead-acid battery, the chopper and the dc motor are examined in detail with the two-fold purpose of minimising losses and modelling the system accurately for computer analysis.

The chopper design is first discussed and transfer equations developed. The minimisation of switching, snubber, on-state, free wheel diode and inductor losses is investigated as well as the choice of chopping strategy.

The motor is regarded as given and design changes are not considered. The copper, brush, iron, mechanical and stray losses are discussed theoretically and their experimental determination described.

The pulses of current in the battery cause increased loss and methods of reducing this are discussed. Modelling the battery as an internal EMF and series resistance is insufficient and a more adequate equivalent circuit is described.

Overall efficiency is improved if both armature and field

current are controlled. The overall system model is analysed by computer to determine the relationship between field and armature currents for optimum efficiency. The efficiency of the optimum control system is also compared with various other control systems.

It is shown that the efficiency improvement of an optimum controller is less than 1% compared with a shunt motor and about 0.25% compared with a series motor for a typical electric vehicle test cycle. A permanent magnet motor is about 0.8% more efficient over the same test cycle. This efficiency saving is very dependent on the chosen test cycle and will vary with the particular application.

Finally, a practical design for an optimum controller based on a microprocessor is developed.

LIST OF SYMBOLS

N	efficiency
I_q	armature current
I_B	battery current
I_f	field current
E_q	armature voltage
E_B	battery voltage
E_f	field voltage
M	mark space ratio
T	torque
W	angular velocity
$K(I_f)$	motor machine constant
k_{rem}	machine constant owing to remnant magnetism
k_{f1}	friction loss constant proportional to speed
k_{f2}	friction loss constant independent of speed
k_H	hysteresis loss constant
k_E	eddy current loss constant
k_s	stray load loss constant
k_{B1}	activation potential drop constant (1)
k_{B2}	activation potential drop constant (2)
R_B	battery resistance
R_q	armature resistance (including interpole resistance)
R_f	field resistance
T	chopping period
TC	time constant
f	frequency
V_B	brush voltage drop
S	sign of torque (+1 or -1)
T_f	torque loss owing to friction
T_i	iron torque loss
T_s	stray load torque loss
L_q	armature inductance
t_c	time snubber capacitor takes to charge to supply voltage

CHAPTER 1

INTRODUCTION

1.1 POWER CONVERSION

In order for electricity to be of practical use, it invariably needs to be controlled. That is the rate of power flow from a fixed source needs to be adjustable. In addition the form of the supply often needs to be modified to suit the particular application.

In general, there are three ways of achieving power conversion. Firstly, linear resistive converters absorb the power not required. This can be implemented using a bank of switched resistors or a transistor used as a controlled resistance (as in Class A, B and C amplifiers). Secondly, two electromechanical machines can be connected to provide power conversion. The DC-DC Ward Leonard converter is a good example of this. Thirdly, switching converters operate by alternately connecting and disconnecting the power source and the load.

The resistive converter is simple and inexpensive but is very inefficient. Electromechanical converters provide excellent conversion but can be large and costly. The switching converter option is becoming increasingly attractive since it theoretically provides lossless conversion.

The topic of this thesis falls into the general field of "switching power converters".

1.2 SWITCHING POWER CONVERTERS

1.2.1 Historical Overview

The idea of using switching power converters was first developed in the early 1920s. Since then, development has been largely tied up with the state of the art of switching devices.

Initially mercury-arc rectifiers and grid-controlled mercury-arc tubes were used. These suffered from many limitations such as cost, reliability and efficiency. In the 1950s high power mercury-arc devices were developed. These were largely used in high voltage direct-current transmission.

During the Second World War magnetic amplifiers or controllable saturable reactors were used, mainly for ac-ac conversion.

The beginning of the semi-conductor industry in 1948 with the development of the transistor was the most significant event in the field of switching power convertors. This led to the development of the thyristor in 1957 and these devices were available by 1961 with ratings of about 200 A and 1000 V. It then took about five years before most of the initial problems were solved and wide spread use became a practicality.

The need for forced commutation was a major limitation in thyristors and toward the end of the 1970s, improved power transistors began to challenge the thyristor in medium and low power applications.

The most recent development in semi-conductor switches has been the development of metal-oxide semiconductor field-effect transistors (MOSFETS) in 1978. These devices are currently available with ratings of about 100 V and 30 A. They are easily paralleled to provide higher current ratings. They have many advantages including absence of second breakdown and very high switching speeds. MOSFETS are likely to become increasingly significant in switching power converters.

Other than the development of switching devices, there have been very few significant developments in converter topology over the past twenty years.

1.2.2 Unified Theory of Switching Converters

In a recent book, "Switching Power Converters" (P.Wood)[1], the author has attempted to bring all the possible combinations of switching power converters under a unified treatment of the subject.

The conversion of polyphase ac to polyphase ac is regarded as the most general case and all other possibilities as special cases. An hierarchy of converters is shown in Table 1.1.

TABLE 1.1

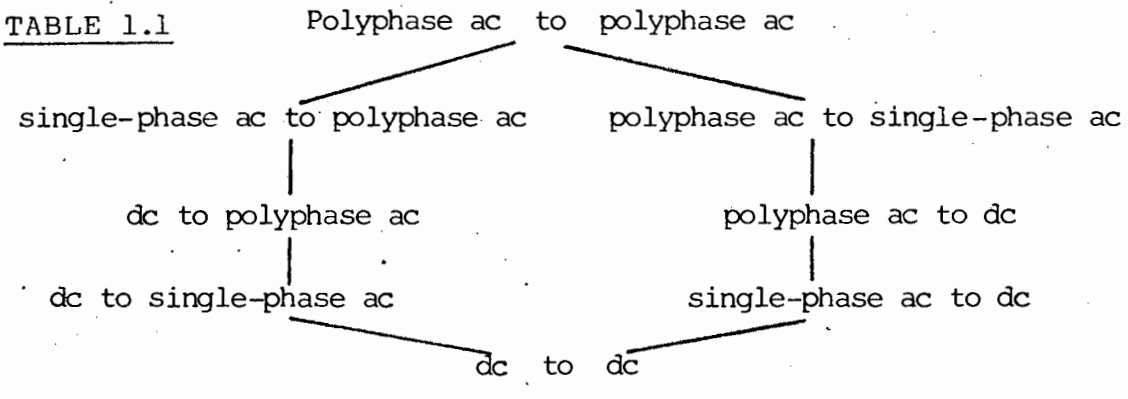

The converter can then be regarded as a matrix of switches and its behaviour mathematically described using existence functions and Fourier series.

1.2.3 Motor Drives

Switching power converters are useful in many applications, one of the most important being motor drives.

Converters are available to drive both ac and dc motors. There is a wide variety of ac motors available, the most common being induction motors and synchronous machines.[2]

Dc motors are generally either shunt or series wound. Recent developments are making the control of both field and armature currents in a separately excited machine a possibility. Development is taking place on permanent magnet motors as well as motors with disc-shaped rotors. Tests have been done on controlling speed by varying the field only, this being done usually in conjunction with a gearbox.

Converters have been developed for each of these machines from polyphase, single phase and dc sources.

1.3 DC TO DC MOTOR DRIVES

The subject of this investigation has been limited to the most specialised case of power switching converters listed in Table 1.1, that of dc-dc conversion. Furthermore, it has been limited to the particular application of dc-dc motor drives.

A large amount of material has been published on the subject over the last decade (references 3 to 20). Until recently, much of this has been concerned with the problem of thyristor commutation with few other creative innovations.

1.3.1 Electrical Vehicles

A brief overview of electrical vehicles provides motivation for this thesis, although its scope is not limited to this application.

Owing to the limitation of oil resources and the problem of pollution, the electric vehicle has been suggested as an alternative to the internal combustion engine.[3, 21, 22] The viability of this option has been a subject of much debate. Many electric vehicles have been built, mostly experimental models. Currently, their practical use has been limited to delivery vehicles and public transport.

There are currently two major limitations to the widespread use of electrical vehicles. The weight and speed of charging of the lead acid battery and, secondly, the initial capital cost is likely to be between 50 and 100% greater than the Internal Combustion vehicles.[22] There is presently little difference in the efficiency of the two systems when traced back to energy source.[22]

The dc motor has traditionally been used for electric vehicles but other possibilities are also being considered. Electronic

dc-ac converters are making the use of induction motors a viable option. Tests on hybrid vehicles, containing both electric and Internal Combustion motors have been done.[23]

Efficiency is one of the most important considerations in the design of an electric vehicle drive. It can be shown that in the case of a commercial one-ton truck a 1% efficiency improvement makes it possible to reduce battery mass by 12-15 kg; hence the need for an efficient control system including regenerative braking.[20]

1.3.2 DC Sources

The lead-acid battery has a long history of use and is currently the most viable option as a DC source. It is relatively cheap and robust. However, it has the disadvantage of a very low energy storage density and is, therefore, very heavy. Attention has been given to reducing the weight of containers and grids.

Much research is being done to develop alternatives. Many possibilities have been proposed, each with limited success and their own problems. A useful survey of the state of the art of some main contenders is given in reference.[21] These include metal-aqueous batteries (nickel-zinc, nickel-iron, nickel-cadmium), metal-oxygen batteries (zinc-air, iron-air) and high temperature batteries (sodium-sulphur, lithium-sulphur). Fuel cells are a further option for use as a dc source.

The future of electric vehicles is largely linked with the development of alternative batteries. However, it is difficult to predict which will be the most likely candidate.

The lead-acid dc source was chosen for investigation in this thesis, since it is the only battery which is commercially available at present and it currently has the most widespread use.

1.4 BREAKDOWN OF SOURCES OF INEFFICIENCY

Electrical losses occur in the battery, chopper and motor. In addition iron and mechanical losses occur in the motor.

A 96 V 3.7 KW motor is extensively analysed in this thesis to illustrate the principles involved. The comparative losses of this shunt motor operating over the standard test cycle in section 5.3.5 are tabulated below.

Battery	Motor			Chopper
Electrical	Electrical	Iron	Mechanical	Electrical
19.0%	44.1%	23.1%	13.3%	$<0.5\%$

TABLE 1.1

1.5 SCOPE OF THESIS

Many factors need to be considered when designing high performance dc-dc converters.[23] Some of these are listed below:

(a) efficiency of conversion
(b) economic considerations
(c) size and weight
(d) complexity
(e) reliability and ease of maintenance
(f) smooth control (particularly in transition between modes)
(g) stability of dynamic characteristics
(h) accuracy of control
(i) speed of response
(j) protection
(k) cycle life of system
(l) availability of components.

From these considerations, the criteria of efficiency is the subject of investigation in this thesis. Many studies on the subject examine the individual components of the system. However, it was felt to be important that the efficiency of the whole system be investigated, including the lead-acid source, the chopper converter and the dc machine.

The chopper design is first examined in detail with a view to minimising losses. The motor and battery are then investigated. These are regarded as given components which are not

open to design changes and, therefore, the goal of these two chapters is to model the motor and battery as accurately as possible for computer simulation. The possibility of controlling both field and armature currents is then analysed with respect to the effect on efficiency of the whole system. An optimum control system is proposed and this is compared to other options. Finally, a practical design is developed.

CHAPTER 2

THE CHOPPER

2.1 PRINCIPLES OF OPERATION

2.1.1 Circuit and Waveforms

A circuit using a simple two-way switch can be used to describe the operation of a two quadrant DC-DC chopper controlling the armature current of a DC motor.[1, 24, 25]

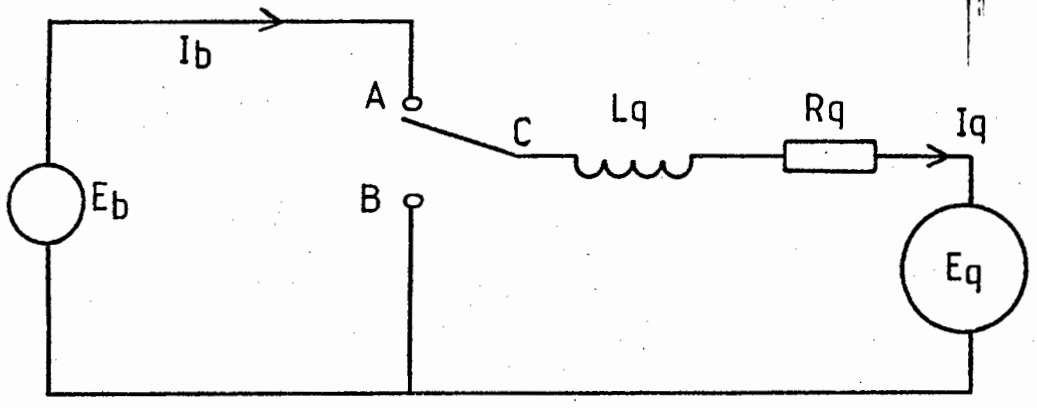

FIGURE 2.1

When the switch is in position A, current will flow from the battery through the armature and when in position B, no current will flow from the battery but armature current will be maintained by the inductance Lq.

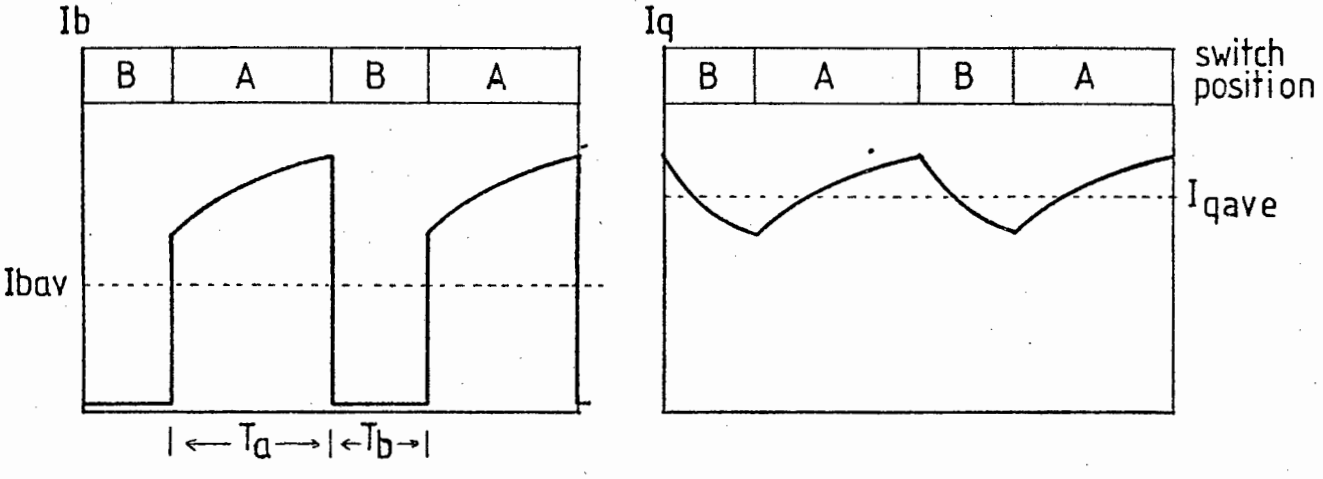

FIGURE 2.2

If T_A equals the time the switch is in position A and T_B the time in position B, then the mark space ratio (M) is defined as

$$M = \frac{T_A}{T_A + T_B} \qquad (2.1)$$

As the mark space ratio is increased, the average current through the motor (I_q) increases.

2.1.2 Regeneration

In order to cause the current to flow from the motor into the battery source, a voltage step-up mode is required since $E_q < E_B$.

The circuit in Figure 2.1 will enable this. If the time T_B is sufficiently long, the voltage E_q will cause I_q to flow negatively. When the switch is changed to position A, the inductance L_q will attempt to maintain this negative current. Current will then be delivered to the battery in pulses.

The critical value of mark space ratio at which regeneration occurs is dependent on E_q (assuming a constant E_B). This armature voltage varies with the machine speed and flux.

2.1.3 Transfer Equations[26, 27, 28]

The relationship between I_B (average) and I_q (average) as a function of

mark space ratio is not immediately obvious, particularly in the case of regeneration. For example if M = 0, a large I_q will flow but zero current will flow through the battery. What is the greatest current which can be regenerated and at what mark space ratio?

An equation relating I_{Bave} to mark space ratio (M) is developed in Appendix 1.1. The constants in the equation are armature resistance (R_q), armature inductance (L_q), battery voltage (E_B) armature voltage (E_q), Chopping Period (T). Mark space ratio is defined in Equation (2.1).

$$I_{Bave} = \frac{E_B - E_q}{R_q} \cdot M + \frac{E_B L_q}{T R_q^2} \frac{(e^{-\frac{R}{L}(1-M)T} - 1)(e^{-\frac{R}{L}MT} - 1)}{(e^{-\frac{R}{L}T} - 1)} \qquad (2.2)$$

This equation tends to a limit as the ratio $\frac{L_q}{T}$ tends to infinity, i.e. for a very large inductance or very high chopping frequency (see Appendix 1.2).

$$I_{Bave} = \frac{E_B}{R_q} M^2 - \frac{E_q}{R_q} M \qquad (2.3)$$

This equation is verified in Appendix 1.3 using an alternative approach of assuming that the power in and out of the chopper are equal.

A similar analysis is done for the average motor current in Appendix 1.1.

$$I_{qave} = \frac{E_B M - E_q}{R_q} \qquad (2.4)$$

This equation is seen to be independent of inductance value (L_q) and chopping frequency ($\frac{1}{T}$).

Equations (2.3) and (2.4) are normalised with respect to $\frac{E_B}{R_q}$ and plotted in Figure 2.3.

2.1.4 Equations for Regeneration

It is important to note that the same equations apply for both motoring and regenerating. Negative current will flow when the mark space ratio is below a critical value.

From Equation 2.3 it can be seen that this critical value occurs when

$$I_{Bave} = \frac{M}{R_q}(E_B M - E_q) = 0$$

therefore, regeneration will begin to occur when $M = \frac{E_q}{E_B}$ (2.5)

The maximum value of current which can be regenerated is also found from Equation (2.3)

$$\frac{d\, I_{Bave}}{d\, M} = \frac{2E_B}{R_q} M - \frac{E_q}{R_q} = 0$$

therefore, maximum regenerated current occurs when $M = \frac{E_q}{2E_B}$ (2.6)

and will have a value

$$I_{Bave} = \frac{E_B}{R_q} \cdot \frac{E_q^2}{4E_B^2} - \frac{E_q}{R_q} \cdot \frac{E_q}{2E_B}$$

$$= \frac{-E_q^2}{4R_q E_B} \quad (2.7)$$

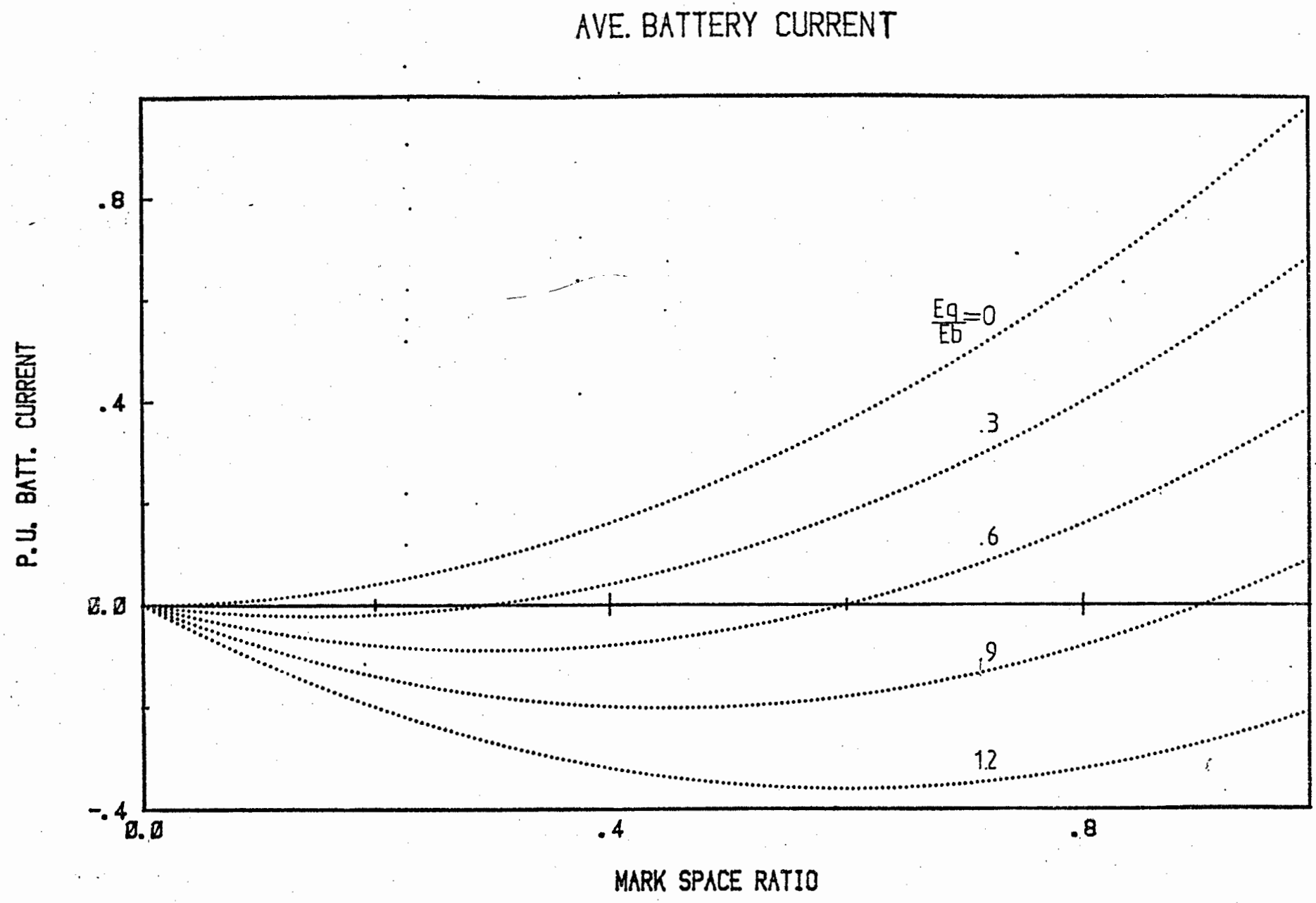
AVE. BATTERY CURRENT
P.U. BATT. CURRENT
.8
.4
Ø.Ø
-.4
Ø.Ø
.4
.8
MARK SPACE RATIO
Eq/Eb=0
.3
.6
.9
1.2

Figure 2.3

2.1.5 A Practical Circuit

The circuit in Figure 2.1 assumes a bidirectional switch, whereas most semiconductor devices are uni-directional.

During motoring (positive I_q), it can be seen by inspection that the required switching function along path B-C can easily be performed using a diode permanently in the circuit. With the switch in position A the diode across B-C will be reverse biased and will not conduct (see Figure 2.4). When path A-C is broken, the inductor supplies a negative EMF in an attempt to maintain the current flow. Thus the diode will be forward biased and path B-C will be switched on.

Similarly, a diode across A-C will provide the required switching during regeneration.

Therefore, two diodes and two uni-directional switching devices will enable the required bidirectional switching.

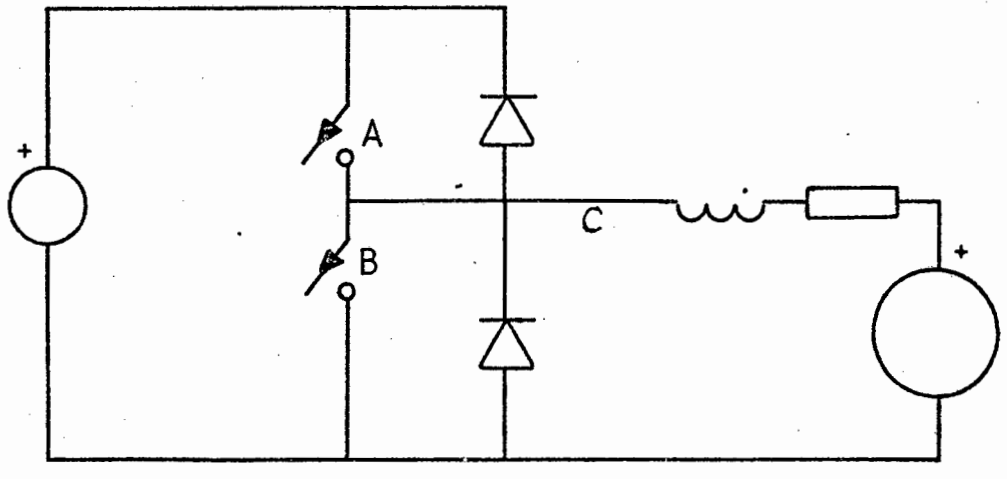

FIGURE 2.4

Switches A and B are always 180° out of phase.

2.1.6 Cúk Converter[29]

A novel adaptation of the ideas developed in this section has been suggested in reference (29). Conceptually, it consists of cascaded step up and step down stages with a large capacitor to transfer the energy between the two.

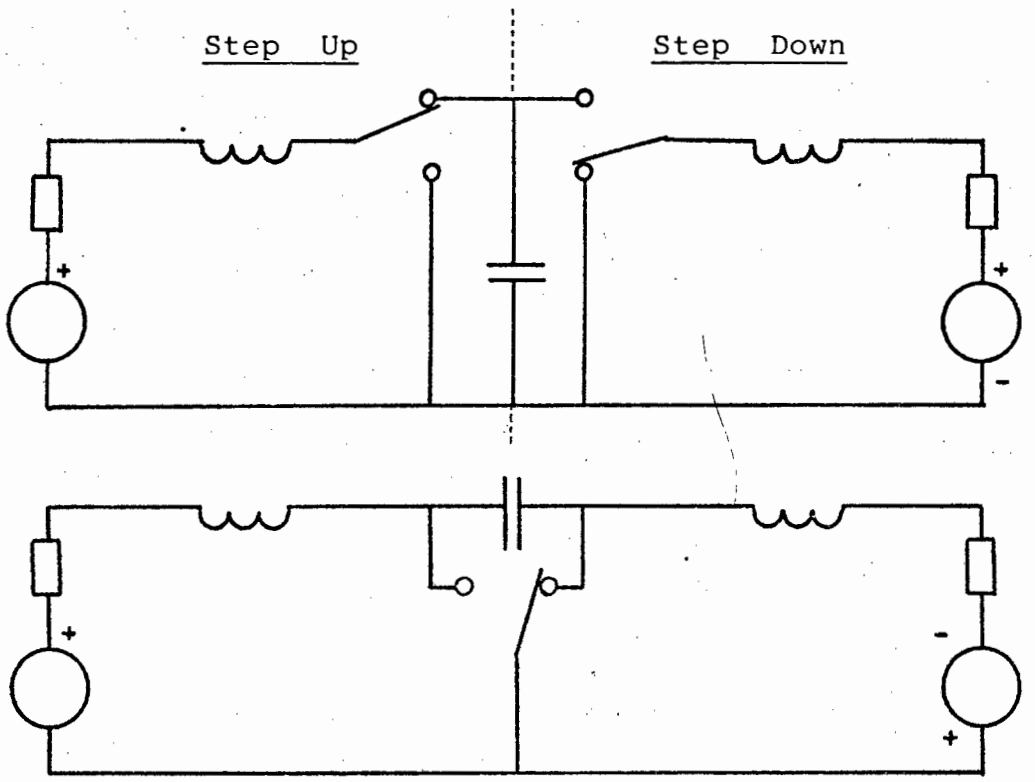

FIGURE 2.5

This can be implemented using a single pole double throw switch. Each end of the capacitor is alternately grounded.

The main advantage of this system is the continuity of both input and output currents. Further improvements are obtained if the two inductors are transformer coupled on the same core.

This converter together with several other adaptations are discussed extensively in the literature by Slabodan Cúk.

2.2 SWITCHING DEVICES

Various semiconductor devices are available to perform the switching operation.

2.2.1 Thyristors[4, 25, 30, 31]

The thyristor is the most commonly used switching device because of its robustness and high current and voltage capabilities.

The major disadvantage of the thyristor is the need for forced commutation, since the device will not turn off until the current through it has been reduced to zero. This affects reliability and switching speeds. Various methods of commutation are discussed in reference (30).

The thyristor switch is inefficient because of the slow switching speeds and the energy required for commutation.

2.2.2 Power Transistors[32, 33, 34, 35]

Power transistors eliminate the need for forced commutation. However, these are limited by their relatively low current and voltage capabilities, particularly their ability to handle surge currents (due to the effect of second breakdown).

The current rating can be increased by parallelling several devices. Transistors need to be carefully matched since the saturation collector-emitter voltages are not identical.

Current sharing resistors may be required which would reduce efficiency.

Unless darlington transistors are used, the base drive current required is fairly high.

The use, protection and choice of power transistors in the switching mode is extensively analysed in reference.[35]

2.2.3 Power Field Effect Transistors[36]

A recent development in power semiconductors is the HEXFET (trade name of a range of power MOSFETS produced by International Rectifier).

The device is controlled by applying a voltage to the gate and the drive current is almost zero (nanoamperes). Therefore, it has a high gain.

Pulsed load current rating is more than double the continuous rating. This is due to the absence of second breakdown. However, the device is very sensitive to overvoltage transients.

Single HEXFETS are available which can switch 28 A (continuous) and 100 V. Because of a positive temperature coefficient, the devices are easily paralleled and current is automatically shared. Unlike the transistor, the saturated on-state can be represented by a resistor. Therefore, paralleling of devices reduces the on-state resistance, thus reducing losses.

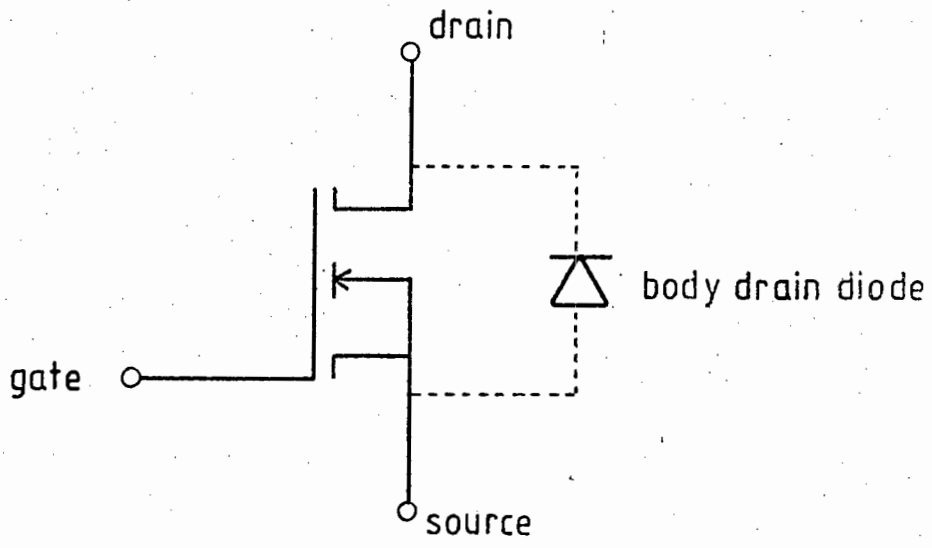

FIGURE 2.6

The HEXFET symbol is shown in Figure 2.6. An internal reverse or body drain diode has the same current rating as the device and can be used as a free-wheeling diode if necessary.

HEXFETS were used in this thesis because of their high switching speed capabilities, (therefore, low losses) and ease of use.

2.3 THE USE AND PROTECTION OF HEXFETS[36]

Three values need to be investigated:gate/source voltage, drain/source voltage and drain/source current, with particular reference to transient spikes.

2.3.1 Gate/Source Voltage

Over-voltage on the gate can punch through the oxide layer and cause damage.

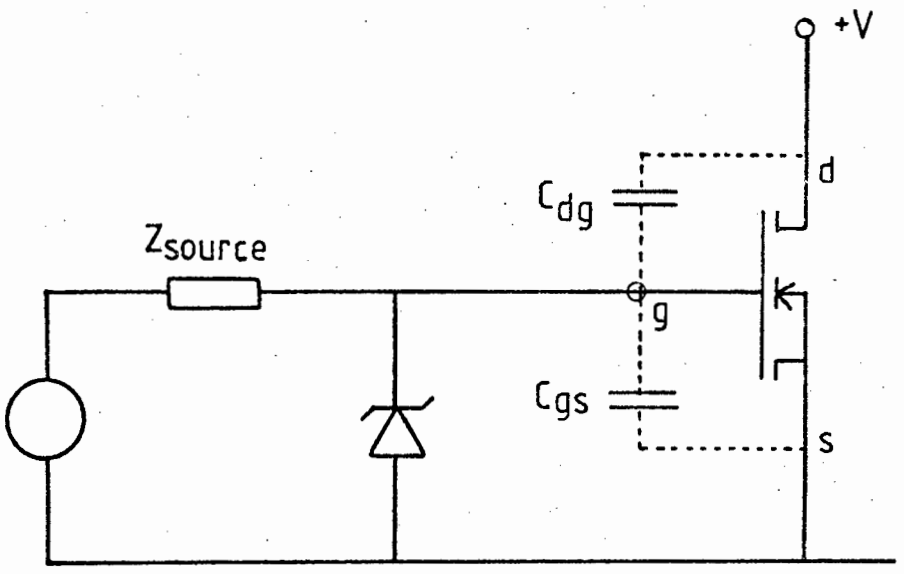

FIGURE 2.7

During turn-off time a positive change in V_{DS} will be reflected as transient on the gate

$$V = \frac{1}{1 + C_{gs}/C_{dg}} \times \Delta V_{DS}$$

since (C_{dg} and C_{gs} act as a potential divider).

This could be sufficient to cause spurious turn on or could damage the device due to over-voltage on the gate. An external zener diode will clamp both negative and positive transients. A low source impedance will prevent spurious turn-on and will also limit voltage transients.

2.3.2 Drain/Source Voltage

During turn-off, the path of an inductive circuit is broken. Therefore, V_{DS} rises in an attempt to maintain the current. The HEXFET is particularly sensitive to these voltage spikes.

2.3.2.1 Free wheel diode

A free wheel diode connected across the inductor to provide an alternative path for the current being switched is essential.

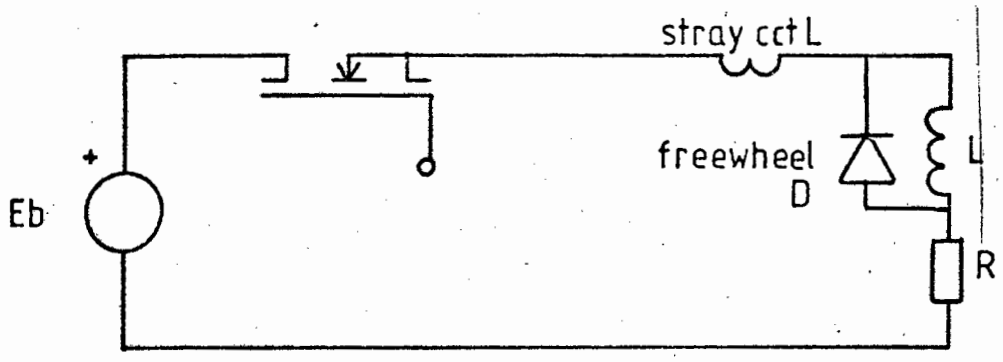

FIGURE 2.8

The diode has a finite switch on time, during which the voltage will rise. Therefore, a high speed Schottky diode is desirable with a switch on time of the order of 50 nS. The use of the body drain diode in the second HEXFET of the chopper in Figure 2.6 was suggested in 2.2.3. This has a reverse recovery time of about 300 nS, which is too slow for high speed switching.

2.3.2.2 Layout

There is a small stray inductance in the leads of the circuit. This is sufficient to cause voltage spikes when switching at high speeds. It is important that the diode is physically located as close to the HEXFET as possible and that leads to the battery be kept short.

2.3.2.3 Snubbers

Despite the above precautions, there still remains a finite

circuit inductance and reverse recovery time for the free wheel diode. A protection snubber circuit is, therefore, required. Three possibilities are described.

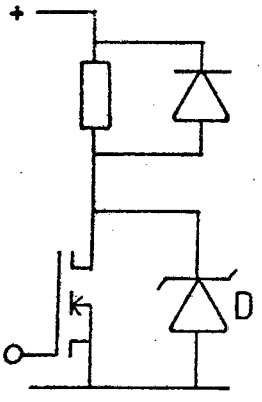

FIGURE 2.9

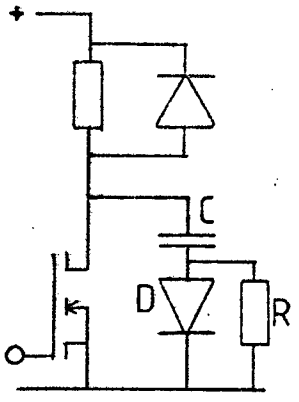

FIGURE 2.10

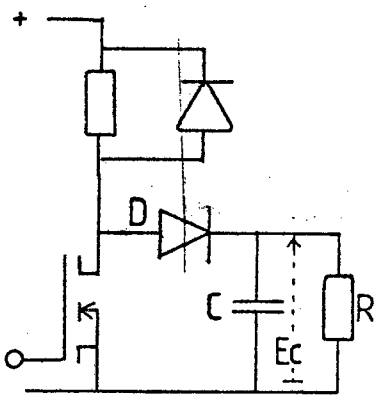

FIGURE 2.11

At turn-off, the voltage across the HEXFET will rise in an attempt to maintain the load current. The snubber in Figure 2.9 will conduct when the zener voltage is exceeded, thus preventing high voltage spikes.

In Figure 2.10 the capacitor C charges via the diode at turn-off, thus absorbing the voltage spike. During the on period of the Hexfet, the energy in C is discharged through resistor R. The value of C is calculated from.

$$C = \frac{I t_c}{V}$$

where I is the full load current. V the supply voltage and the value of t_c is discussed in Section 2.4.2.4 and optimised in Equation 2.18. R is calculated such that the time constant

$$RC \ll \frac{1}{f}$$

where f is the chopping frequency. The value of R must be high enough to keep the sum of load and capacitor discharge current below the peak rated value of the hexfet.

In Figure 2.11 the capacitor is charged to a value greater than the supply voltage. Thus diode D is reverse biased except when a voltage spike of greater than E_c appears during turn-off. The resistor needs to be carefully chosen to discharge the capacitor while maintaining the required voltage E_c.

Both Figure 2.9 and 2.11 are voltage clamping devices which dissipate energy only when an over-voltage appears. The load-line characteristic is shown in Figure 2.12. The snubber in Figure 2.10 absorbs energy throughout the switching period and alters the load line characteristic. (Figure 2.13)

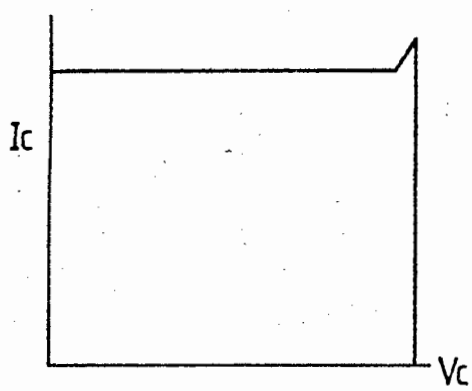

FIGURE 2.12

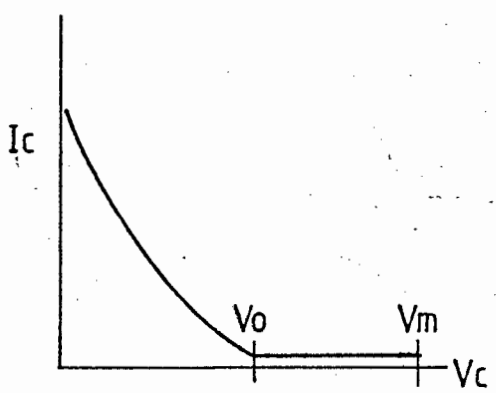

FIGURE 2.13

The load line characteristic in Figure 2.13 enables the device to operate further into the safe operating area of the device. Power is dissipated in the snubber rather than in the silicon. Snubber and switching losses are examined in Section 2.4.

The diode in Figures 2.10 and 2.11 and the zener in Figure 2.9 must be chosen for their fast forward recovery characteristics. Snubbers should be mounted physically as close as possible to the hexfet terminals to avoid circuit inductance.

2.3.3 Drain Source Current

The total continuous RMS current rating should not be exceeded. The hexfet also has a peak current rating which is more than double the continuous RMS rating. This should not be exceeded.

When the hexfet is switched on, the reverse recovery of the free wheeling diode can cause a high current spike.

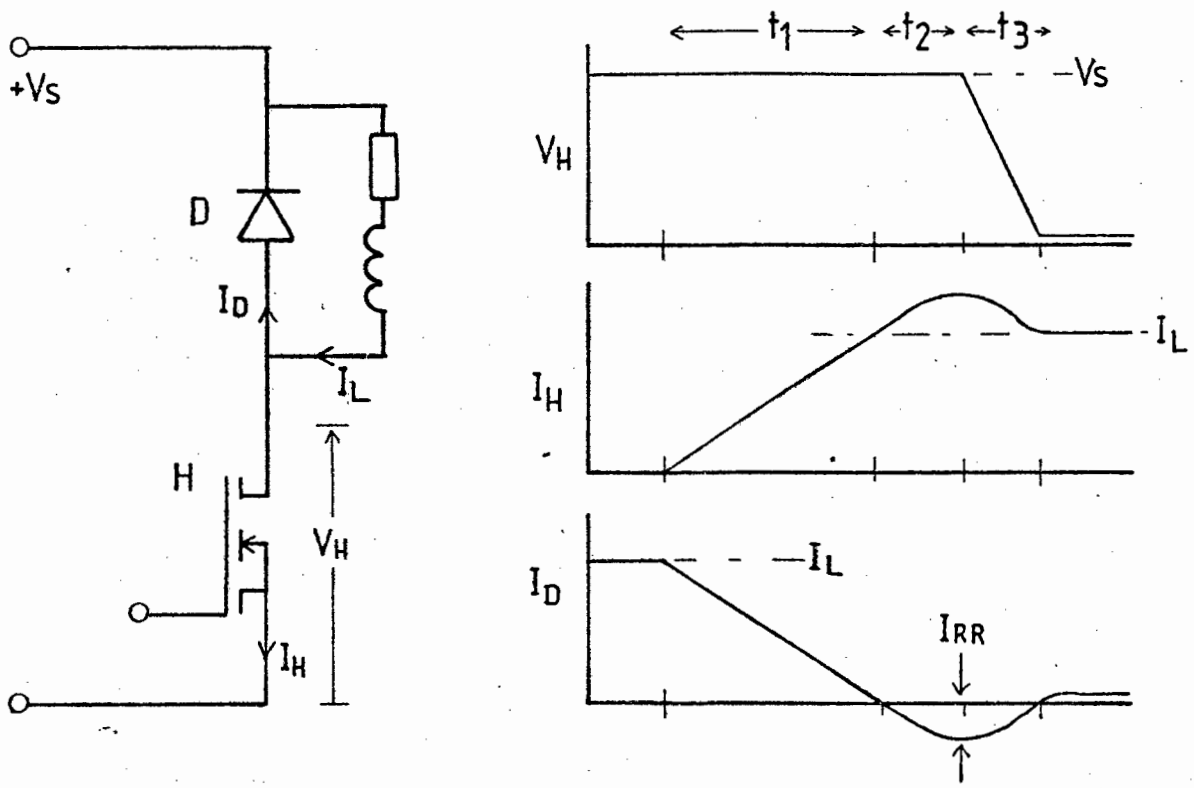

FIGURE 2.14

During time t_1 the value of I_D decreases and I_H increases. With a perfect diode, commutation should be complete after t_1. However, owing to minority carrier reverse recovery, the diode is unable to support reverse voltage, and thus the current I_D reverses direction. The value of I_H also increases because $I_H = I_L - I_D$. After time t_2, the diode begins to support reverse voltage and diode current tends to zero (I_H tends to I_L). The voltage V_H remains high till the end of time t_2 and then begins to drop.

Parasitic capacitance will also tend to increase this current peak.

There are four ways of reducing this effect.

1. Slowing down the gate drive signal.
2. Using a fast recovery diode.
3. Using a small linear inductance in series with the switch (together with a fast recovery free wheel diode).
4. Using a small saturable inductance in series with the switch.

The efficiency of these methods is examined in Section 2.4.

2.4 SWITCHING AND SNUBBER LOSSES[35, 37, 38]

2.4.1 Switching Losses With No Snubber

Assuming zero stray inductance and zero recovery time for the diode, the following simplified waveforms are obtained:

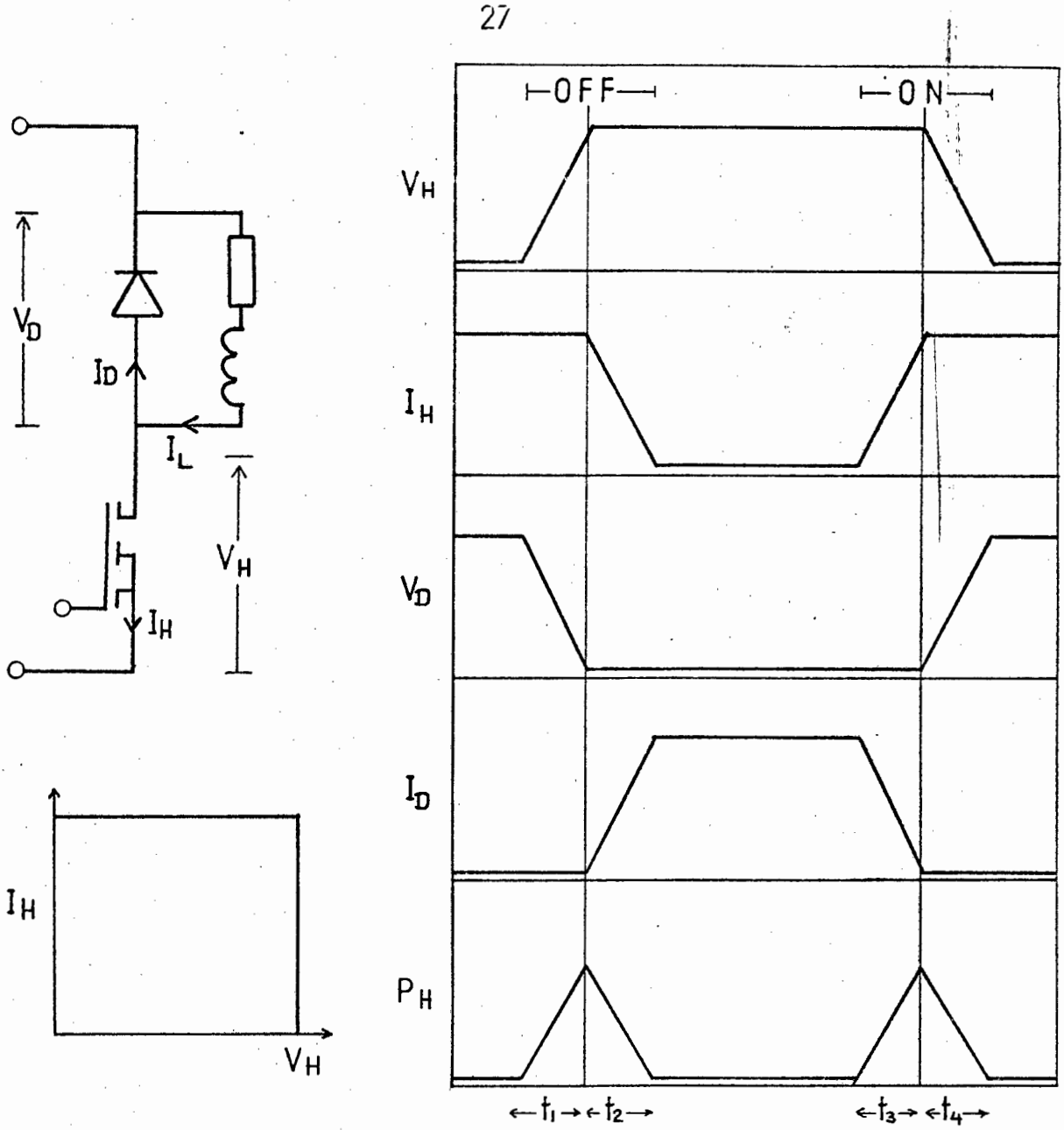

FIGURE 2.15

During turn off, the voltage V_H will rise until the diode becomes forward biased. At this point the diode current begins to increase and the hexfet current begins to decrease.

The power loss in the hexfet.

$$P = \frac{1}{T}\left[\int_0^{t_1} V_H I_H dt + \int_0^{t_2} V_H I_H dt + \int_0^{t_3} V_H I_H dt + \int_0^{t_4} V_H I_H dt\right]$$

$$= \tfrac{1}{2} V_S I_L \left[t_1 + t_2 + t_3 + t_4\right] \times f \qquad (2.8)$$

where f is the chopping frequency.

From the waveforms it can be seen that either the voltage or the current in the diode is always zero. Therefore, switching losses are zero in the diode.

From the equation 2.8 it can be seen that switching losses in the chopper can be reduced by decreasing the switching time or decreasing the chopping frequency.

2.4.1.1 Switching Speed

If a power loss of 0.1% of the load power being switched is regarded as negligible then the switching loss will be insignificant, for

$$P_S = \tfrac{1}{2} V_S I_L t_S f < .001\ V_S I_L$$

therefore, $f < \frac{.002}{t_S}$

where f is the chopping frequency and t_s is the total on and off switching time $t_1 + t_2 + t_3 + t_4$. Using hexfets a t_s of about 300 nS was achieved. Thus with a chopping frequency of less than 6.6 KHz, the switching loss will be negligible.

2.4.1.2 Achieving High Switching Speeds[36]

The gate drive signal is an important factor in providing high switching speeds and, therefore, low losses.

During steady state operation, very low drive current is required. However, at switch ON, a certain charge is required to raise the gate to the desired voltage owing to the capacitance. Thus the drive should be able to supply a large current in a short time, i.e. very low impedence.

A NPN-PNP transistor pair enables this requirement to be met.

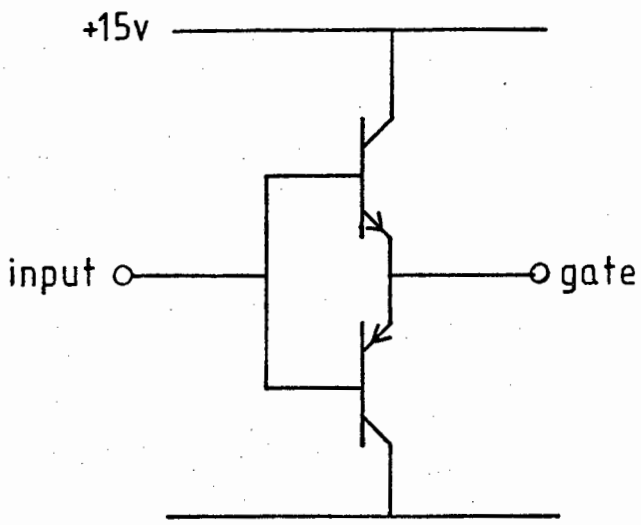

FIGURE 2.16

The final system was driven from the output port of an INTEL 8085 micro-processor. The following circuit was used.

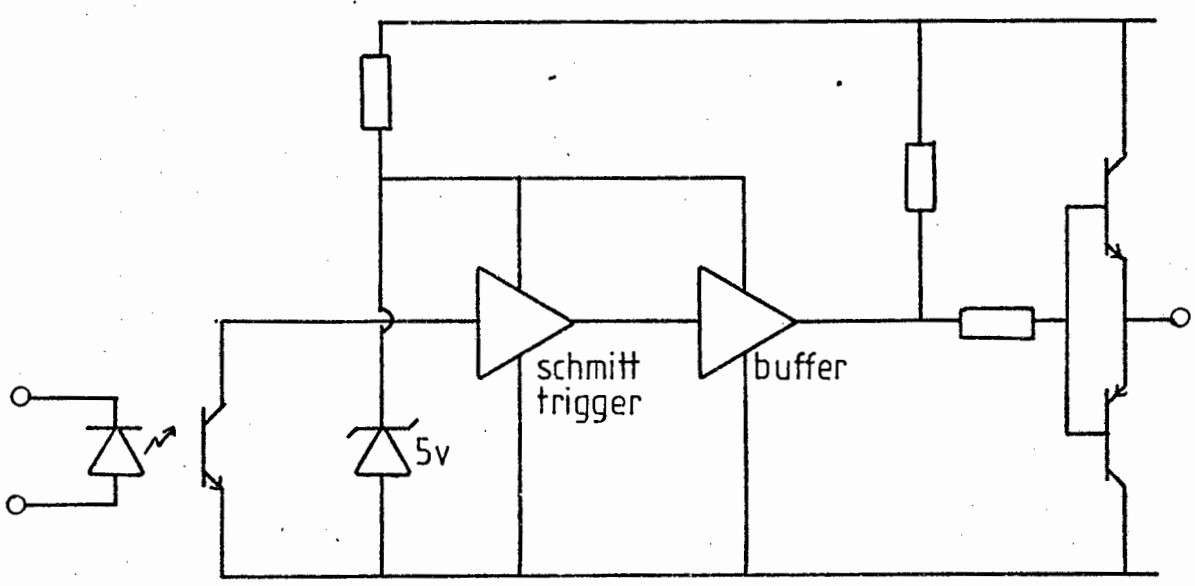

2.4.2 "Turn-Off" Capacitive Snubber

2.4.2.1 Snubber and switching losses[35]

Equations for the energy loss when using a capacitive snubber (see Figure 2.10) are developed in Appendix 2. These equations assume zero stray inductance and diode recovery time. Power losses are obtained by multiplying by chopping freqencies.

Switching turn off power loss in the hexfet (symbols are defined in Appendix 2.3.1)

$$P_{H(\text{turn off})} = \frac{V_S I_L}{2} \cdot \frac{t_s^2}{6(2t_c - t_s)} \cdot f \quad W \tag{2.9}$$

$$P_S = \frac{I_L V_S}{2} \left(t_c - \frac{t_s}{2}\right) \cdot f \quad W \tag{2.10}$$

At turn on, the only effect of the snubber is to contribute a small discharge current from the capacitor. This is assumed to remain constant over the relatively short switching period and has a value of $\frac{V_S}{R}$. The loss due to this effect can be regarded separately and the total loss found by superposition.

Thus the turn on loss can be regarded as the same as when no snubber is present. This case was dealt with in Section 2.4.1.

$$P_H(\text{turn-off}) = \frac{V_S I_L}{2} (t_3 + t_4) \cdot f \qquad (2.11)$$

where t_3 and t_4 are described in figure 2.15.

2.4.2.2 Effect of stray inductance[35]

The effects of stray inductance on voltage and current waveforms are marked in Figure 2.17. The frequency of ringing is obtained from

$$2\pi f = \frac{1}{\sqrt{L_S C}}$$

therefore $$\text{period } T = 2\pi\sqrt{L_S C} \qquad (2.12)$$

where L_S is the stray inductance and C is the snubber capacitor.

The peak voltage

$$\Delta V = |I| \cdot |Z| = I_H W L_S \quad \text{and} \quad W = \frac{1}{\sqrt{L_S C}}$$

therefore $$\Delta V = I_H \sqrt{\frac{L_S}{C}} \qquad (2.13)$$

(See Figure 2.17 overleaf.) I_H is the load current through the Hexfet.

2.4.2.3 Effect of diode recovery time

At turn-off, the forward recovery time of the diode will have the effect of delaying the rising edge of I_D at time t_c by a small constant. This will also cause a further overshoot in V_H.

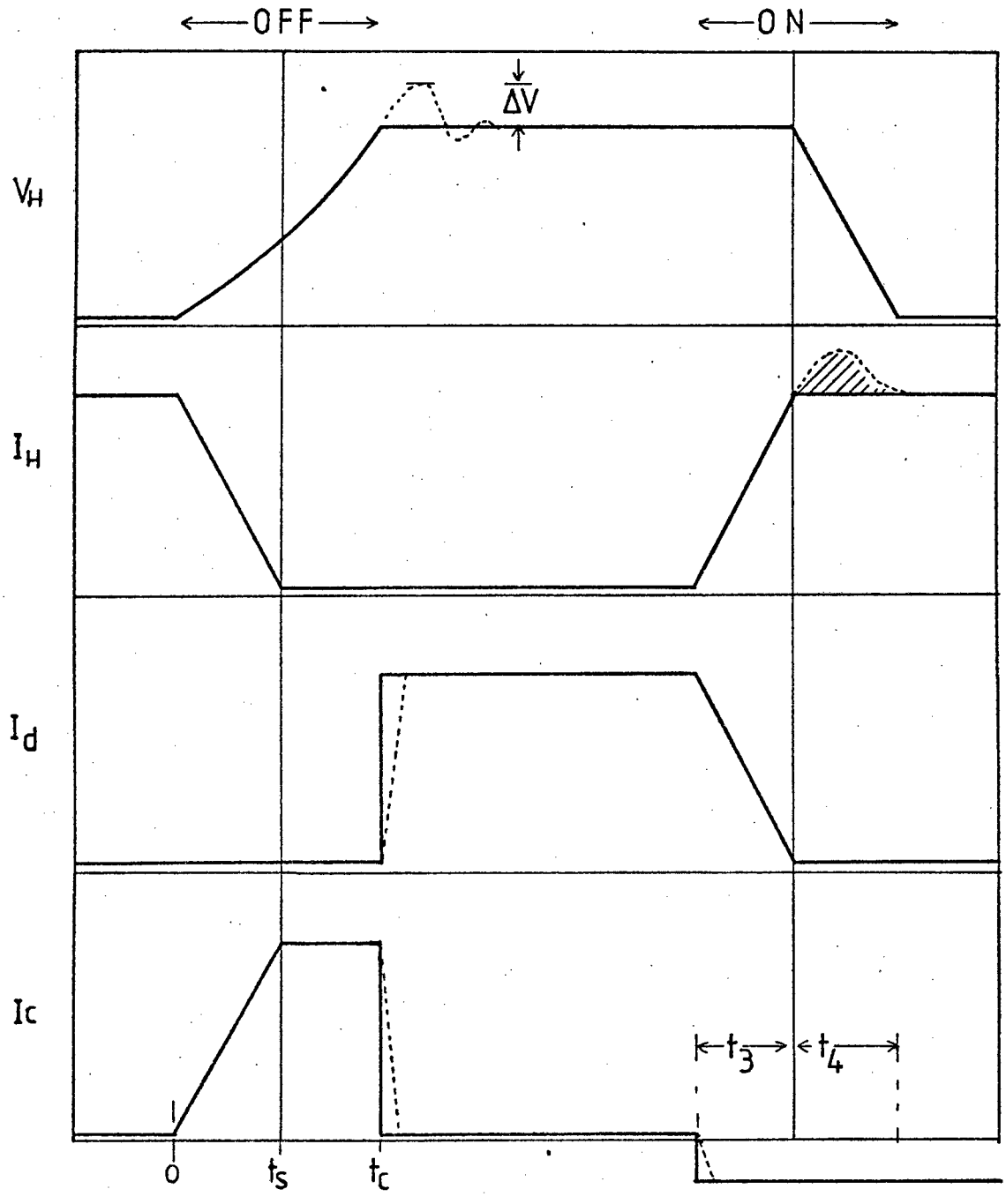

——— waveforms neglecting stray L + D. recovery

-------- including stray L

▨ reverse recovery

FIGURE 2.17

At turn on, the reverse recovery time causes an overshoot in the hexfet current I_H.

Both recovery time and stray inductance will have the effect of slightly increasing the power loss equations developed above.

2.4.2.4 Comparison of "turn off" losses with and without capacitive snubber[35]

The total turn off power loss with a snubber is given by equations 2.9 and 2.10.

$$P_S = \frac{V_S I_L}{2} \cdot f \left[\frac{t_s^2}{6(2t_c - t_s)} + (t_c - \frac{t_s}{2}) \right] \qquad (2.14)$$

If the voltage rise time and the current fall time are assumed to be equal in Figure 2.15, then the turn off power loss without a snubber is

$$P' = \tfrac{1}{2} V_S I_L (t_1 + t_2) \cdot f$$

$$\text{therefore } P' = V_S I_L f t_s \qquad (\text{since } t_1 = t_2 = t_s) \qquad (2.15)$$

Using equations 2.14 and 2.15, it is possible to determine under which conditions the overall efficiency is improved by using a capacitive snubber. The controllable variable in the equation is t_c which is determined by the value of capacitance.

Equation 2.14 is rearranged so that the quantity $\frac{t_c}{t_s}$ is the equation variable. This eliminates the need to know the value of t_s

$$\text{Therefore } P_S = V_S I_L . t_s . f \left[\frac{1}{12(2\frac{t_c}{t_s} - 1)} + \frac{t_c}{2t_s} - \frac{1}{4} \right] \quad (2.16)$$

Equation 2.16 is normalised with respect to P' since these are the two quantities being compared.

$$\text{Therefore } \frac{P_S}{P'} = \frac{1}{12(2\frac{t_c}{t_s} - 1)} + \frac{t_c}{2t_s} - \frac{1}{4} \quad (2.17)$$

The normalised values $\frac{P_S}{P'}$ are then plotted on a graph (Figure 2.18). The area where $\frac{P_S}{P'} < 1.0$ is the region where efficiency is improved by using a snubber.

By inspection of the graph (Figure 2.18) it can be seen that efficiency is improved when

$$t_c < 2.5\ t_s \quad (2.18)$$

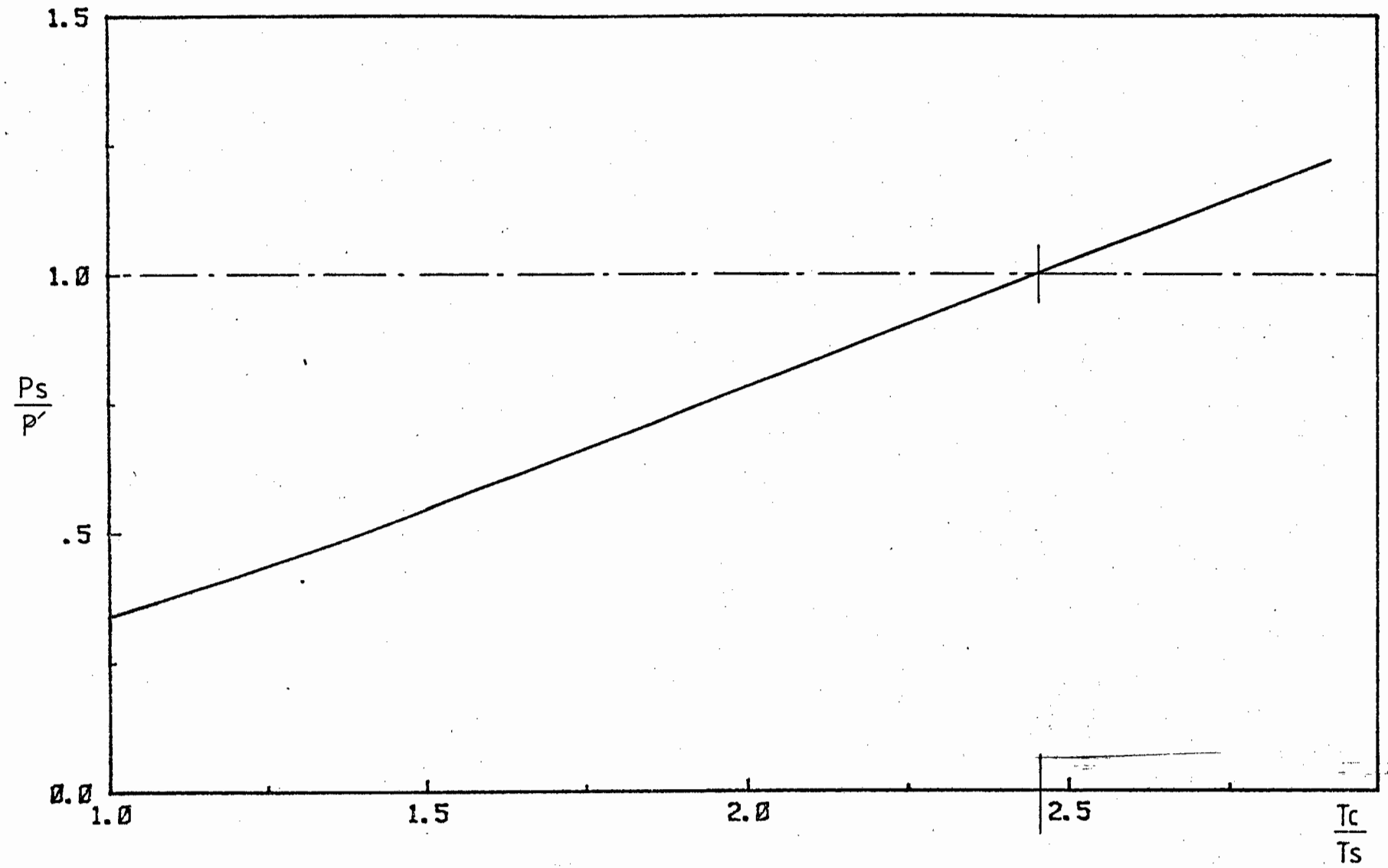

Figure 2.18

2.4.2.5 Zener "snubber"

The zener is a voltage clamp which absorbs voltage peaks but does not affect the load-line switching characteristic. Therefore, no part of the switching loss is dissipated in the zener. The only losses dissipated in the zener will be those due to stray inductance and diode forward recovery at turn off. The switching loss equation is the same as that described in Section 2.4.1.

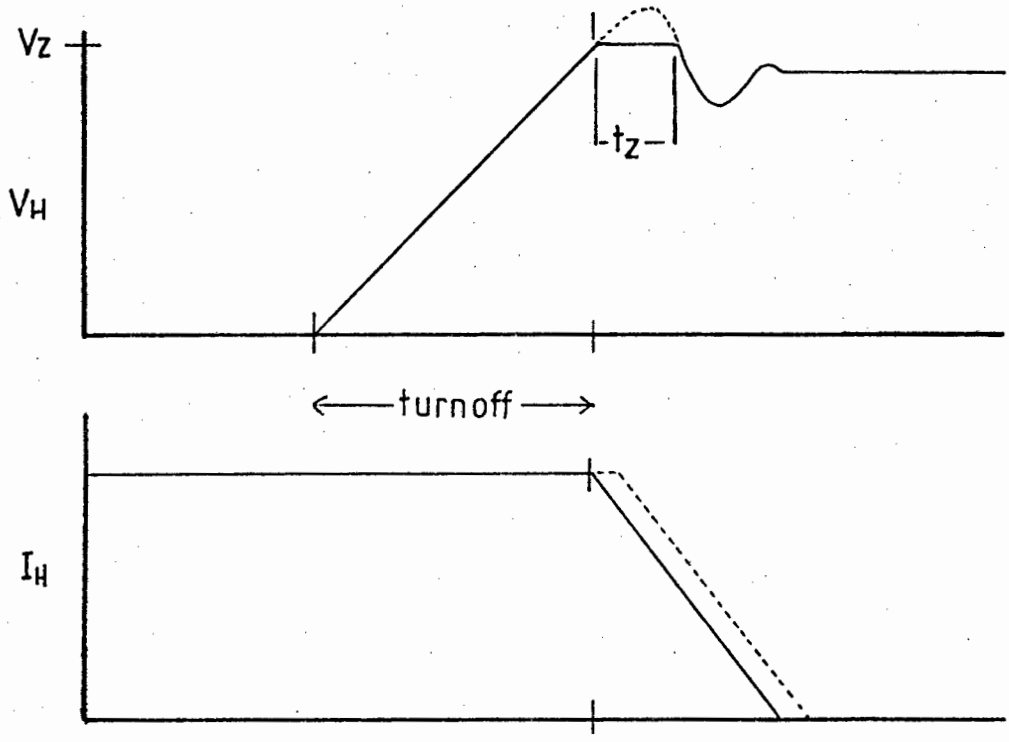

FIGURE 2.19

The stray inductance causes V_H to overshoot. The diode forward recovery time causes the diode current to be delayed by a constant. This results in a further voltage overshoot.

The maximum loss in the zener is

$$P = V_z \cdot I_L \cdot t_z \cdot f$$

In practise t_z is very small and P is negligible in a well designed circuit.

It should be noted that a well designed capacitive snubber reduces switching losses whereas a zener clamp does not alter the load-line switching characteristic.

2.4.3 "Turn On" Snubber and Switching Losses[35]

Four methods of protection against current spikes caused by reverse recovery are described in Section 2.3.3.

Slowing down the gate drive signal is effective but increases the loss since the switching time is increased.

Using a fast recovery diode reduces the losses caused by reverse recovery, but does not affect the switching losses.

Using a small series inductor reduces the reverse recovery current spike and also reduces the overall switch-on loss by altering the load-line switching characteristic. The switching waveforms and load line of a linear series inductor are shown in Figure 2.20 (overleaf).

The switching loss without a turn-off snubber was found in Section 2.4.1.

$$P_H \text{ (no snubber)} = \frac{V_S I_L}{2} (t_3 + t_4) \cdot f \qquad (2.19)$$

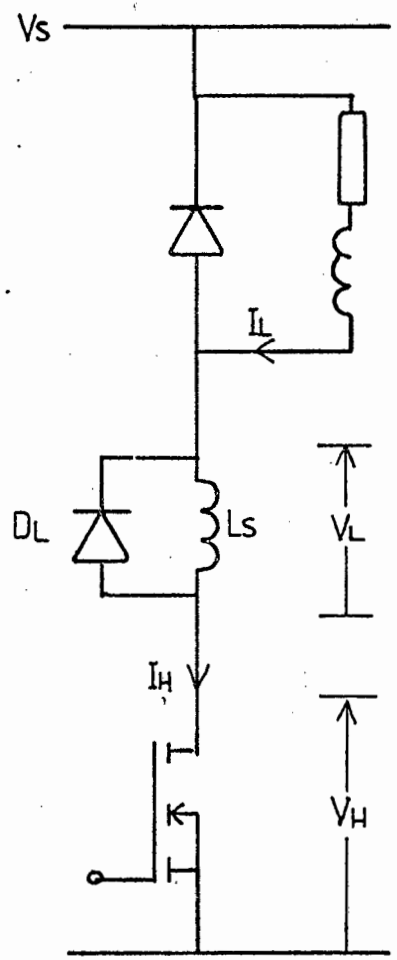

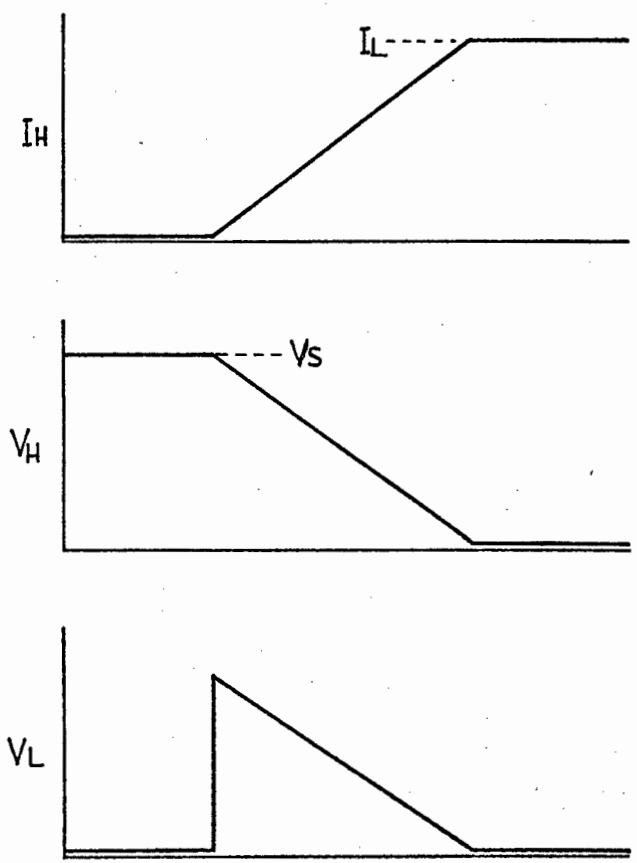

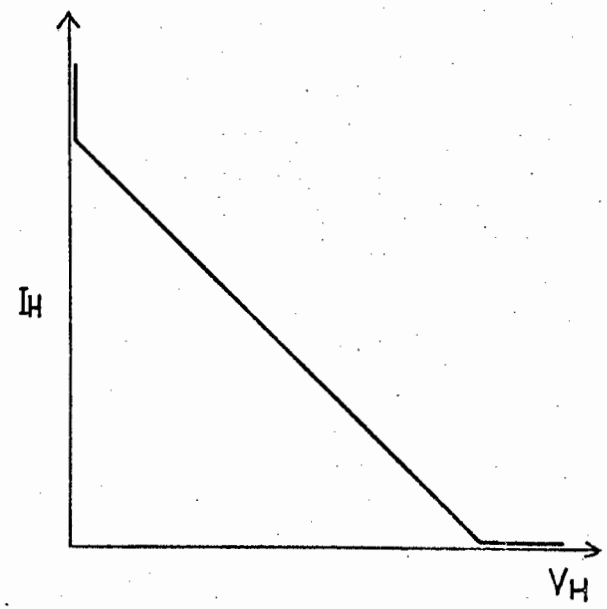

figure 2.20

The loss in the hexfet with a linear inductance

$$P_{H\ (\text{linear } L)} = \frac{1}{T}\int_{o}^{t_s} V_H(t)I_H(t)dt = \frac{V_H I_L t_s f}{6} \qquad (2.20)$$

The power dissipated in diode D_L at turn off owing to energy stored in L_S

$$P_L = \frac{1}{T}\int_{o}^{t_s} V_L(t)I_L(t)dt = \frac{V_H I_L t_s f}{6} \qquad (2.21)$$

If, for example, $t_3 + t_4$ in equation 2.19 equals t_s in equation 2.20 and equation 2.21, then the total loss with a snubber is a third less than when a snubber is not used.

If a small saturable inductance is used instead of the linear inductance, then the waveforms shown in Figure 2.21 are obtained.

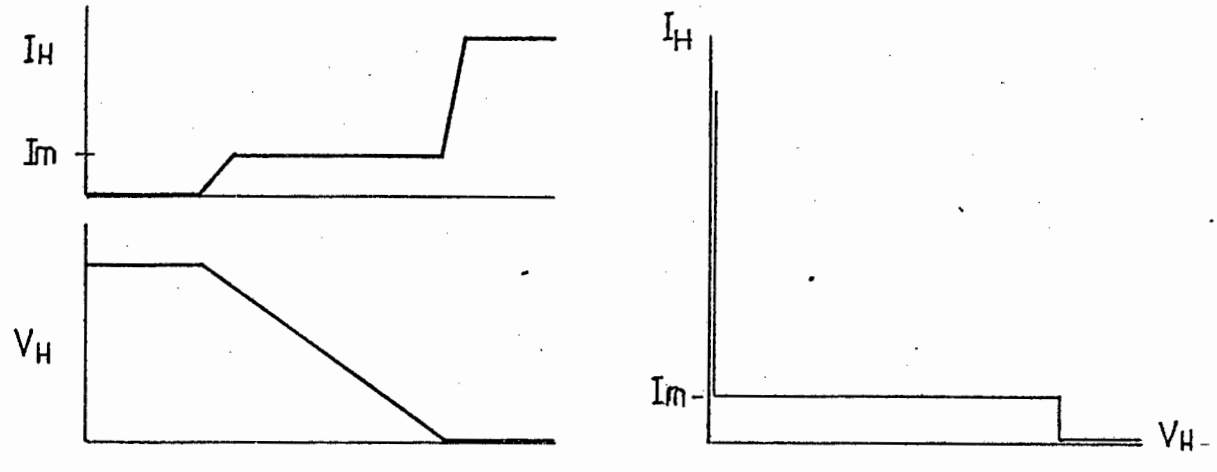

FIGURE 2.21

If a well defined saturable inductance is used, both hexfet and snubber switch on losses become negligible.

2.4.4 Energy Recovery Snubbers[38]

The "switch on" snubber can return the snubber energy through a small step up transformer. In the "switch off" snubber, energy absorbed by C is discharged through D1 and the resonance of L and C reverses Vc for the next cycle.

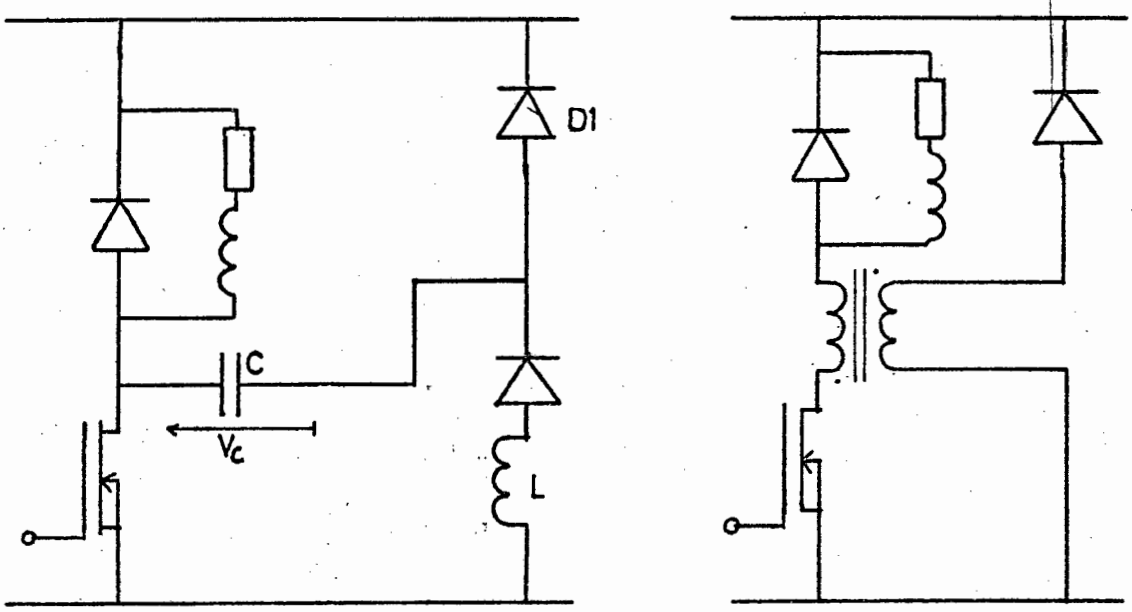

Switch off snubber Switch on snubber

FIGURE 2.22

2.4.5 Conclusion

Careful layout and choice of components can virtually eliminate the need for protection snubbers. Stray inductance can be made very small by keeping leads short (less than a few centimeters). Fast recovery Schottky diodes can be used. The peak current of a hexfet is about twice its continuous rating and in addition if the hexfets are underrated to reduce on state losses (as suggested in Section 2.5), then the current peak caused by the diode's reverse recovery will not pose a problem.

Using hexfets, high switching speeds can be obtained and switching losses can be reduced to negligible proportions (e.g. 0.1% of load being switched).

If this is not sufficient then switching losses can be further reduced by using load-line shaping snubbers and snubber loss recovery circuits.

2.5 ON STATE LOSSES

2.5.1 Hexfet

The on state of a hexfet is approximated by a resistance, therefore

$$P_{ON} = I_H^2 R_{D(on)} \qquad (2.22)$$

where I_H is the RMS value of the hexfet current and $R_{D(on)}$ is the ON-resistance of the hexfet at 25°C. A typical R_D value for an IRFI50 hexfet is 0.055Ω.

A more accurate expression which includes temperature effects is

$$P_{ON} = I_H^2 R_{D(ON)} \left[1 + 0.007 \left(\Delta T_{JA} + T_A - 25\right)\right] \qquad (2.23)$$

where T_A is the ambient temperature in °C and ΔT_{JA} is the junction-to-ambient temperature rise.[36]

By paralleling hexfets the on-state loss can be reduced by as much as is required. If N hexfets are paralleled, the loss in

each one will be

$$P_N = (\frac{I_H}{N})^2 R_{D(ON)}$$

where I_H is the total current. The total on state loss is thus

$$P_{ON} = N \times P_N = \frac{I_{H^2} R_{D(ON)}}{N} \qquad (2.24)$$

P_{ON} is thus reduced by a factor of N. This will require a smaller heatsink and losses will be further reduced since ΔT_{JA} is smaller. (See Equation 2.23) However, although it is efficient to use the hexfets at well below their rated current values, it is also more expensive.

2.5.2 Freewheel Diode

Unlike the hexfet the diode in the on-state is represented by a constant voltage drop. The only way to reduce this loss is by selecting a diode with a lower forward voltage drop. A Schottky diode (SD51), for example, has a maximum forward voltage drop of 0.60 V compared to 1.70 V in the hexfet's (IRF150) own integral reverse diode.

2.5.3 Heatsink Design[39]

The effective value of $R_{D(ON)}$ is increased if the junction temperature is allowed to become too great. This, therefore, is a source of inefficiency. The heatsink must be designed to keep ΔT_{JA} as small as possible.

2.6 INDUCTOR LOSSES

2.6.1 The Inductor

An inductor is required to keep the output current continuous when motoring and is also used as a storage element when the chopper is in the step up mode. The armature inductance of the motor may be sufficient, but in some cases an external inductor needs to be added.

This inductor has a great effect on the additional motor losses caused by chopping which are observed in reference (40).

2.6.2 Losses Owing to Form Factor

If the ratio of switching period (T) to time constant (TC = L/R_q) is too high, then the output current waveform will have a high ripple.

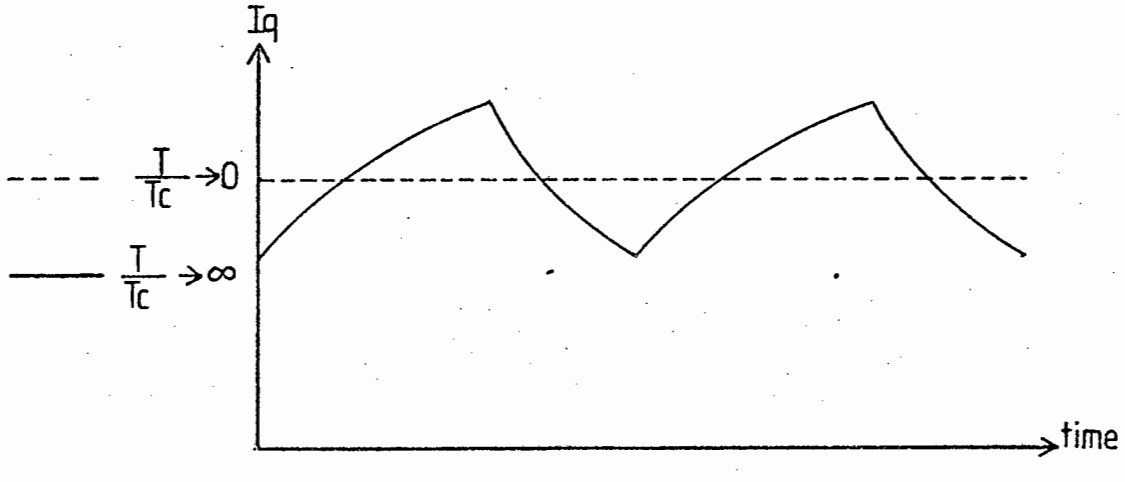

FIGURE 2.23

Therefore, if $\frac{T}{TC} \neq 0$ then a loss will result because of the current form factor:

This loss is analysed in Appendix 3, and normalised with respect to E_{B^2}/R_q it is shown to be.

$$P_{N(loss)} = M - M^2 + \frac{e^{-(1-M)\frac{T}{TC}} - 1)(e^{-M\frac{T}{TC}} - 1)}{\frac{T}{TC}\,(e^{-\frac{T}{TC}} - 1)} \qquad (2.25)$$

This per unit loss is plotted in Figure 2.24 against $\frac{T}{TC}$ for various values of mark space ratio M.

The loss is seen to be greatest when M = 0.5 and has a maximum value of

$$P_{N(max)} = \frac{1}{4} + \frac{(e^{-\frac{T}{2TC}} - 1)}{\frac{T}{TC}\,(e^{-\frac{T}{2TC}} + 1)} \qquad (2.26)$$

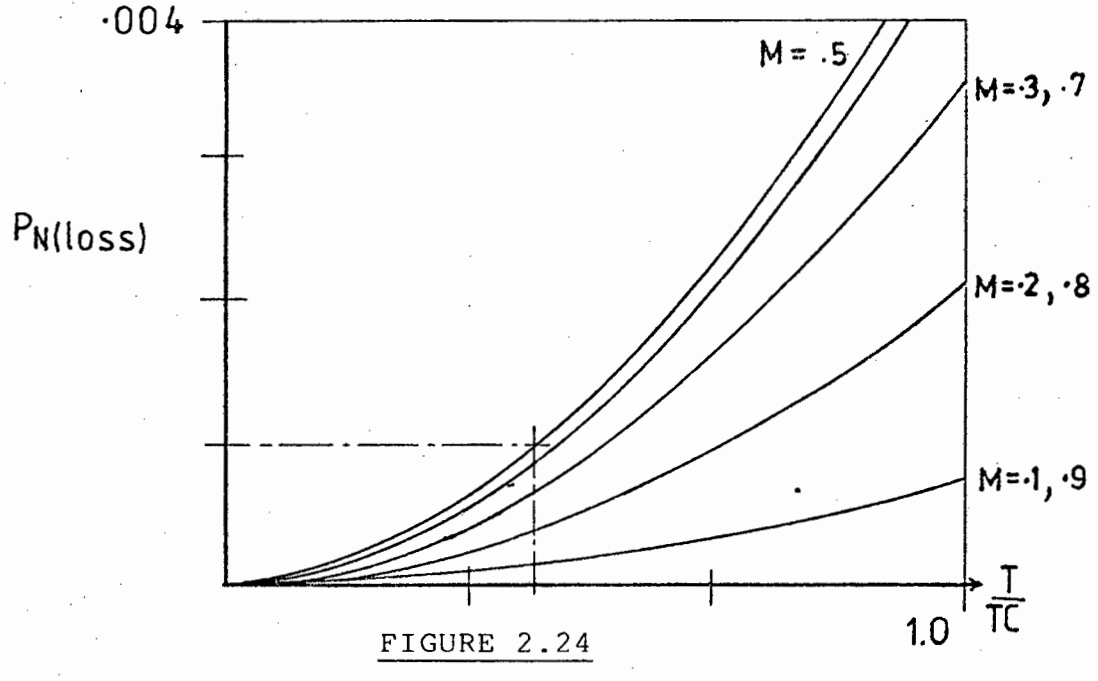

FIGURE 2.24

The chopping frequency must, therefore, be high enough and the value of L large enough, so that this loss is negligible. A power loss of 0.1% of E_{B^2}/R_q can be assumed to be negli-

gible. Therefore, a value of $\frac{T}{TC} < 0.45$ would be adequate.

2.6.3 Output Current Discontinuity

In a unidirectional chopper, discontinuous current by the inductor being too small will decrease the form factor and will be a further loss in the chopper. The effect of this discontinuity is analysed in reference (27).

However, in a bidirectional chopper discontinuity in the output current does not arise since current flows naturally in both directions. (Assuming both chopping switches are alternatively switched .)

2.6.4 Hysteresis Loss

The ripple current in the inductor subjects the iron core to changes in magnetic flux. This is the cause of eddy current and hysteresis losses in the inductor.

The hysteresis loss is expressed by[41]

$$P_H = K_H V f B_{max}^n$$

where K_H is a constant of the material, V the volume, f the chopping frequency, B max the peak value of flux density and n is the Steinmetz exponent (varies from about 1.5 to 2.0, typically 1.6). Hysteresis loss is independent of the wave shape of the flux.

The maximum ripple current when using pulse width modulation is shown in Section 2.7.3.1 to be

$$\Delta I_{max} \doteq \frac{T}{4.TC} \cdot \frac{E_B}{R_q} = \frac{E_B}{4.f.L} \quad \text{since } TC = \frac{L}{R_q}$$

also

$$B_{max} = \frac{\phi_{max}}{A} = \frac{LI_{max}}{A.N} = \frac{E_B}{4ANf} \qquad (2.27)$$

where A is cross-sectional area and N the number of turns.

The hysteresis loss is thus

$$P_H = K_H V \frac{E_B}{4ANf^{n-1}} \qquad n > 1 \qquad (2.28)$$

Contrary to initial expectations it can be seen that hysteresis losses actually decrease as frequency increases. This is because an increase in frequency decreases the ripple current which decreases B_{max}^n.

2.6.5 Eddy Current Loss

The eddy current loss is expressed by[41]

$$P_E = K_E V (F_F . f . t . B_{max})^2$$

where K_E is a constant of the material, V is the volume, F_F is the form factor of the flux wave, f is the chopping frequency, t is the thickness of the laminations and B_{max} is the peak value of flux density.

Using the value of B_{max} from Equation 2.27

$$P_E = K_E V \left(\frac{F_F . t . E_B}{4 AN}\right)^2 \qquad (2.29)$$

It can be seen that eddy current loss is independent of frequency. To reduce this loss it is important that a laminated core is used with t as small as possible.

2.6.6 Copper Loss

If an external inductor is used, it must have a finite resistance which will be an additional copper loss

$$P_{cu} = I_L^2 R_L$$

2.6.7 Choice of Inductor and Chopping Frequency

There are six factors which affect the choice of inductor and chopping frequency.

(a) Switching loss: (Section 2.4.1) - This increases in proportion to frequency.

(b) Loss owing to output form factor (Section 2.6.2): This favours a low value of $\frac{T}{TC}$, therefore, a high value of frequency and inductance.

(c) Hysteresis loss (Section 2.6.4) - This favours a high chopping frequency and is independent of inductance

(d) Eddy current loss (Section 2.6.5) - This is independent of frequency and inductance

(e) Loss owing to battery current form factor and battery capacitor (Section 4.1.2) - Overall, this favours a high frequency. (Although the effect of frequency on the capacitor is not extensively analysed.)

Switching loss is the only factor that increases with frequency. If switching losses are minimised using snubbers, then the highest practical frequency will be the most efficient.

The optimum inductance is merely to use the armature inductance, thus eliminating the need for additional copper losses. This is true if the frequency is high enough so that (see Section 2.6.2)

$$\frac{T}{TC} = \frac{R}{f.L} < 0.45 \qquad (2.30)$$

2.7 CHOPPING STRATEGIES[26, 3]

2.7.1 Introduction

In a control system, the mark space ratio of the chopper is determined by the required current and motor back EMF (see equation 2.3). The purpose of a chopping strategy is to adjust either the ON time or the frequency or both to achieve the required mark space ratio.

The choice of chopping strategy will affect the size of the ripple current and chopping frequency for any required motor current. The best strategy will give the least ripple and highest frequency (see Section 2.6.7) over the range of operation.

Three commonly used strategies are examined:

1. Pulse-width modulation (PWM)
2. Pulse-frequency modulation (PFM)
3. Two-level control (TLC)

A strategy which resembles TLC is described in reference (42) and a strategy particularly suited to microprocessor implementation is proposed in reference.[43] These two methods are not examined. Each strategy is investigated with respect to ripple vs motor current and frequency vs motor current.

2.7.2 Ripple Current[26]

Using equation 2.2 a formula for the peak ripple current ΔI can be derived.

$$\frac{\Delta I}{IN} = \frac{(1 - e^{-\frac{MT}{TC}})(1 - e^{-(1-M)\frac{T}{TC}})}{(1 - e^{-\frac{T}{TC}})} \qquad (2.31)$$

where $IN = \frac{E_B}{R_q}$ and $M = \frac{T_{ON}}{T}$

By applying Taylor series, a first approximation can be obtained.

$$\frac{\Delta I}{IN} = \frac{T}{TC} M(1 - M) \qquad (2.32)$$

from equation 2.3 . $M = \frac{I_q}{I_N} + \frac{E_q}{E_B}$

therefore $$\frac{\Delta I}{I_N} \doteq \frac{T}{TC}\left(\frac{I_q}{I_N} + \frac{E_q}{E_B}\right)\left(1 - \frac{I_q}{I_N} - \frac{E_q}{E_B}\right) \qquad (2.33)$$

The ripple current, therefore, depends on frequency, time constant, back EMF and the required motor current.

2.7.3 Pulse Width Modulation

The period of the control pulse is fixed and the mark space ratio is varied.

2.7.3.1 Ripple current vs motor current

Using equation 2.33 with $\frac{T}{TC}$ constant, ripple current is plotted against motor current.

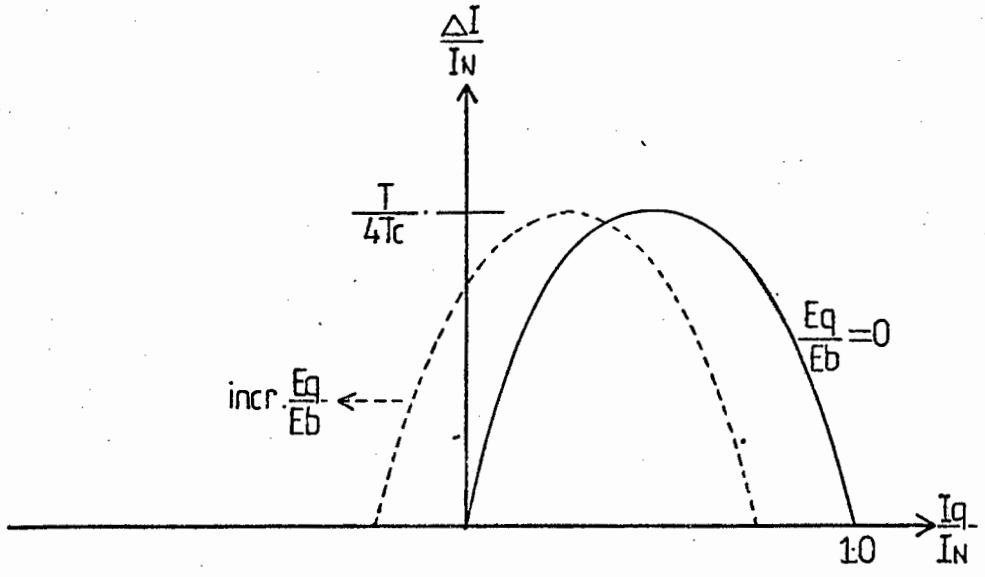

FIGURE 2.25

From this graph it can be seen that the maximum ripple current is

$$\left.\frac{\Delta I}{I_N}\right|_{max} = \frac{T}{4.TC} \qquad (2.34)$$

From equation 2.32 it can be seen that this occurs at $M = 0.5$ (by differentiation).

2.7.3.2 Frequency vs motor current

Frequency is constant and independent of motor current.

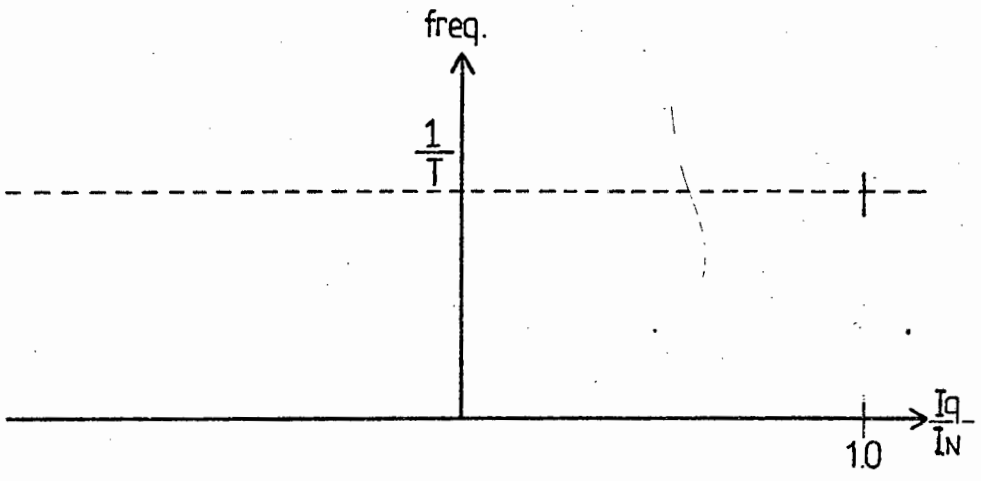

FIGURE 2.26

2.7.4 Pulse Frequency Modulation

In this case, the ON time is fixed and the period adjusted.

2.7.4.1 Ripple current vs motor current

Since $T_{ON} = MT$, equation 2.32 becomes

$$\frac{\Delta I}{I_N} = \frac{T_{ON}}{TC}(1 - M)$$

$$= \frac{T_{ON}}{TC}\left(1 - \frac{I_q}{I_N} - \frac{E_q}{E_B}\right)$$

$$= \frac{T_{ON}}{TC} \left(1 - \frac{I_q}{I_N} - \frac{E_q}{E_B}\right) \qquad (2.35)$$

Therefore, ripple current can be plotted against required motor current.

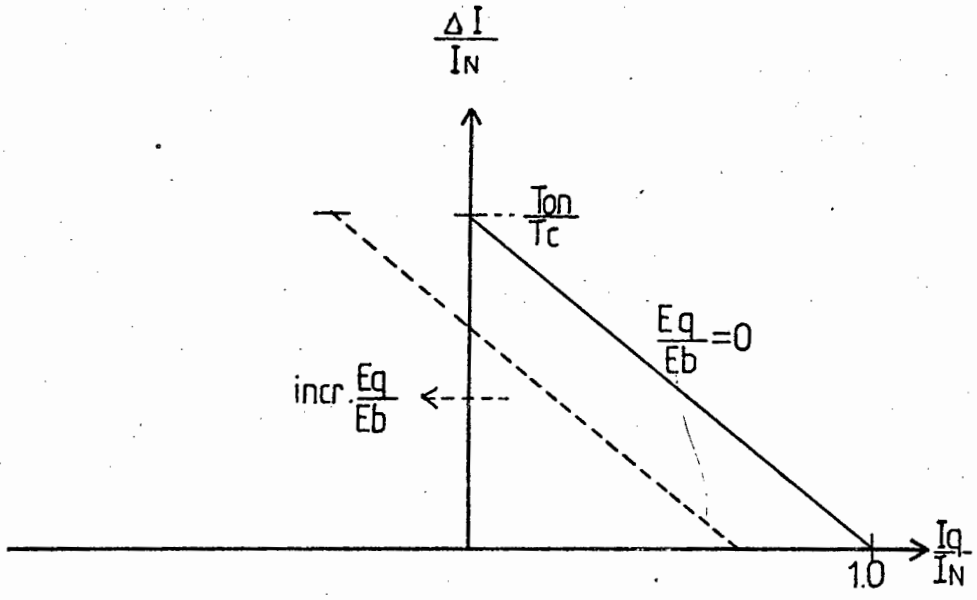

FIGURE 2.27

2.7.4.2 Frequency vs motor current

Frequency increases with motor current.

$$\frac{T_{ON}}{T} = M = \frac{I_q}{I_N} + \frac{E_q}{E_B}$$

Therefore $$f = \frac{1}{T_{ON}} \left(\frac{I_q}{I_N} + \frac{E_q}{E_B}\right) \qquad (2.36)$$

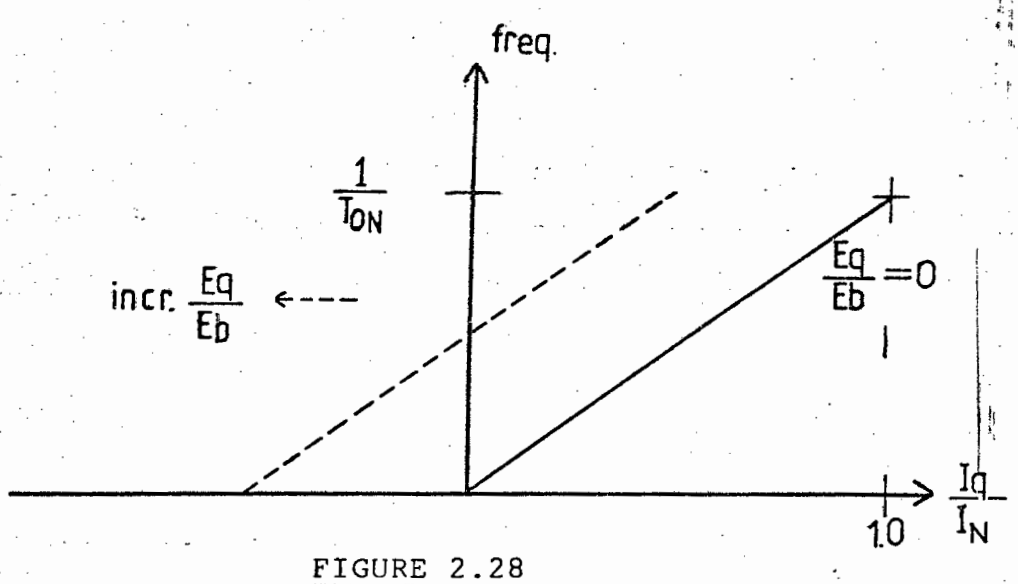

FIGURE 2.28

2.7.5 Two Level Control

In this case two current levels are set a fixed amount ΔI above and below the required average current. The output current is monitored and switching takes place when current reaches these limits. Thus frequency and pulse width are adjusted to maintain the current between the two set levels.

2.7.5.1 Ripple current vs motor current

The ripple current is a constant.

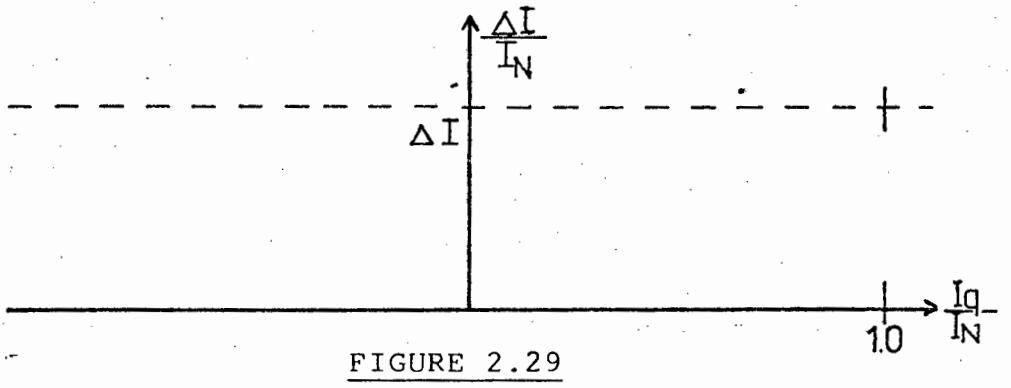

FIGURE 2.29

2.7.5.2 Frequency vs motor current

In equation 2.33 $\frac{\Delta I}{I_N}$ is a constant and by rearranging the formula,

$$f = \frac{1}{TC} \cdot \frac{I_N}{\Delta I} \left(\frac{I_q}{I_N} + \frac{E_q}{E_B}\right) \cdot \left(1 - \frac{I_q}{I_N} - \frac{E_q}{E_B}\right) \qquad (2.37)$$

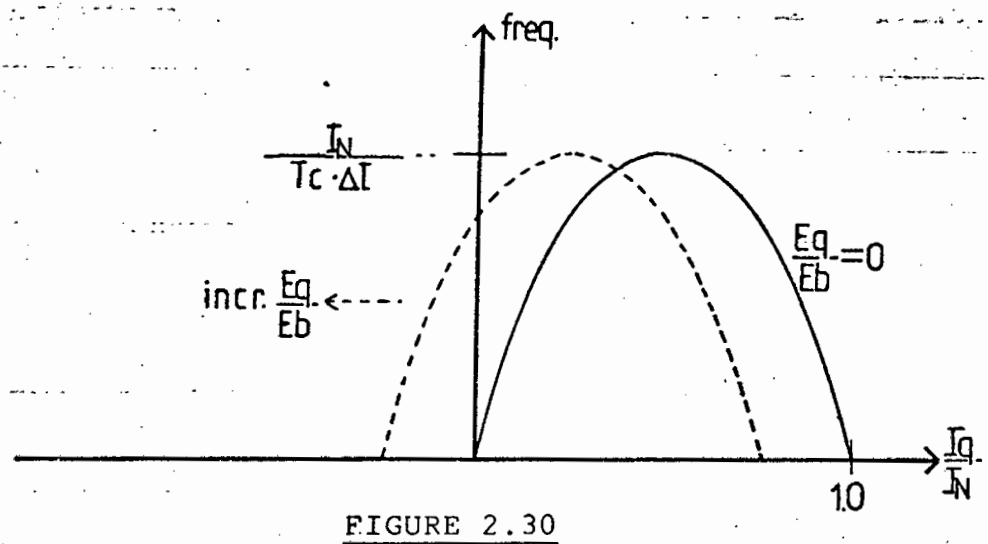

FIGURE 2.30

2.7.6 Selection of Control Strategy

PFM is unattractive since the ripple is high and the frequency is low for small motor currents.

From an efficiency point of view, PWM and TLC are similar.. for PWM the frequency is constant and the ripple parabolic and for TLC the ripple is constant while the frequency is parabolic. Selection between these two methods should be based on ease of implementation.

The effect of the timeconstant is to adjust the height of the parabola in Figures 2.25 and 2.30 and the slope of the graph in Figure 2.27.

CHAPTER 3

THE MOTOR

3.1 INTRODUCTION

In the chopper there is much room for efficiency improvement by careful design. However, the motor is accepted as a given and the only possibility for efficiency improvement is in the appropriate control of field and armature currents which is discussed in Chapter 5.

The purpose of this chapter is to model the motor as accurately as possible so that the system may be analysed by computer to find the control system which produces optimum efficiency. The simplified equations

$$T = K(I_f)I_fI_q \quad \text{and} \quad E_q = K(I_f)I_fW + I_qR_q \tag{3.1}$$

Need to be modified to include all losses.

The losses in the machine are listed below.[44-50]

(i) Electrical losses
- Copper losses in windings
- Brush drop loss

(ii) Iron Losses
- Hysteresis
- Eddy current
- Stray load

(iii) Mechanical losses
- Brush friction
- Bearing friction
- Windage

The machine constant is first measured and then each loss is discussed in general terms. The experimental determination

of the losses in a 3.7 KW 3000 rpm motor are then described. The ratings for the motor are listed in Appendix 4.

Finally, torque and speed equations are proposed and their relative and absolute accuracy discussed.

3.2 THE MACHINE CONSTANT

The machine constant is a constant defining the total torque produced by the motor as function of armature current and the induced back EMF as a function of speed ($K(I_f)$ in equation 3.1). It is affected by the flux saturation of the machine and is, therefore, a function of field current.

3.2.1 Experimental Measurement of $K(I_f)$

With the machine generating there are no I^2R losses on open circuit. Therefore

$$E_q = K(I_f)I_fW \qquad (3.2)$$

And thus $K(I_f)$ can be calculated for various values of I_f. It was shown (within experimental error) that $K(I_f)$ is independent of speed.

Values of open circuit voltage for increasing and then decreasing values of field current are plotted in Figure 3.1. The effect of remnant magnetism and hysteresis on the value of $K(I_f)$ can be seen. Remnant voltage is reflected in the fact that

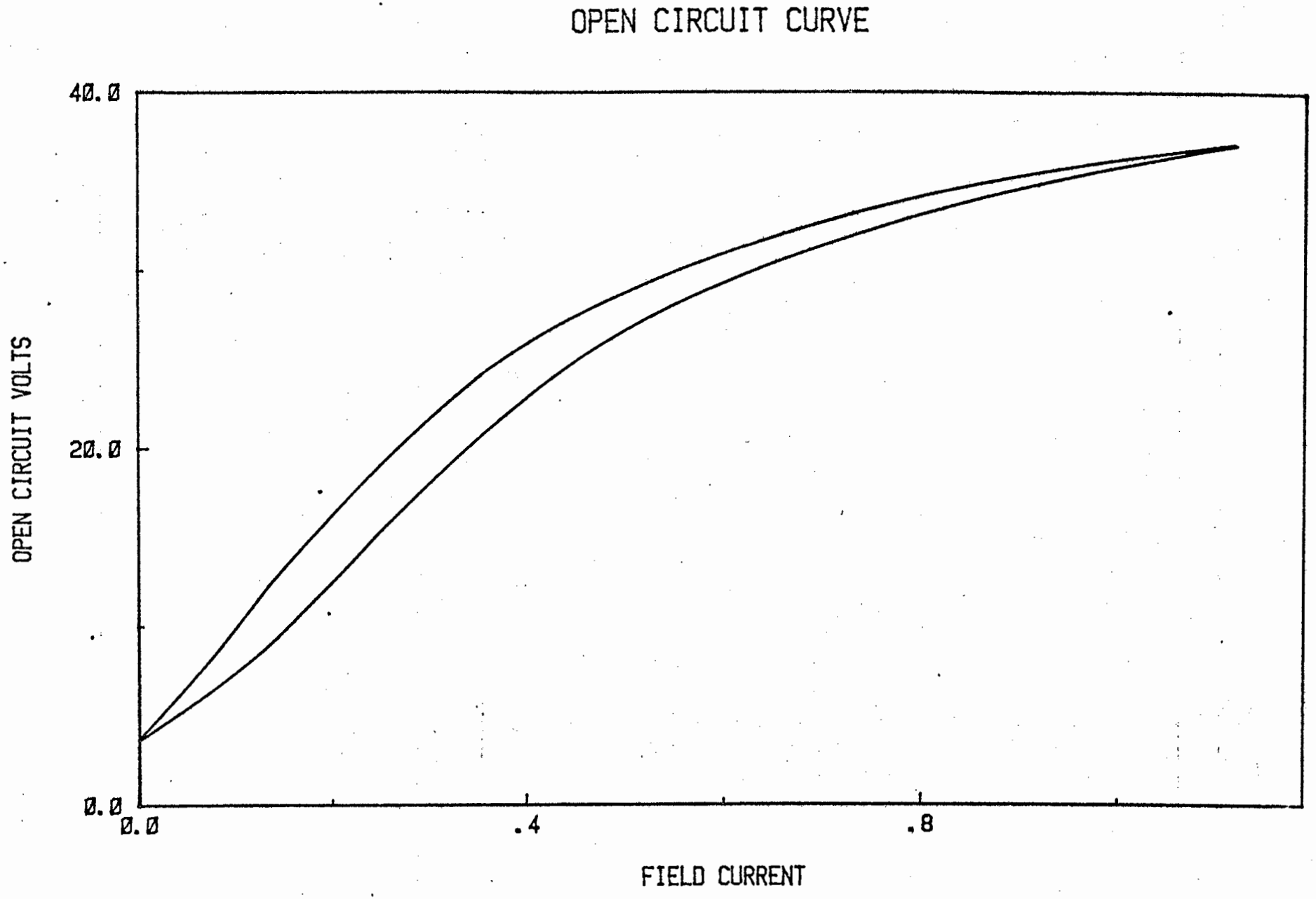
OPEN CIRCUIT CURVE
40.0
20.0
0.0
OPEN CIRCUIT VOLTS
0.0
.4
.8
FIELD CURRENT

Figure 3.1

$$K(0) \neq 0$$

To correct for this, the values of $K(I_f)$ are split into two components

$$K(I_f) = k'(I_f) + \frac{k_{rem}}{I_f}$$

where $$k_{rem} = \frac{V_{remnant}}{W_{measured}}$$

Substituting this into equation 3.2 gives the correct value of E_q at $I_f = 0$. A table of $k'(I_f)$ values and the value of k_{rem} is listed in Appendix 4.

The effect of hysteresis is dependent on the history of field current variation and is very difficult to model when an arbitrary test cycle is selected.

3.2.2 Discussion on Accuracy of $K(I_f)$

Using the procedure in Appendix 5.1, the accuracy of measurement was estimated to be within 3.0% at $I_f = 0.1$ and 0.7% at $I_f = 1.2$.

The error due to hysteresis is over 10% in some instances but this figure is dependent on the history of current variation. This factor is not really an error but rather the actual deviation of the machine parameter.

The machine constant $K(I_f)$ is a set of discrete values rather than a continuous function and this results in a quantisation error. This is virtually eliminated in the final model by regarding the $K(I_f)$ curve as a piecewise linear graph. This is illustrated in Figure 3.2.

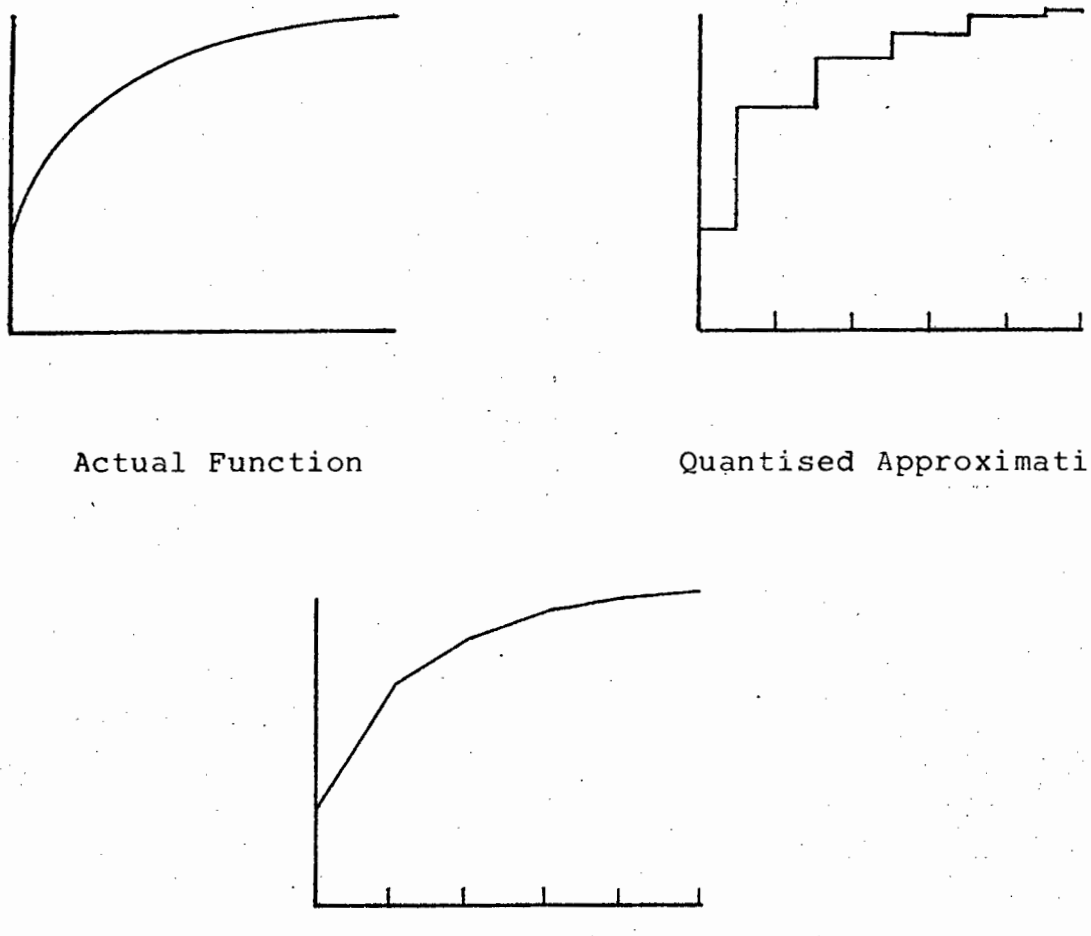

FIGURE 3.2

It is possible that an error could be introduced if the copper oxide layer between the brush and commutator displayed a semi-conductor characteristic. However, no evidence of this was discovered during experimentation.

3.3 COPPER LOSSES

3.3.1 Theory

The resistance in all wires carrying current will cause an I^2R loss. This will occur in the armature, interpole and field windings.

$$P_{cu} = I_q^2 (R_{armature} + R_{interpole}) + I_F^2 R_{field} \qquad (3.3)$$

Resistance is temperature dependent, and if measured at temperature T_1 it can be corrected for temperature T_2 by the equation

$$R_2 = R_1 \left(\frac{K + T_2}{K + T_1}\right) \qquad (3.4)$$

where R_2 is the resistance at T_2. The value of K for copper is 234.5.[41]

Equations describing the heating and cooling of the copper and the iron in the motor are developed in reference (51).

3.3.2 Experimental Measurement

Measurement can be made either by using a Kelvin bridge or by measuring volts and amps.

The latter method was used with rated current so as to test the machine at rated temperature. This is the condition under which the machine would mostly run.

The position of the armature affects the reading of armature resistance. In Figure 3.3 it can be seen that $R_{armature}$ consists of two parallel paths which are not exactly equal, owing to variance in solder resistance, wire thickness and number of turns(r_1). In addition the brush may contact one or two commutator segments and thus a winding may be short circuited (r_2). The solution is to average a set of readings at various armature positions.

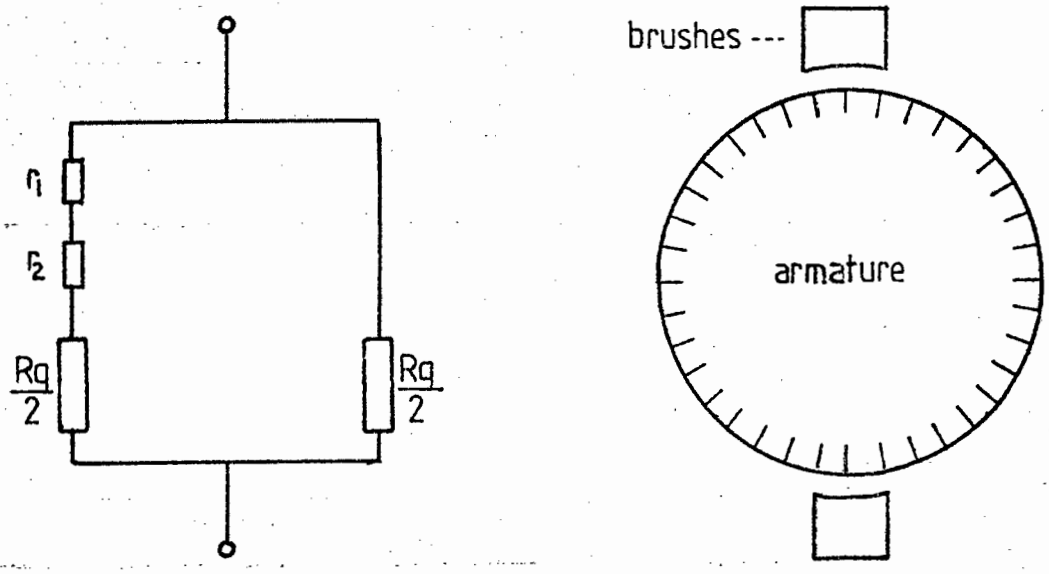

FIGURE 3.3

The test current is fed through the terminals, but the voltage probes must be placed directly on the commutator segments. The interpole resistance is measured with the same current but with voltage between one motor terminal and one brush terminal.

Results are shown in Appendix 4.

3.3.3 Accuracy of Results

Accuracy estimates are based on the procedure described in Appendix 5.1.

The inaccuracy due to errors in reading volts and amps using digital meters is less than 1%. The standard deviation of readings taken at various positions of the armature is 1.6%. Therefore, an inaccuracy of less than 2% can be assumed.

The model used for copper loss was

$$P_{cu} = I_{q}^{2} R_{q} + I_{F}^{2} R_{F} \qquad (3.5)$$

where R_q is the sum of armature and interpole resistance.

Temperature was not included as a variable since the model would become too complex when used on an arbitrary test cycle. Resistance was measured at the final temperature caused by rated current. The resistance values were about 20% lower when measured cold.

3.3.4 Skin Effect

The armature resistance is measured with direct current. However, individual conductors experience a large a.c. component. The equivalent a.c. resistance is greater than the d.c. resistance owing to the skin effect (this reduces the effective area of the conductor by concentrating currents on the circumference).[41]

The skin effect is proportional to the square of the a.c. frequency which is proportional to speed.

This effect is difficult to isolate and measure. The armature may be removed and resistance measured with a.c. The iron surrounding the conductors may also affect the theoretical value.

In this thesis the skin effect was included in the stray load loss term which is also a function of $(I_q.W)^2$. (See Section 3.7.)

3.4 BRUSH LOSSES[50 52]

3.4.1 Brush Voltage Drop

This quantity is very difficult to model accurately since it depends on several variables which are difficult to determine. (These are discussed below.)

3.4.2 Interface Film

A thin layer of copper oxide develops on the surface of the commutator segments and is covered by a thin deposit of graphite from the brush. Water vapour and an oxygen film provide boundary lubrication (hence the short brush life at high altitudes). The film is influenced by the water content of the air and ambient air pressure.

The effect of this layer is difficult to model but is important in the commutation process.

3.4.3 Temperature

Increased temperature affects the interface film by hastening the oxidation of copper.

Carbon shows a negative temperature coefficient and the brush coefficient of friction decreases with a temperature greater than 80°C. Losses thus decrease as temperature increases.[41]

3.4.4 Brush Pressure

This is an important factor for both brush losses and brush wear. An optimum value for each grade of brush is obtained. A value which is too low will increase electrical losses and a value which is too high will increase mechanical wear.

3.4.5 Other Factors

The brush drop is also dependent on area, grade of brush and the elasticity of the brush.

3.4.6 Experimental Measurement

The voltage drop was measured between the commutator segments beneath the brush and the armature terminal for various values of current with the armature stationary. The graph in Figure 3.4 was obtained.

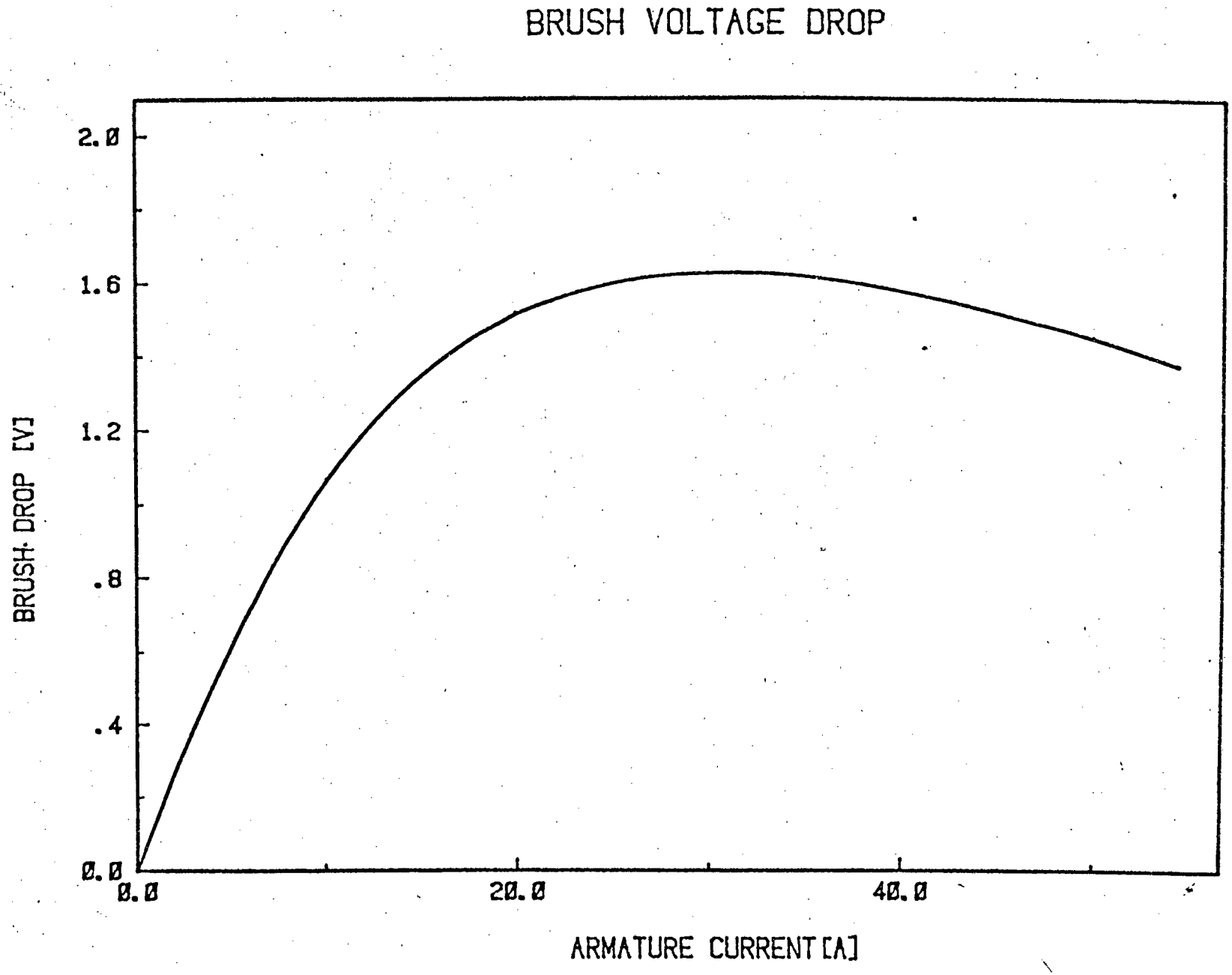
BRUSH VOLTAGE DROP
2.0
1.6
1.2
.8
.4
0.0
BRUSH-DROP [V]
0.0
20.0
40.0
ARMATURE CURRENT [A]

FIGURE 3.4

A constant value of $V_B = 1.4\ V$ was used in the model. This will be inaccurate at low values of current.

The accuracy of this approximation is difficult to determine since conditions change greatly during rotation (especially the interface film).

3.5 NO LOAD IRON LOSSES

Hysteresis and eddy current losses are present since the machine iron is subjected to variations of magnetic flux.

3.5.1 Hysteresis Loss[44]

Hysteresis loss is dependent on the range and frequency of flux variation

$$P_H = K_H f B_{max}^n$$

where K_H is a constant, f is the frequency, B_{max} is the magnitude of flux density variation and n is the Steinmetz exponent.

The frequency f is proportional to speed W and the flux density B is proportional to field current I_f.

Therefore $$P_H = K W I_f^n \qquad (3.6)$$

3.5.2 Eddy Current Loss[44]

A loss is caused by I^2R losses in the core owing to induced eddy currents.

$$P_E = K_E f^2 t^2 B^2_{max}$$

Frequency is proportional to speed W and B_{max} is proportional to I_f, and t is the lamination thickness.

therefore, $$P_E = K W^2 I_f^2 \qquad (3.7)$$

Leakage flux causes eddy currents to be induced in the armature end plates. Losses in the end plates and sides of the slots are greater since leakage flux is normal to the plane of lamination. Burrs on the edge of stampings increase eddy losses since laminations then have an electrical link.

A ripple is superimposed on the main flux wave owing to variations in magnetic reluctance caused by the slots. This ripple moves with respect to the pole face and thus induces eddy currents in the pole. The frequency of the ripple is the product of motor frequency and number of slots. In this thesis a 3000 rpm motor was used with 36 slots; giving a ripple frequency of 1.8 KHz.

From a design point of view, the losses in the armature teeth should be considered separately from the rest of the core losses since flux distributions are greatly different.[49]

3.5.3 Experimental Determination of Constants

From an efficiency point of view, there is no need to separate hysteresis and eddy current losses. The total no load iron loss can be determined using the apparatus shown in Figure 3.5.

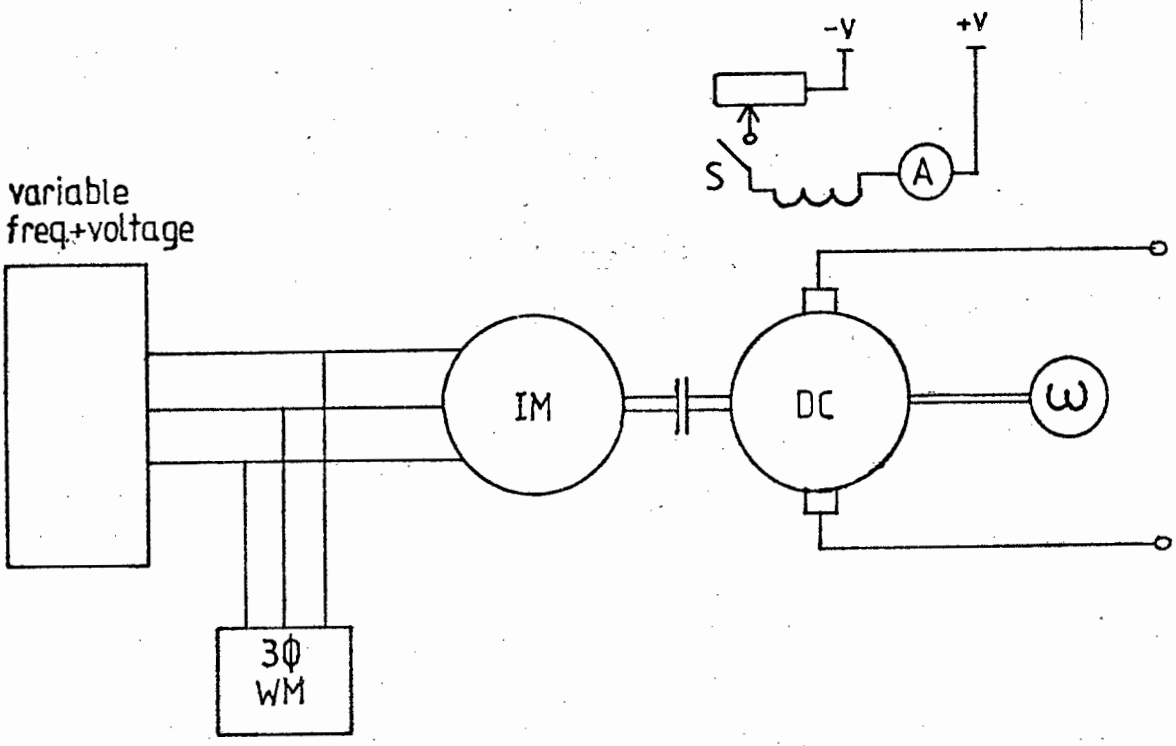

FIGURE 3.5

The difference in input power measured with 'S' open and closed is a measure of total no load loss at the corresponding speed and field current values. Readings were taken for a series of I_f values keeping W constant and then W was varied keeping I_f constant. The results in Figures 3.6 and 3.7 were obtained.

Using a dc driving motor, it was found that the input current

varied with time even when running at exactly the same speed and torque. The cause of this effect was not established but may possibly be linked to the brush voltage characteristic. An ac induction motor with a more complicated speed controller was, therefore, required.

3.5.4 Discussion on Results

An expression of the form

$$P_I = k_H W I_f + k_E W^2 I_f \qquad (3.8)$$

with values of k_H and k_E listed in Appendix 4, accurately, fitted the results obtained. The effect of I_f was not as pronounced as expected by the theory.

Probable errors were estimated using the procedure in Appendix 5.1, and are discussed in three sections.

(i) **Measuring instruments** - At low values of field current the difference in power readings is small. Thus an inaccuracy of 14% can be expected at low I_f and this reduces to 1% at full I_f. . While 14% seems high, it represents an absolute value of 1.5 watts which is not excessive.

(ii) **Speed** - This is measured to within 0.5% using a digital timer and an opto-sensor on the motor shaft.

(iii) The relation between iron loss and speed was investi-

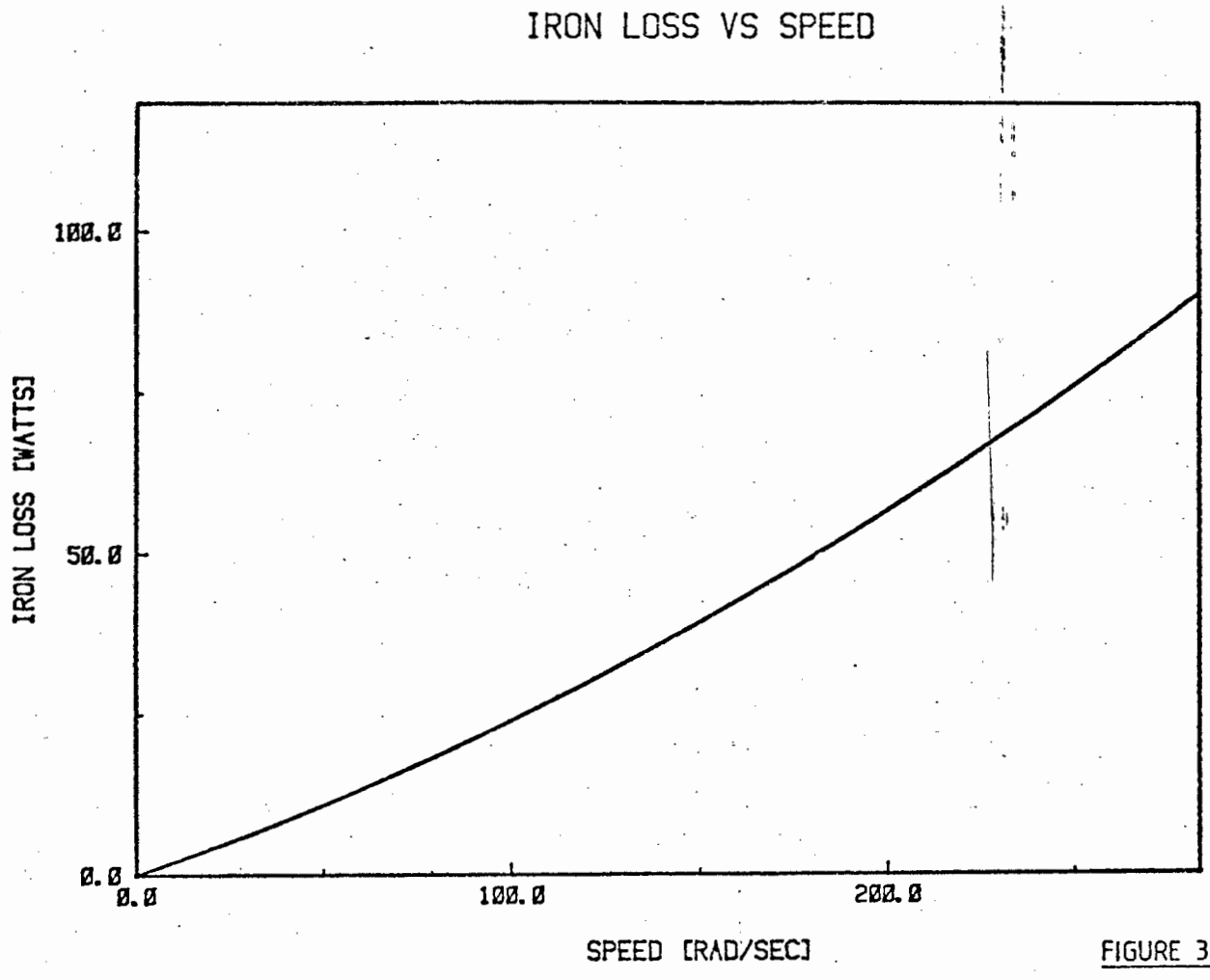

FIGURE 3.6

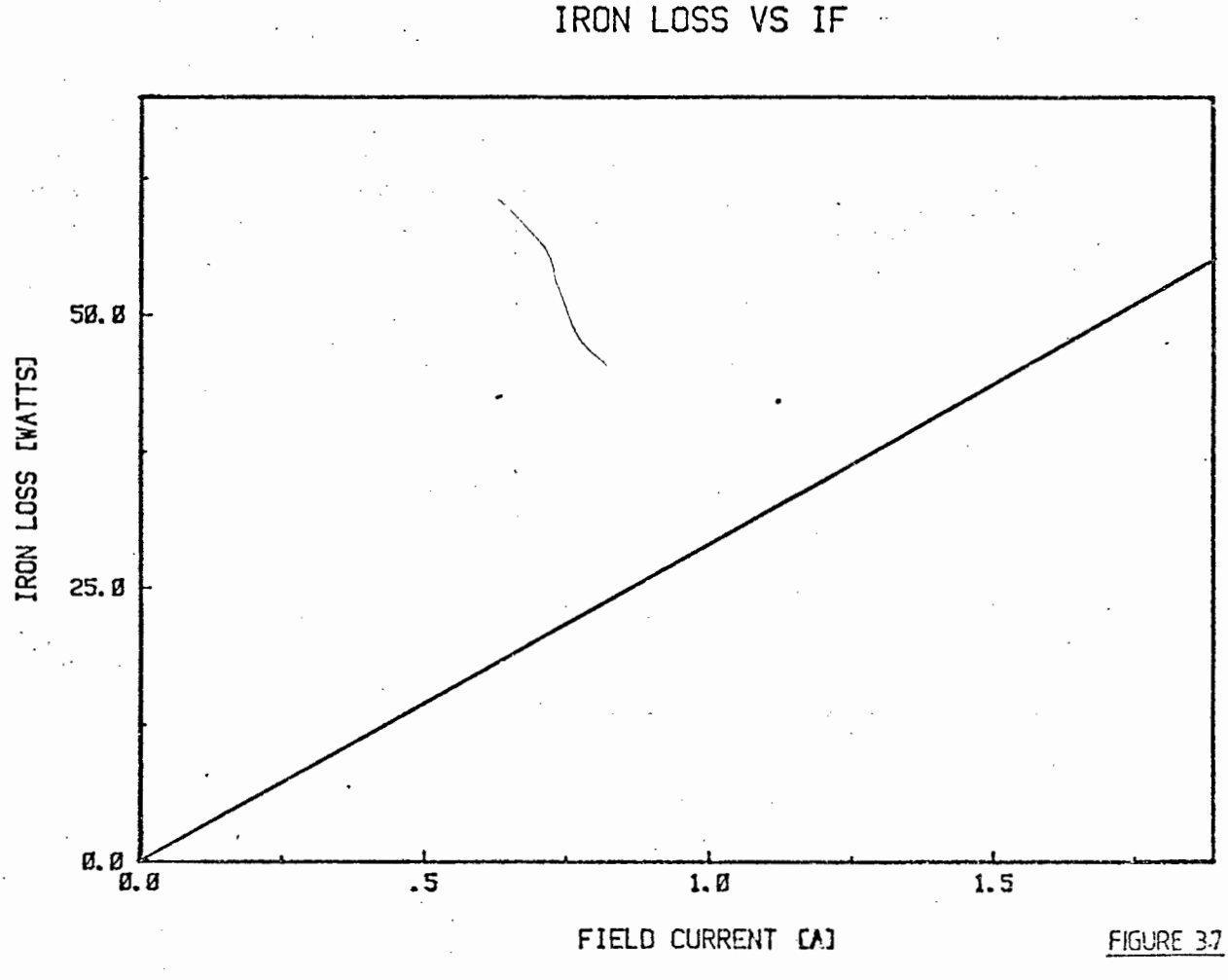

FIGURE 3.7

gated at a constant field current of 1.5 amps. This was taken to be representative for other values of field current. The accuracy of the model may, therefore, decrease at other values of I_f.

Similarly, the relation between iron loss and field current was investigated at a constant speed of 1500 rpm.

A random set of test values ($I_f \neq 1.5$ amps and $W \neq 1500$ rpm), showed that the model was always within 5 watts of the results obtained.

3.6 MECHANICAL LOSSES[47, 48]

The mechanical loss has three main components.

3.6.1 Brush Friction Loss

An expression for brush friction loss is

$$P_{Br} = k\,u\,P\,A\,V_c \qquad (3.9)$$

where k is a constant, u is the coefficient of friction, P is the brush pressure, A is the contact area and V_c is the peripheral speed of the commutator (which is proportional to motor speed W).

The coefficient of friction varies with brush grade, surface speed and brush face temperature.

3.6.2 Bearing Friction Loss

An expression for journal or sleeve bearing friction loss is

$$P_B = k D L V_b^{1.5} \tag{3.10}$$

where k is constant, D is the diameter of the shaft, L is the length of the bearing and V_b is peripheral shaft speed in the bearing.

The losses in roller and ball bearings are too variable to be expressed in a simple formula. However, using well lubricated roller or ball bearings these losses are so small compared to windage and brush friction that they may be regarded as negligible.

3.6.3 Windage

Windage loss depends on many variable factors. For a large motor with no fan, a rough expression is

$$P_W = kA V_A^2 \tag{3.11}$$

where k is a constant, A is the armature surface area and V_A is the armature surface speed.

For smaller motors with a fan (as used in this thesis) an approximate expression is

$$P_W = k V_A^n \tag{3.12}$$

where n varies between 2 and 3.

Mechanical losses are all largely independent of load.

3.6.4 Experimental Determination of Mechanical Losses

Mechanical losses were all measured together. Brush losses may be separated if required by measuring the difference in input power of a driving motor with the brushes up and then down.

Similar apparatus was used to that used in determining no load iron loss (see Figure 3.5). No field current was supplied and power readings were taken with the two motors alternatively coupled and uncoupled, the difference being the windage and friction loss. Readings were taken at various speeds and the results are shown in Figure 3.8.

The expression,

$$P_{Wf} = k_{f1}W^2 + k_{f2}W \qquad (3.13)$$

with k_{f1} and k_{f2} listed in Appendix 4, accurately reflects the results obtained.

Using the procedure in Appendix 5.1, together with the rated accuracy of the wattmeter, the inaccuracy of the above model is 15% at speed 600 rpm and 2% at speed 3000 rpm. While 15% seems high, it represents an absolute value of 1.7 watts which is not excessive.

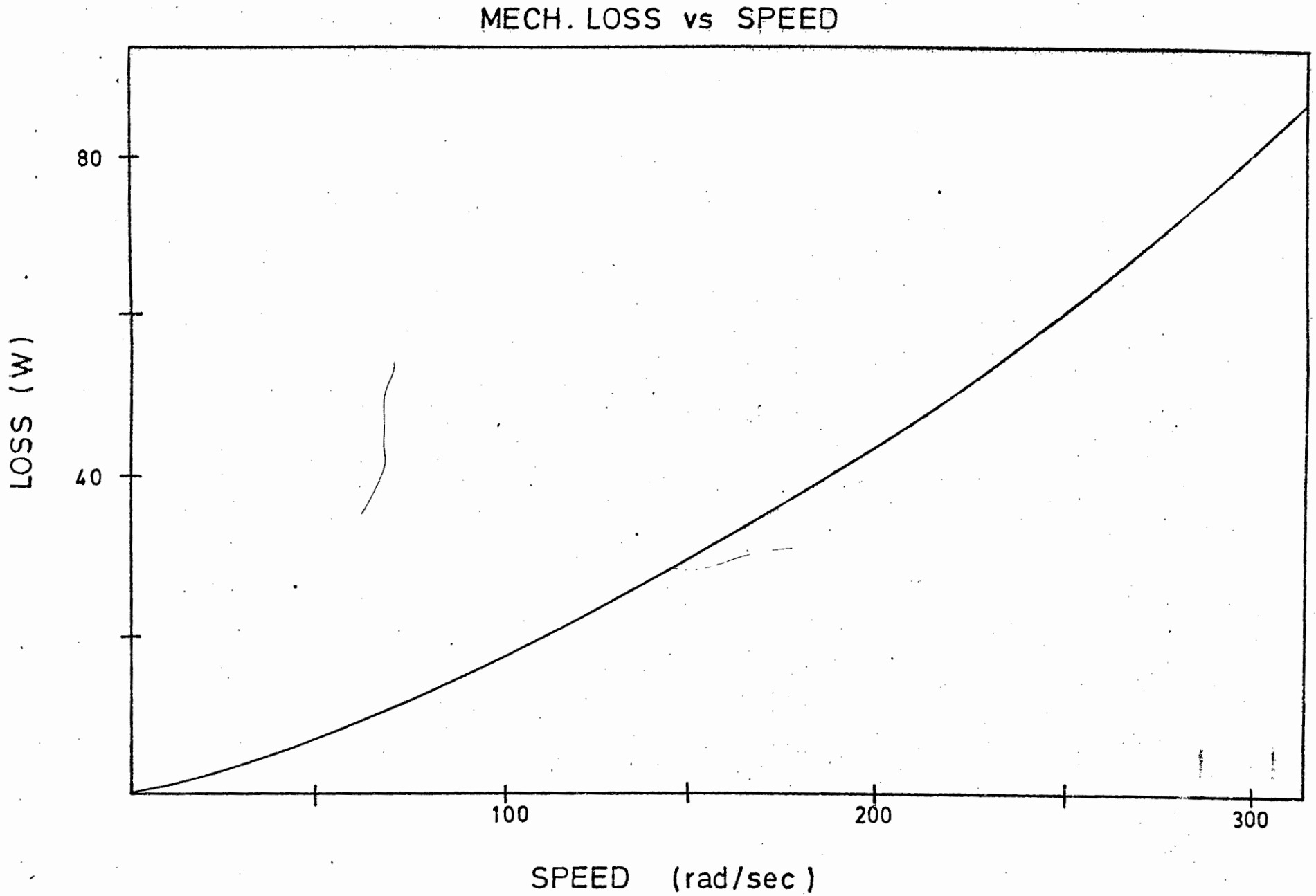

fig 3-8

3.7 STRAY LOAD LOSSES

Additional losses exist which are dependent on load.

3.7.1 Distortion of Flux Wave

The effect of armature reaction causes the space distribution of the flux density to change with load. Iron losses, therefore, increase because the peak flux density in the teeth and core is increased. Eddy current losses caused by flux leakage also increases with load.

3.7.2 Experimental Measurement of Stray Load Losses

For the purpose of modelling the motor, all additional losses (i.e. other than those already measured) are included in this term. The main contributions will, however, be from flux wave distortion and the skin effect factor (Section 3.3.4).

The stray load loss was measured by the difference in torque predicted using losses already measured and the torque actually measured in practice.

The accurate measurement of torque is extremely difficult. In this thesis a sophisticated strain gauge torque transducer (HBM type T2/20 Nm)[53] and instrumentation amplifier (HBM) was used. Torques of up to 20 Nm could be measured to an accuracy of 0.5% of full load.

Values of stray load loss were measured for various armature

current values with speed fixed at 1500 rpm. Armature current was then fixed at 19.5 amps and stray load loss was measured for various values of speed. The graphs in Figures 3.9 and 3.10 were thus obtained.

The following expression was found to fit the data obtained

$$T_s = k_s W I_q^2$$

therefore, $$P_s = k_s W^2 I_q^2 \qquad (3.14)$$

and k_s is listed in Appendix 4.

3.7.3 Discussion on Results

The torque meter was able to read to an accuracy of 0.1 Nm. The limitation being in the ability to initially zero the amplifier owing to static friction in the torque transducer bearings.

This error is very significant when expressed as a percentage of the stray load loss. The above equation is, therefore, not very helpful in predicting the absolute value of the stray load loss.

However, for the purpose of this thesis, the relative value of stray load loss (or the shape of the curve in Figure 3.9 and 3.10) is a helpful function to know, especially when the model is being used to predict the relative change in efficiency

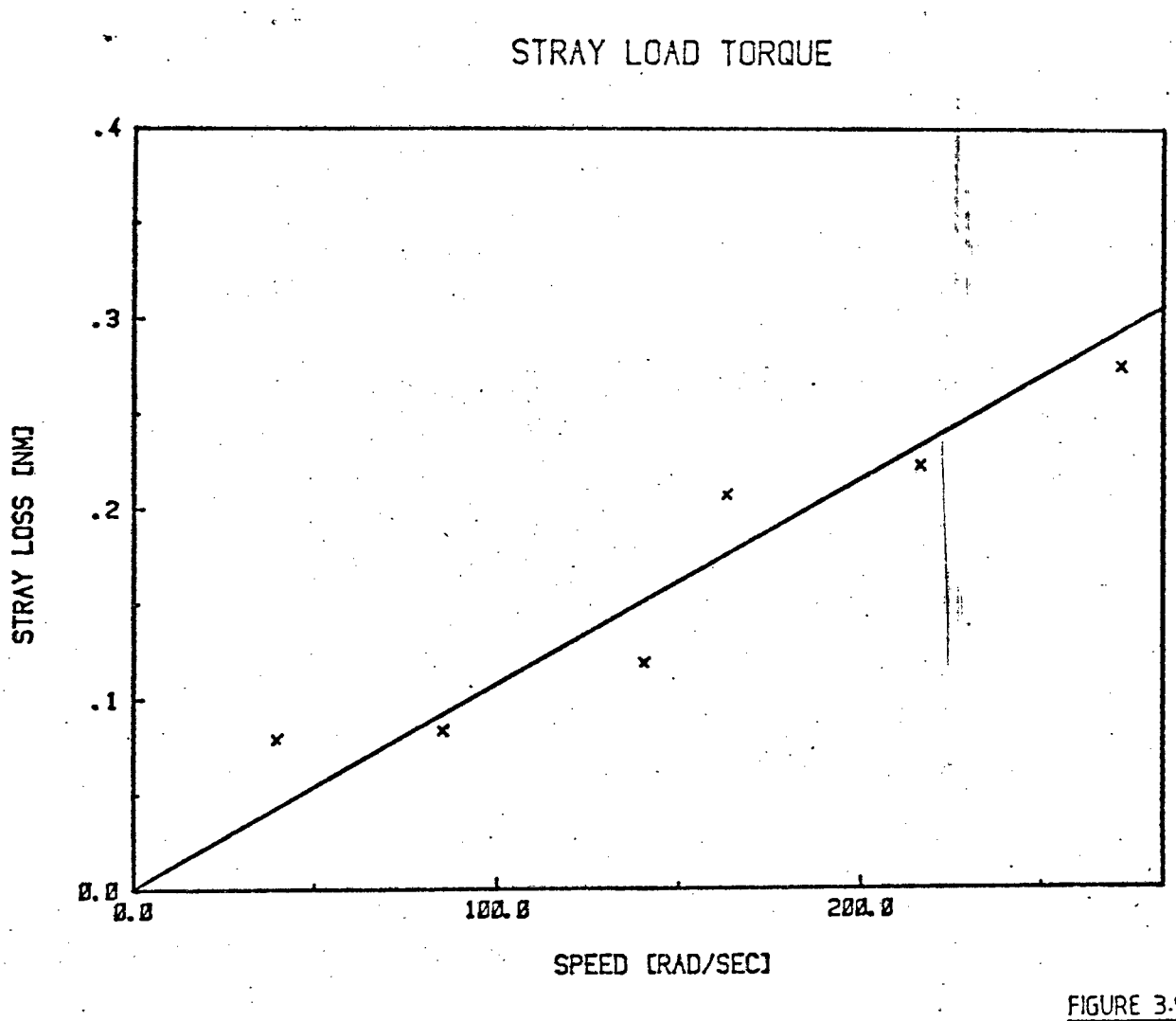

FIGURE 3.9

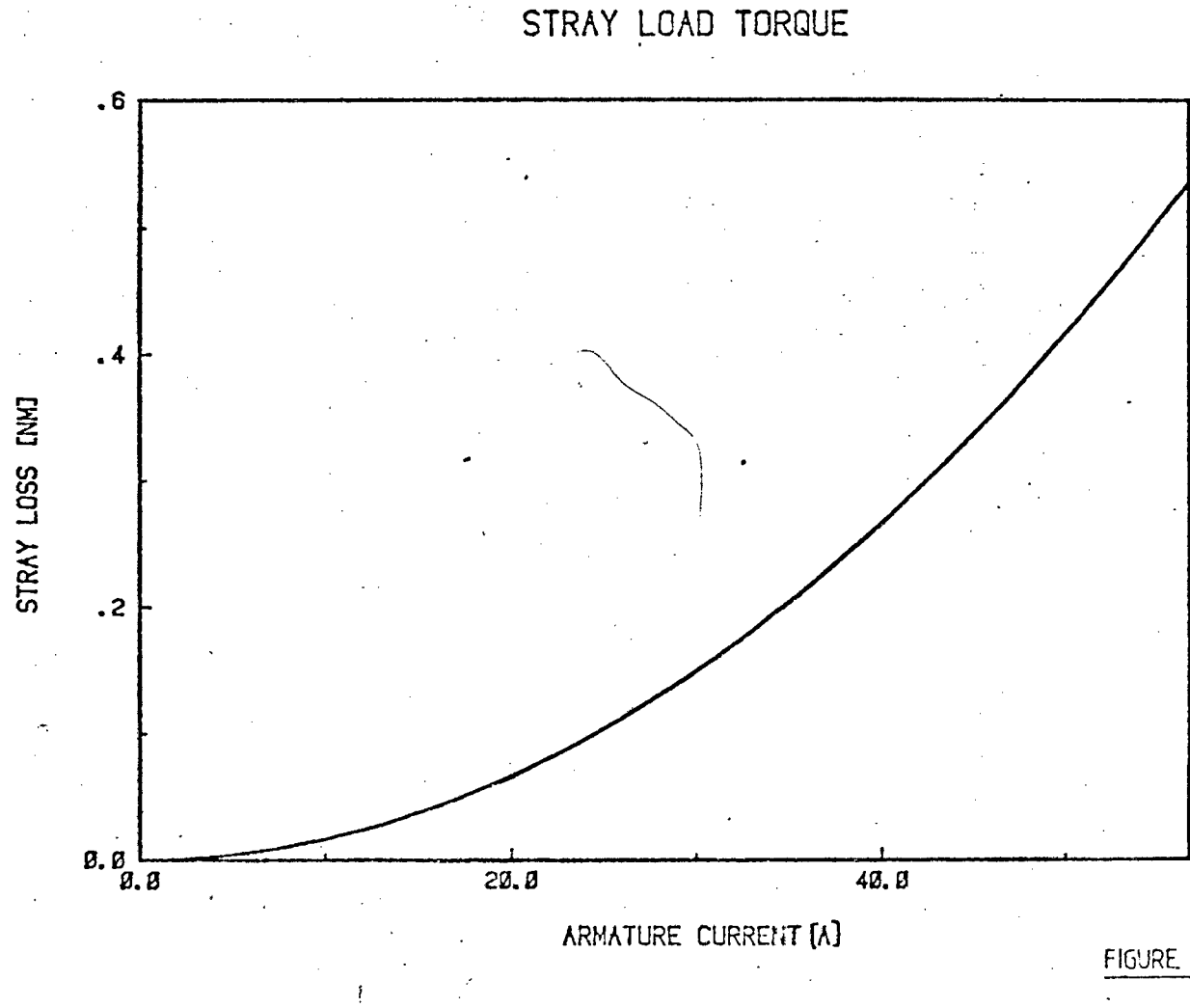

FIGURE 3.10

with certain criteria. The relative accuracy of the torque meter is greater by a factor of ten since it does not depend on static bearing friction or calibration factor.

The formula used to calculate torque owing to stray load loss is

$$T_s = T_{measured} - K(I_f)I_fI_q - k$$

where k is the sum of all calculated losses. The inaccuracies of the constants used to calculate T_s should be kept in mind, especially $K(I_f)$.

3.8 CONCLUSION

The electrical losses will have the effect of reducing armature voltage and the mechanical losses will reduce the effective output torque. Stray losses are also assumed to reduce output torque. This is not strictly accurate since it includes skin effect losses. However, this will not affect the calculation of efficiency which is the purpose of the model. The basic machine equations, therefore, become

$$E_q = K(I_f)I_fW + I_qR_q + S.V_B \qquad (3.15)$$

where S = +1 for a motor

S = -1 for a generator

and $$T = K(I_f)I_fI_q - (k_{f1}W + k_{f2}) - (k_H + k_EW)I_f - (K_sW\ I_q^2) \qquad (3.16)$$

(These equations may be compared to those used in reference (20).) Using these, efficiency can be calculated.

$$N = \left[\frac{E_q I_q + I_F^2 R_F}{TW}\right] - S \qquad (3.17)$$

For regeneration the efficiency is defined as the battery power divided by the shaft power (TW) and hence the need for the S term in (3.17).

It should be noted that other methods of efficiency measurement are available such as the Kapp-Hobkinson test[45, 46] which employ two identical motors. However, this is inadequate for the purpose of this thesis since the motors will have different field current settings and, therefore, iron losses will not be equivalent.

The inaccuracy of the model proposed in predicting torque is analysed in Appendix 5 and is shown to be less than 2% (except at very low torques).

CHAPTER 4

THE BATTERY

INTRODUCTION

Battery losses have a significant effect on the efficiency of the system and therefore cannot be neglected.

4.1 DISCONTINUITY IN BATTERY CURRENT

4.1.1 Current Discontinuity Over A Standard Test Cycle

Over a typical operational cycle the current will not be smooth, and there will be periods of peak current demand. If a method of smoothing the current was available (thus reducing I_{Brms} to I_{Bave}), an efficiency improvement would result.

The battery losses over a standard electric vehicle test cycle (Figure 5.21) are thus shown in Appendix 6.2 to be reduced by a factor of 2. This amounts to an overall efficiency saving of about 3% (see Table 1.1).

This peak load smoothing can be achieved using a flywheel coupled to the motor shaft. Alternatively a Nickel Cadmium battery connected across the terminals of the lead acid battery could be used. This has a lower internal resistance and should be large enough to supply the peaks of power demand.

The practicalities of this method of efficiency improvement were not fully explored in this thesis and hold possibilities for further development.

4.1.2 Battery Losses With Chopped Current[54]

The battery is initially assumed to be an internal EMF E_B, with an internal series resistance, R_B. The loss in the battery is

$$P_B = I^2_{B(RMS)} \cdot R_B \qquad (4.1)$$

If the battery current is rectangular with a mark space ratio M, then the RMS current will be greater than the average.[55] It is shown in Appendix 6.1 that

$$I_{B(RMS)} = \frac{1}{\sqrt{M}} I_{B(ave)}$$

therefore

$$P_B = \frac{1}{M} I^2_{B(ave)} \cdot R_B \qquad (4.2)$$

Thus the effect of discontinuous current is to increase battery losses by a factor $\frac{1}{M}$. Methods of reducing this extra loss are discussed in the following sections.

4.1.3 Capacitive Filtering[32]

Using a large enough capacitor at a high enough chopping frequency, the battery current can be smoothed to a continuous value I_{Bave} and the RMS battery current is reduced to $I_{B(ave)}$ with a resulting reduction in battery loss. However, there will be an additional loss in the capacitor owing to its equivalent resistance (ESR) R_c.

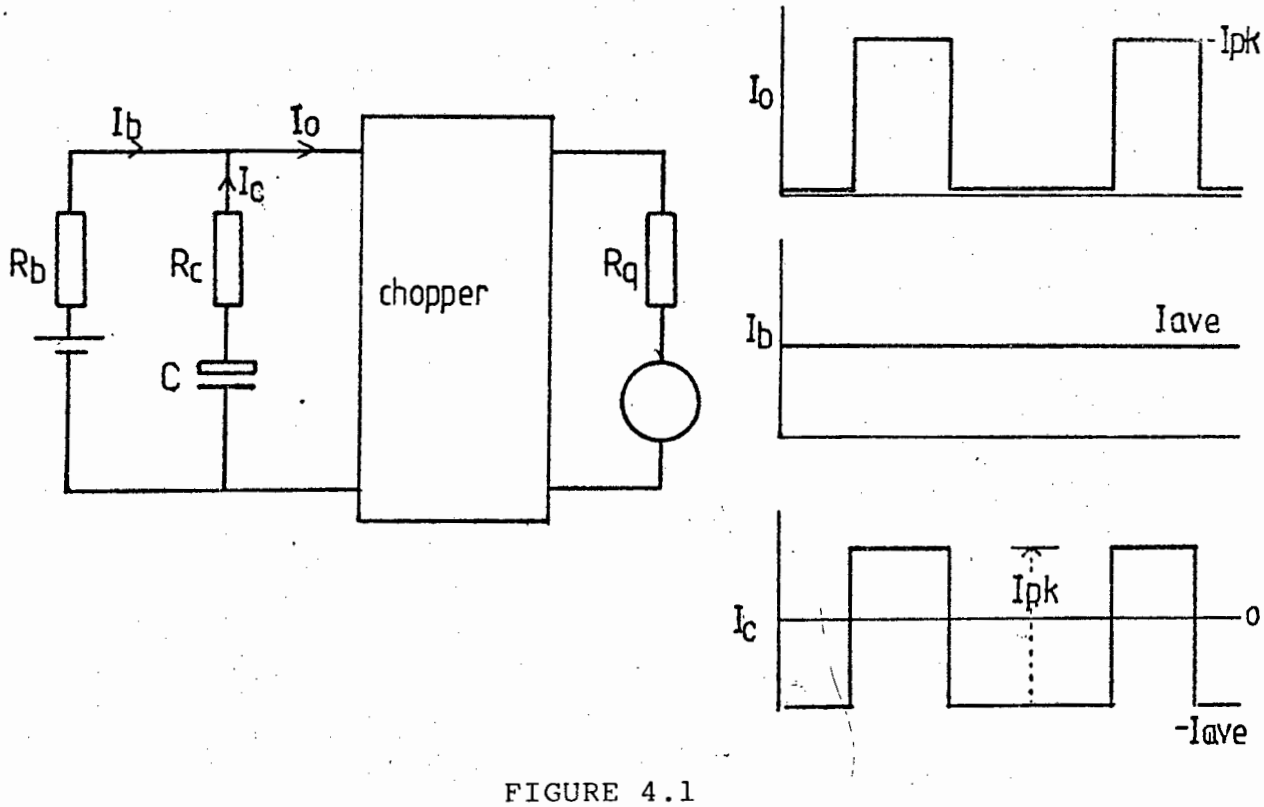

FIGURE 4.1

It is shown in Appendix 6.3 that

$$I_{c(rms)} = \sqrt{\frac{1 - M}{M}}\, I_{B(ave)}$$

The total power loss with a capacitor is thus

$$P_{BC} = I^2_{B(ave)} \cdot R_B + \left(\frac{1 - M}{M}\right) I^2_{B(ave)} R_c$$

Thus using a capacitor represents a net per unit saving

$$\frac{P_{BC}}{P_B} = M + \frac{R_C}{R_B}(1 - M) \qquad (4.4)$$

For example if $R_C/R_B = 0.1$, losses will be reduced by 46% at M = 0.4 by using a capacitor. In this thesis, two 14 000 μF capacitors were connected in parallel, each having an ESR rating of 0.025Ω and 25 A ripple current.

For a more accurate analysis of efficiency saving the behaviour of the capacitor at high frequencies should be considered. It is also shown in Section 4.2 that the approximation of losses using an internal battery resistance is simplistic.

4.1.4 Sequentially Switched Choppers[18, 19]

Battery losses can also be reduced by using a chopper with several switches operating sequentially.[18, 19] The circuit in Figure 4.3 using two switches is compared with a normal single switch chopper.

In Figure 4.3 (overleaf) each switch carries half the current and they are switched alternately with a phase difference of $\frac{T}{2}$. It is shown in Appendix 6.1 that

$$I_{B(RMS)} = \frac{1}{\sqrt{2\sqrt{M}}} I_{B(ave)} \qquad (4.5)$$

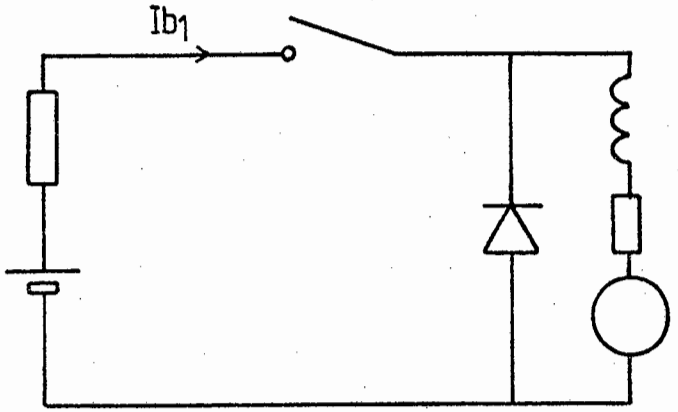

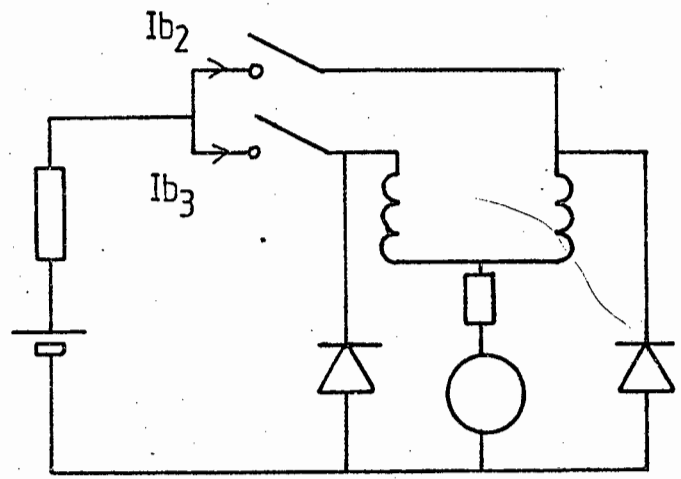

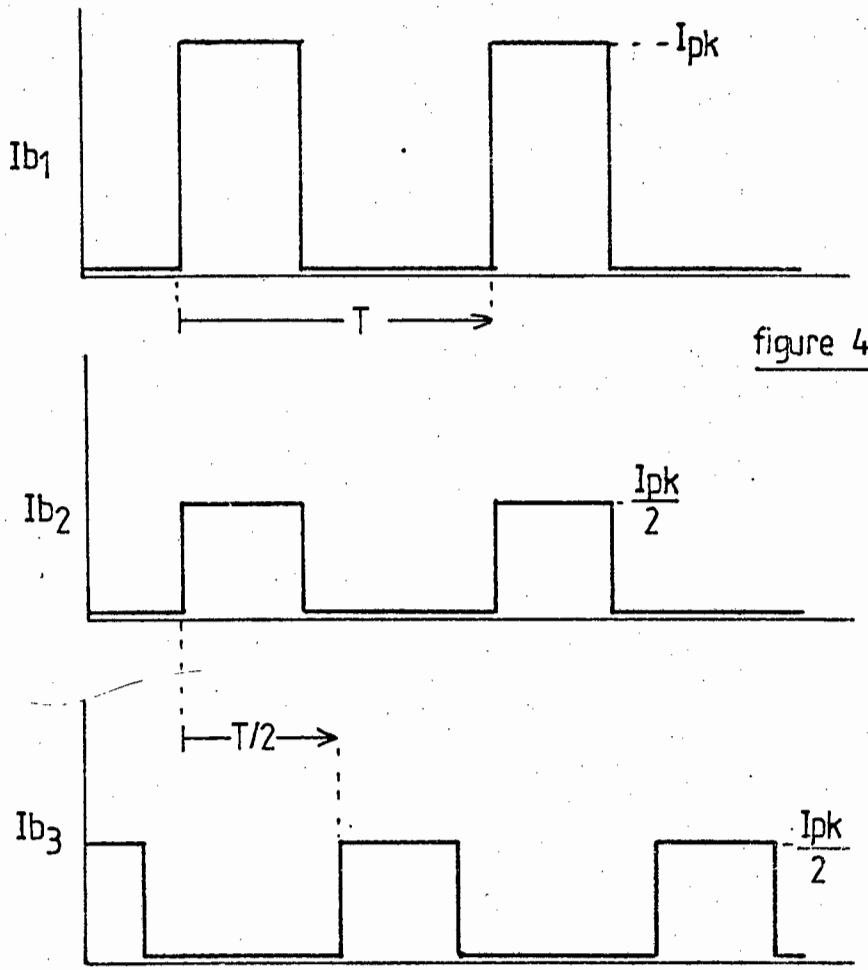

figure 4.2

figure 4.3

Comparing this with equation 4.2 it can be seen that losses are halved under all conditions. This reduction in losses will only be realised when M is less than 0.5. However, this may represent a significant portion of a typical drive cycle.
The main disadvantage of this system is the need for extra inductors.

4.1.5 Battery Switching[19]

Several batteries are usually used. Battery losses can be reduced by paralleling batteries when a lower voltage would be sufficient.

In a lossless chopper

$$I_{B(ave)} = MI_{q(ave)} \tag{4.6}$$

also, for any required motor current I_q, M can be found from equation

$$M = \frac{I_q R_q + E_q}{E_B} \tag{4.7}$$

Substituting 4.6 and 4.7 into 4.2

$$P_B = (I_q R_q + E_q) I_q^2 \cdot \frac{R_B}{E_B} \tag{4.8}$$

Switching out series cells when not required reduces R_B and E_B by the same factor resulting in no net efficiency improvement.

Switching N cells from series to parallel connection, reduces

E_B by N and R_B by N^2, resulting in a net reduction in losses by a factor of $\frac{1}{N}$. This analysis is based on Equation 4.2 and is thus only valid if a capacitive filter is not used.

4.1.6 Cúk Convertor[29]

The Cúk convertor is discussed in Section 2.1.6 and more extensively in reference (29). Here the author claims conversion efficiencies which are substantially greater than those of conventional design. Presumably this is because of the continuous nature of the input current which reduces $I_{B(RMS)}$ to $I_{B(ave)}$ and thus results in a reduction of losses (as in Section 4.1.3).

However, it should be noted that the capacitor in Figure 2.5 carries full load current and, therefore, has the same losses as the capacitor in Section 4.1.3. Thus from an efficiency point of view, it is unlikely that the Cúk converter will be much more efficient than a standard circuit with a capacitive input filter.

4.2 MORE ACCURATE MODEL OF BATTERY[56, 57]

In most applications, the battery is modelled by an internal EMF and a series resistance. However, for a detailed analysis of efficiency this is insufficient. The battery is in itself a very complicated electro-chemical system and is difficult to model accurately.

4.2.1 Equivalent Circuit

A simplified equivalent circuit for a lead acid battery is proposed in reference (57) and is shown in Figure 4.4.

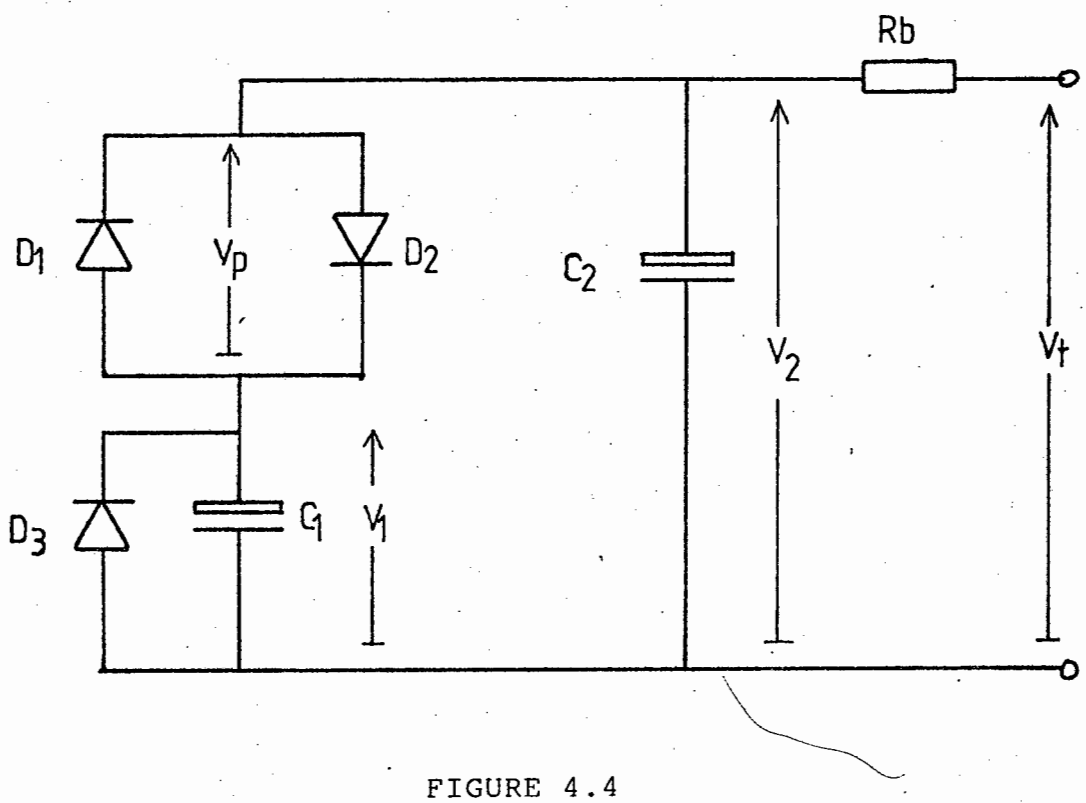

FIGURE 4.4

The basic electrochemical storage element is represented by an extremely large capacitor C_1. The value of this capacitance is of the order of 10^5 farads for a 300 Ah cell.[56] R_B is the ohmic resistance in the plate conduction path (electrolyte and plates).[58] The diode D_3 represents shunt dissipation and accounts for over-charge current losses. This amounts to a loss of battery capacity of about 1% per day[59] and can usually be neglected.

An important effect in the battery is known as activation polarisation[59, 60, 61] which causes a terminal voltage drop with load. This is due to the effect of the double layer at

the surface of the electrodes. The polarisation voltage, V_p is logarithmically related to current. It can, therefore, be modelled as a pair of back-to-front diodes D_1 and D_2.

In addition the double layer also has the effect of storing charge. This can be represented by a capacitor C_2 which is of the order of 100 Farads/Ah for a 300 Ah cell. It should be noted the activation polarisation has the effect of decreasing terminal voltage on discharge and increasing it on charge.

4.2.2 Experimental Verification

From tests on a 72 V lead acid set, the model was shown to be fairly accurate. Using a digital storage oscilloscope the graph in Figure 4.5 was obtained for a step current load.

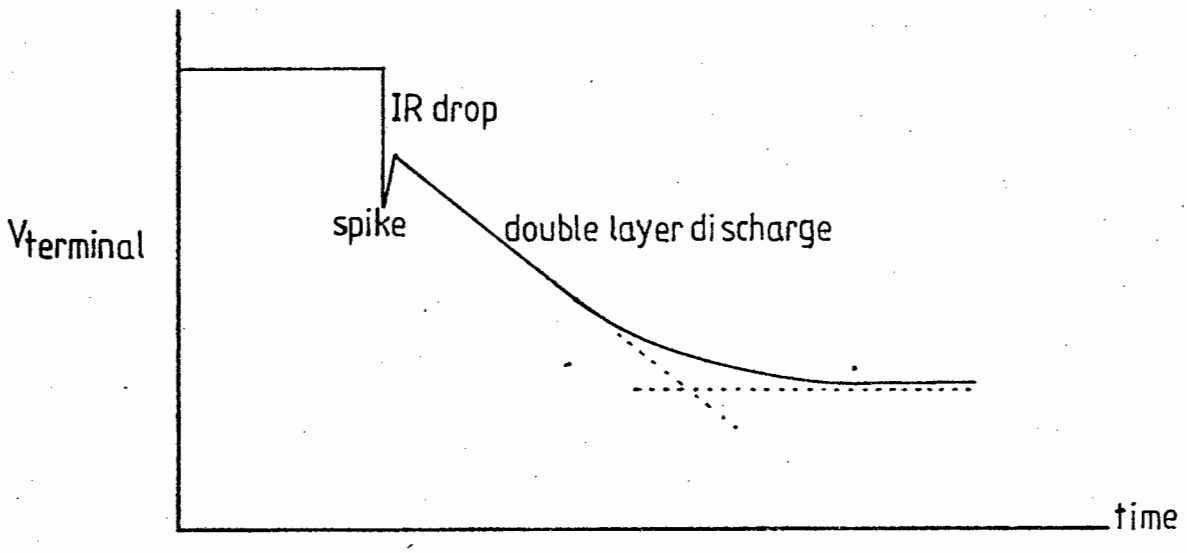

FIGURE 4.5

The presence of R_B was confirmed by the instantaneous voltage drop IR_B, and its value was calcualted from this. A brief voltage spike caused by lead inductance was observed at switch on.

The subsequent linear voltage drop is assumed to be the discharge of the double layer capacitance C_2. By inspecting the circuit diagram we see that C_2 initially supplies all the current as it discharges. When the voltage difference between the capacitors is sufficiently high, current is forced through the diode D_1 and C_1 begins to supply current. This is observed as a tailing off of terminal voltage to a constant value. When the voltage is observed over a long period, the slow discharge of C_1 can be seen.

When the load was disconnected, C_2 was charged via C_1. As V_2 approached V_1, the charge current decreased logarithmically. C_2 eventually charges infinitely close to V_1 but it takes a long time, about 20 times longer than when it is discharged. This observation helped to verify the proposed model.

4.2.3 Battery Losses

There are two main sources of loss. The I^2R loss in R_B and the loss caused by the voltage drop V_p across the diodes D_1 and D_2. The latter is calculated as the product of voltage V_p and current.

4.2.4 Experimental Results

All tests were performed with a specific gravity of 1.26 per cell and an electrolyte temperature of 20°C.

4.2.4.1 Battery resistance

The instantaneous voltage drop was measured and the value of R_B listed in Appendix 4 was obtained. The inaccuracies due to the instruments was about 1%. Results were taken at different times and under a variety of circumstances. The standard deviation from the value quoted above was 18%.

4.2.4.2 Activation potential V_p

It is assumed that the open circuit terminal voltage V_t will eventually settle at a value equal to V_1 in Figure 4.4. A step load is applied. Sufficient time is allowed for C_2 to discharge (see Figure 4.5) but not sufficient for the discharge of C_1. At this stage

$$V_t = V_1 - V_p - IR_B$$

From this, V_p can be calculated since the other variables are known. The results obtained are shown in Figure 4.6.

It is shown in reference (57) that the voltage and current relationship in the diode pair D_1, D_2 can be reduced to

$$V_p = \frac{1}{K_{B1}} \operatorname{Sinh}^{-1} \left(\frac{I}{K_{B2}}\right) \qquad (4.9)$$

This function with values of K_{B1} and K_{B2} listed in Appendix 4, described the experimentally obtained results to within 4%.

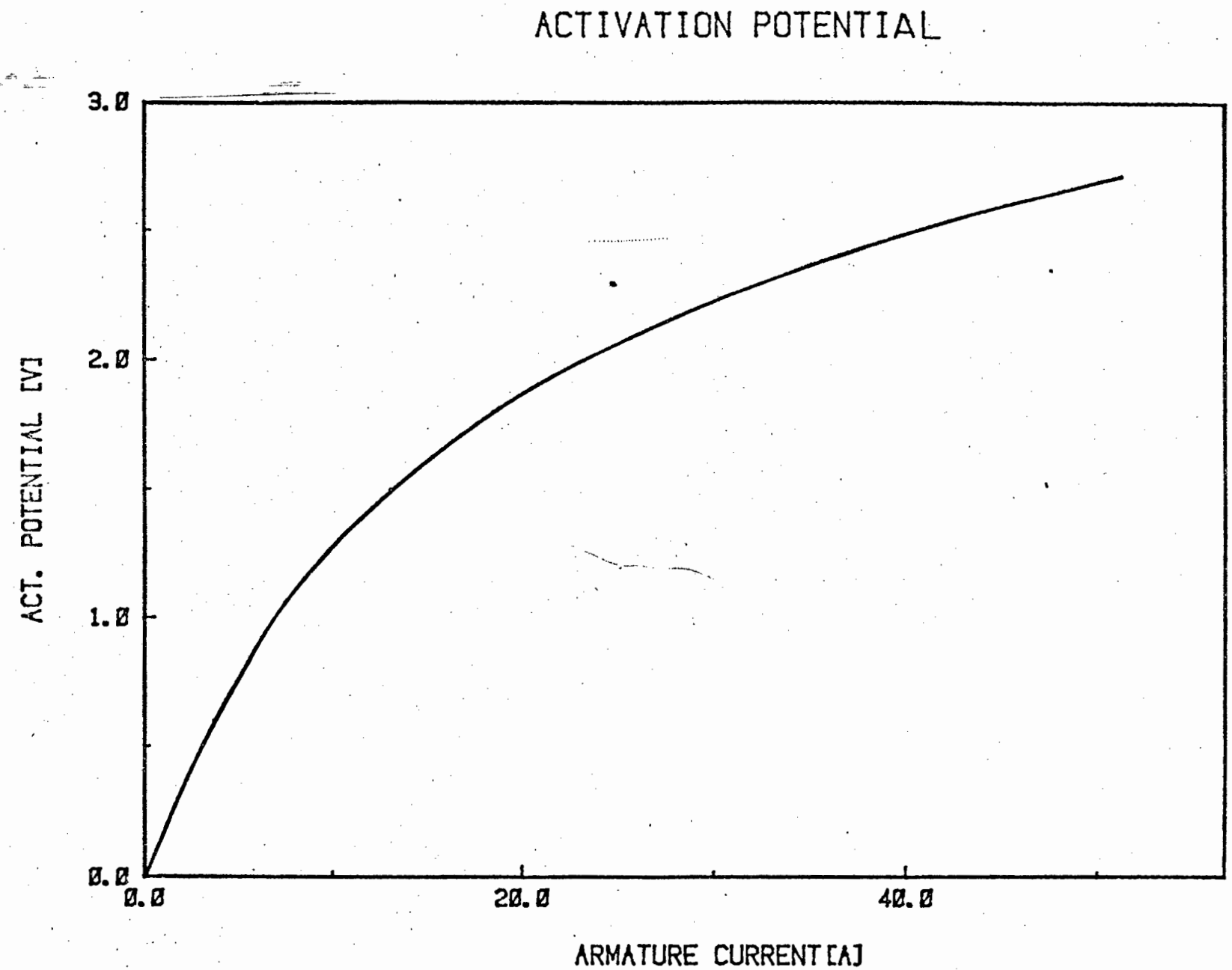
ACTIVATION POTENTIAL
3.0
2.0
1.0
0.0
ACT. POTENTIAL [V]
0.0
20.0
40.0
ARMATURE CURRENT [A]

FIGURE 4.6

The standard deviation between results at various times was approximately 15%.

4.2.4.3 Discussion on results

The electro-chemical system of a battery is difficult to model accurately. Variables such as specific gravity, temperature and ageing[59] affect the results. For example, the variation of battery resistance with discharge is demonstrated in reference (59).

If more detailed studies were undertaken as to the effect of the temperature and specific gravity, it may be possible to incorporate these factors in a feedback system.[62] However, to predict them for any given situation is very difficult since they are determined by the history of the system.

It is important to note that equation 4.9, assumes that voltages have settled to a steady state. This is valid if the smoothing capacitor suggested in Section 4.1.2 is used. The results are not valid for discontinuous current. The relatively long time constants, especially when the load current is reduced, are not included in the model.

CHAPTER 5

RELATIONSHIP BETWEEN FIELD AND ARMATURE CURRENTS

5.1 INTRODUCTION

To control a DC motor, both armature current and field current may be controlled to produce the required torque and speed. This section will investigate the effect on efficiency of being able to control both these variables.

If no saturation or losses occur, the torque equation becomes

$$T = KI_f I_q \tag{5.1}$$

Clearly there are many combinations of I_f and I_q which will produce the same required torque. The question is how the selection of this combination affects efficiency. Alternatively, is there a constant combination of I_f and I_q which consistently provides the optimum efficiency.

5.1.1 Control Equation

The relationship between I_f and I_q can be arbitrarily defined. However, most control systems relate these two variables by a control equation

$$I_f = f(I_q)$$

The control equations of three special cases of this general rule are listed below.

shunt motor	I_f = constant
series motor	I_f = constant x I_q

$$\text{field controlled motor} \quad I_f = \left(\frac{E_B}{KW}\right) - \left(\frac{R_q}{KW}\right) I_q$$

The series motor condition can be simulated on a separately excited motor using the appropriate control equation to control field and armature currents.[11, 63] The field control equation is derived from

$$V_{terminal} = KI_f W + I_q R_q$$

and $V_{terminal}$ is kept constant at the battery voltage E_B.

The effect of the different control equations are illustrated in Figure 5.1. The machine equation for any given torque T is plotted

$$I_f = \frac{T}{K} \times \frac{1}{I_q}$$

For any given torque the I_f, I_q combination must be somewhere on this curve. The control equation determines the particular point on this curve for various torque values. Therefore, the I_f, I_q operating point is determined by the intercept between the motor torque equation and the control equation.

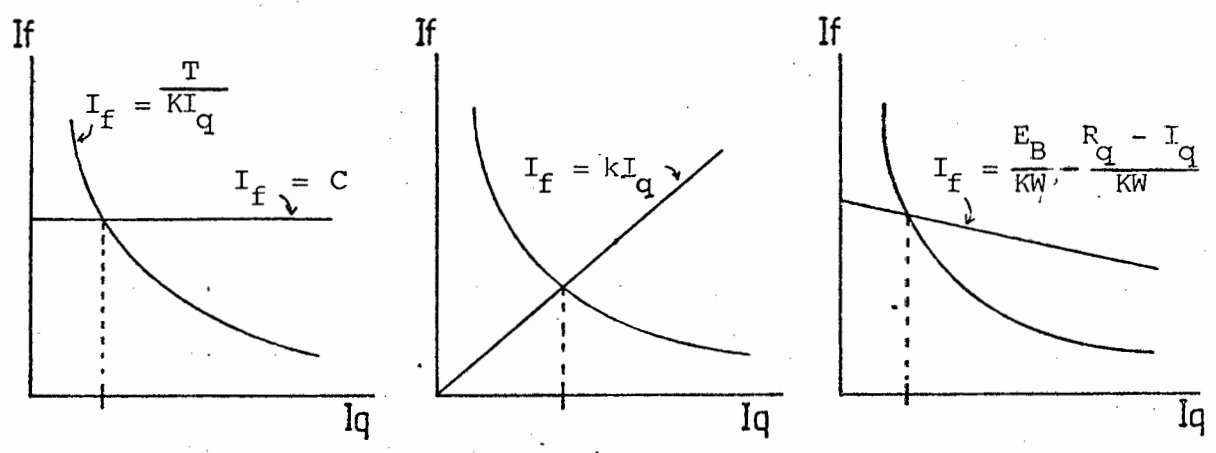

FIGURE 5.1

If a microprocessor is used to control field and armature currents, it is possible for any other control equation to be implemented. The problem is, therefore, to find the appropriate control equation which provides optimum efficiency under all conditions and also to find to what extent the above special cases differ from the optimum efficiency.

5.1.2 Torque Speed Characteristics

Fixing the control equation relating field and armature currents also determines the shape of the open loop torque speed characteristic.

This is illustrated with the torque speed characteristics of the three special cases described above, shown in Figures 5.2 to 5.4. The actual torque-speed operating point is found from the intercept between these curves and the T-W characteristic of the load.

In a shunt motor:

$$T = k' I_q$$

$$W = \frac{V_t - I_q R_q}{k'}$$

therefore

$$T = \left(\frac{k' E_B}{R_q}\right) - \left(\frac{k'^2}{R_q}\right) W$$

(See Figure 5.2 overleaf.)

In a series motor:

$$T = k' I_q^2$$

$$W = \frac{V_t - I_q R_q}{k' I_q}$$

therefore

$$T = k' \left(\frac{V_t}{k'W + R_q}\right)^2$$

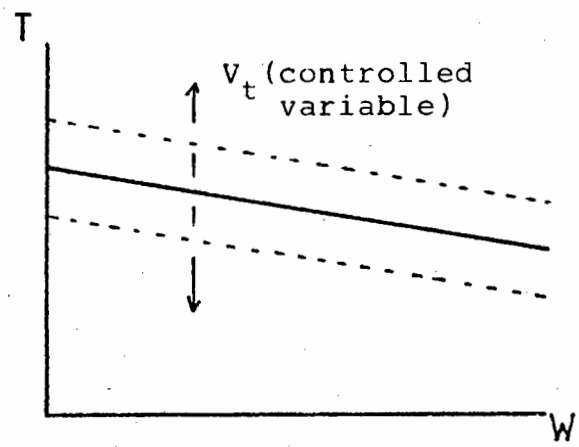

FIGURE 5.2

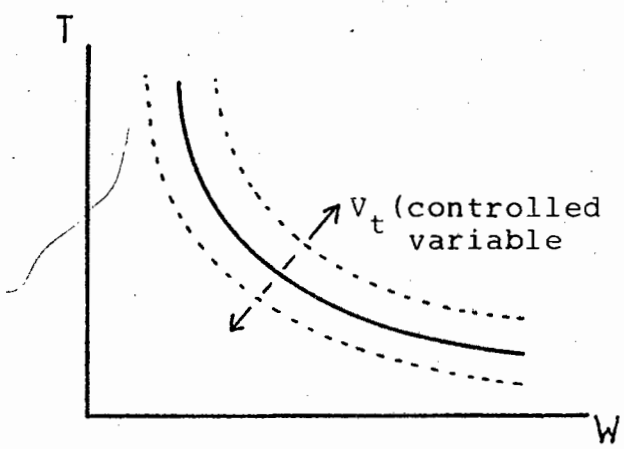

FIGURE 5.3

In a field controlled motor:

$$I_f = \frac{E_B}{KW} - \frac{R_q}{KW} \cdot I_q$$

$$T = K I_f I_q$$

therefore

$$T = \left(\frac{K I_f E_B}{R_q}\right) - \left(\frac{K^2 I_f^2}{R_q}\right) W$$

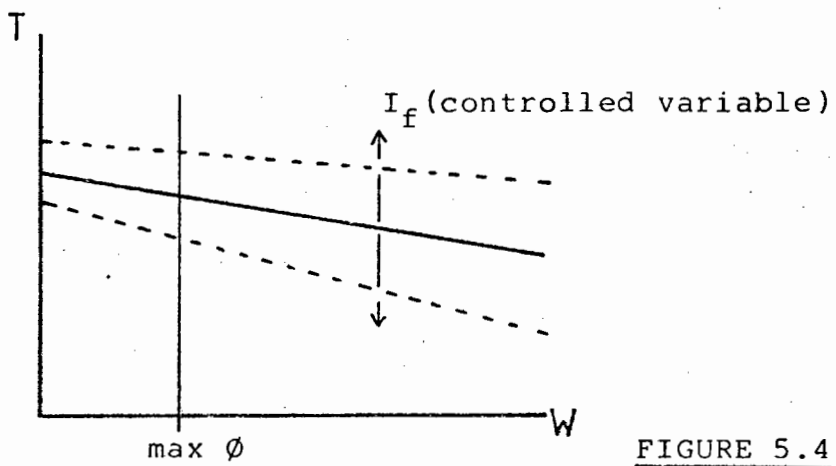

FIGURE 5.4

It should be noted that the curves in Figures 5.2 to 5.4 describe what happens to speed if the load torque is changed and the control variable is kept constant. However, in a feedback system the control variable is continuously adjusted to maintain the desired torque speed operating point. Therefore in a feedback system, any required overall torque speed characteristic may be implemented by the controller. For example a constant torque (Figure 5.5) or constant power characteristic (Figure 5.6) may be realised.

An attractive torque speed characteristic combines those in Figures 5.5 and 5.6 in Figure 5.7. This has the advantage of using maximum power available and giving maximum speed range. It is easily implemented if a microprocessor is used. An interesting idea is described in reference (11) which determines maximum power, not from the ratings but using temperature feedback from sensors near the field and armature.

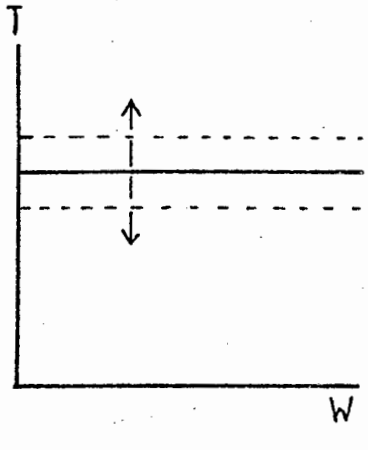

FIGURE 5.5

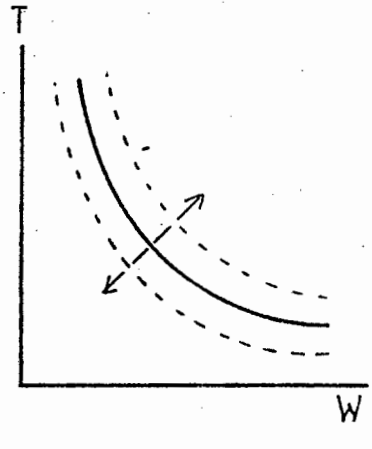

FIGURE 5.6

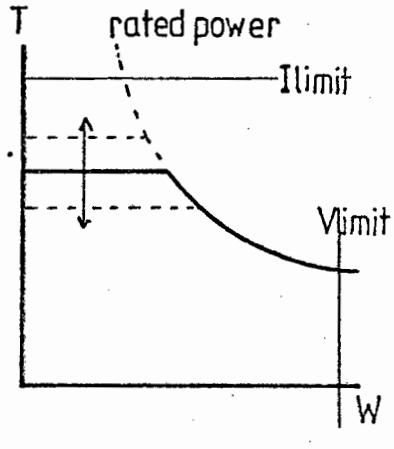

FIGURE 5.7

It has been shown in this section that the choice of control equation affects the open loop torque speed characteristic. The efficiency is not affected by the torque speed characteristic since the operating point is set by the required speed and the load on the motor. The torque speed characteristic merely describes what happens to the speed as load increases and this is overridden by the controller characteristic. It is true, however, that the efficiency at a given torque speed operating point is dependent on the choice of control equation.

5.1.3 Regenerative Braking

Referring to Figure 2.3 it can be seen that the regenerated battery current increases as I_f increases (since the ratio E_q/E_B increases). On inspection it seems that the field current should be kept at a maximum since this is the condition where maximum current is regenerated. However, the next section will show that this is not the optimum control equation.

5.2 OPTIMUM CONTROL EQUATION

The goal of this section is to find the control equation which relates field current and armature current to give optimum efficiency. Insight is initially gained by making simplifying assumptions and the system is then analysed more accurately using a computer.

5.2.1 First Approximation

Several assumptions are made during the first stage of investigation. It is assumed that no saturation occurs and,

therefore, the machine constant is truly constant. Only field and armature copper losses are considered and all other losses are neglected. The machine torque equation is, therefore, the same as equation 5.1.

It is shown in Appendix 7.1 that the optimum efficiency is when

$$I_f = \sqrt{\frac{R_q}{R_f}}\, I_q \qquad (5.2)$$

This control equation has the same form as the series motor with a constant equal to $\sqrt{R_q/R_f}$. The constant in a normal series motor is determined by the number of field turns and this can be optimised. In a simulated series characteristic the constant is determined by the controller.

The above result is not unexpected, since it is wasteful to have full field current when low torques are required and the series characteristic reduces field current with torque. Also it is not illogical that the optimum condition appears when the armature and field copper losses are equal. That is,

$$I_{q^2} R_q = I_{f^2} R_f \qquad (5.3)$$

which is the same as the equation above. This result is noted in references (44 and 50) when they state the constant losses must equal load dependent losses and also more specifically in references (10 and 63).

The slope of a normal series control equation would be the

ratio of rated field current to armature current as in Figure 5.8. However, the optimum slope described above means that a discontinuous function is preferable.

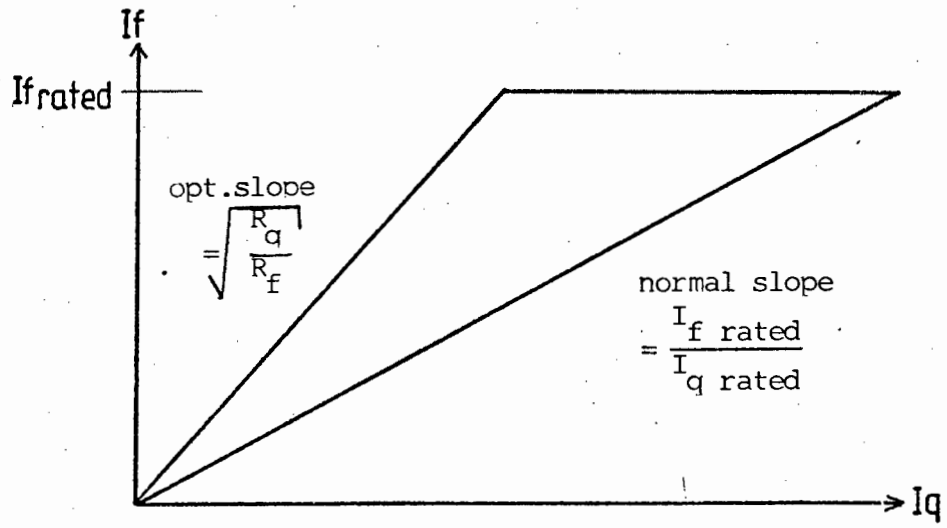

FIGURE 5.8

5.2.2 Second Approximation

During the second stage of investigation, all losses are included but three simplifying assumptions are made.

Saturation is neglected and the machine constant K is assumed to be truly constant.

It is assumed that the losses do not affect the relationship between I_f and I_q defined by

$$T = KI_fI_q$$

This means that all losses are included, but they are assumed not to be reflected as a reduction in torque.

Thirdly, it is assumed that battery current I_B is constant and

independent of the particular I_f, I_q combination chosen for any given torque and speed. Although not immediately obvious, this is a valid assumption because power into the chopper is equal to the motor output power divided by efficiency.

$$I_B E_B = \frac{TW}{\text{efficiency}}$$

Since E_B is constant, I_B will only vary by the percentage that efficiency changes.

With these three assumptions it is shown in Appendix 7.2 that the control equation for optimum efficiency must satisfy.

$$2(R_q + k_s W^2) I_q^2 + V_B I_q = 2R_f I_f^2 + (k_E W^2 + k_H W) I_f \qquad (5.4)$$

Again, this can be seen to mean that the losses caused by the armature current must equal the losses caused by the field current, where the copper losses are weighted by a factor of two because of their higher powers.

Equation 5.4 is plotted in Figure 5.9. The initial slope $\frac{dIf}{dIq}$ is shown in Appendix 7.2 to be

$$\text{Initial Slope} = \frac{V_B}{k_E W^2 + k_H W} \qquad (5.5)$$

The graph tends to a final slope

$$\text{Final Slope} = \sqrt{\frac{R_q}{R_f}} \qquad (5.6)$$

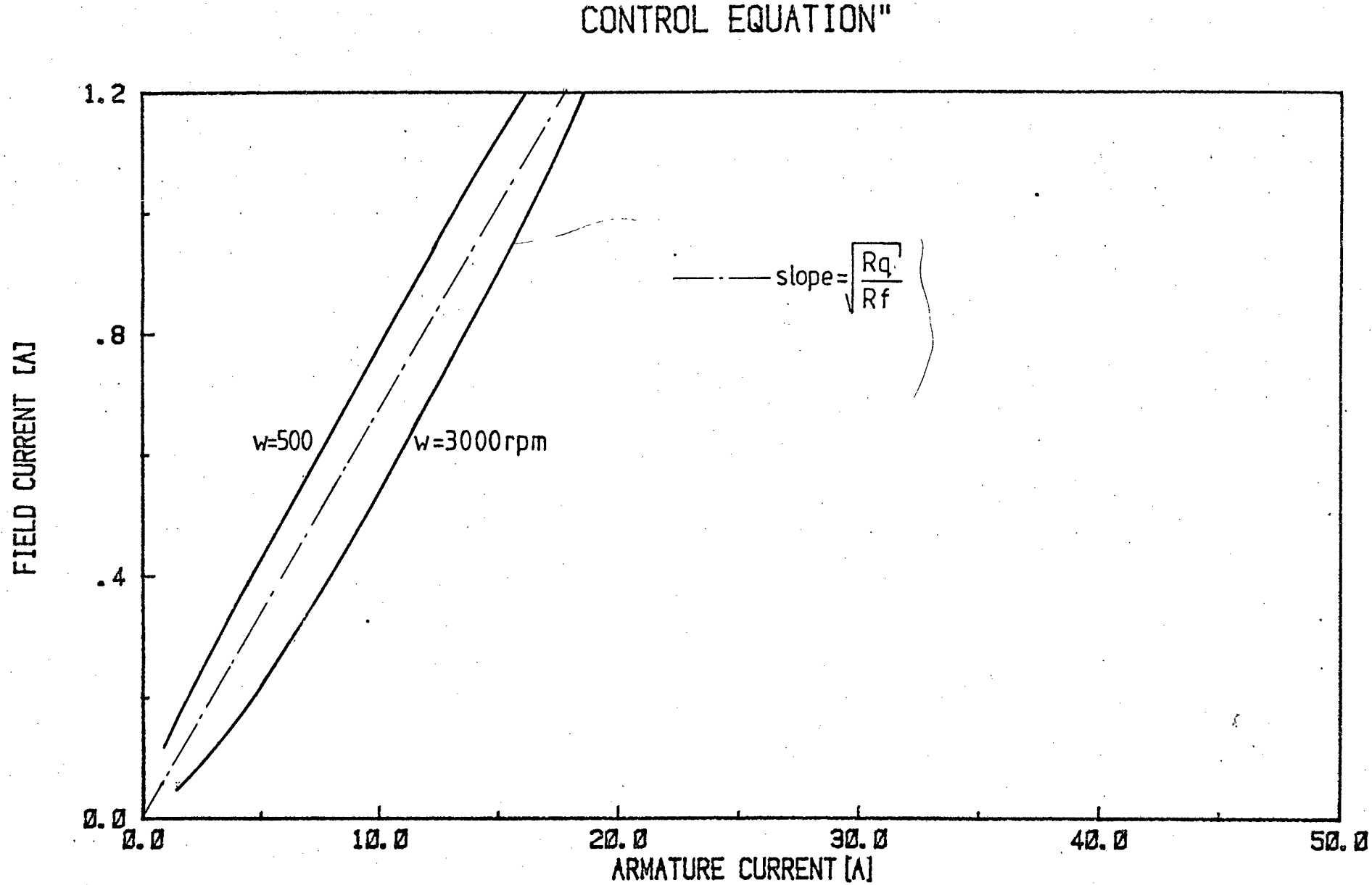
CONTROL EQUATION"
1.2
.8
.4
0.0
FIELD CURRENT [A]
w=500
w=3000rpm
slope=√(Rq/Rf)
0.0
10.0
20.0
30.0
40.0
50.0
ARMATURE CURRENT [A]

figure 5.9

Comparing with the first assumption, this graph is fairly similar because brush and iron losses are of similar magnitude (coefficients of I_f and I_q in equation 5.4). It was noted that using a slightly lower value of R_q had a large effect on the influence of speed.

5.2.2.1 Effect of assumptions

This second approximation is useful in gaining insight into the nature of the optimum control equation, particularly the shape of the curve and the effect of speed.

It is shown in Section 5.1.1 that the I_f - I_q operating point is found from the intercept between the control equation and the motor torque equation. The first two assumptions in Section 5.2.2have the effect of altering the shape of the motor torque equation. This is shown in Figure 5.10. At very low torques the assumptions are seen to be reasonable but this is not true as the torque increases.

5.2.3 Computer Model

As a third approximation, all losses are included and the effect of saturation is taken into account. The only assumptions are that the equations in Section 5.2.3.1 are accurate.

5.2.3.1 Equations used in model

The symbols used are defined in Figure 5.11

Effect of assumptions in 2nd approx.

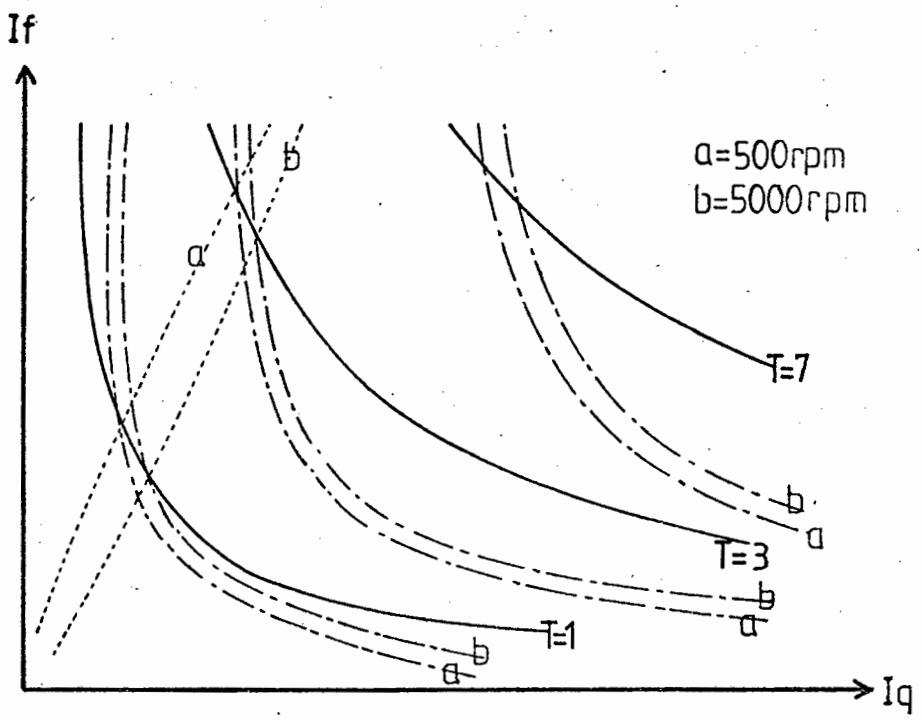

——— torque equation T = K If Iq

—·—·— torque equation incl. losses + saturation

---------- control equation

figure 5.10

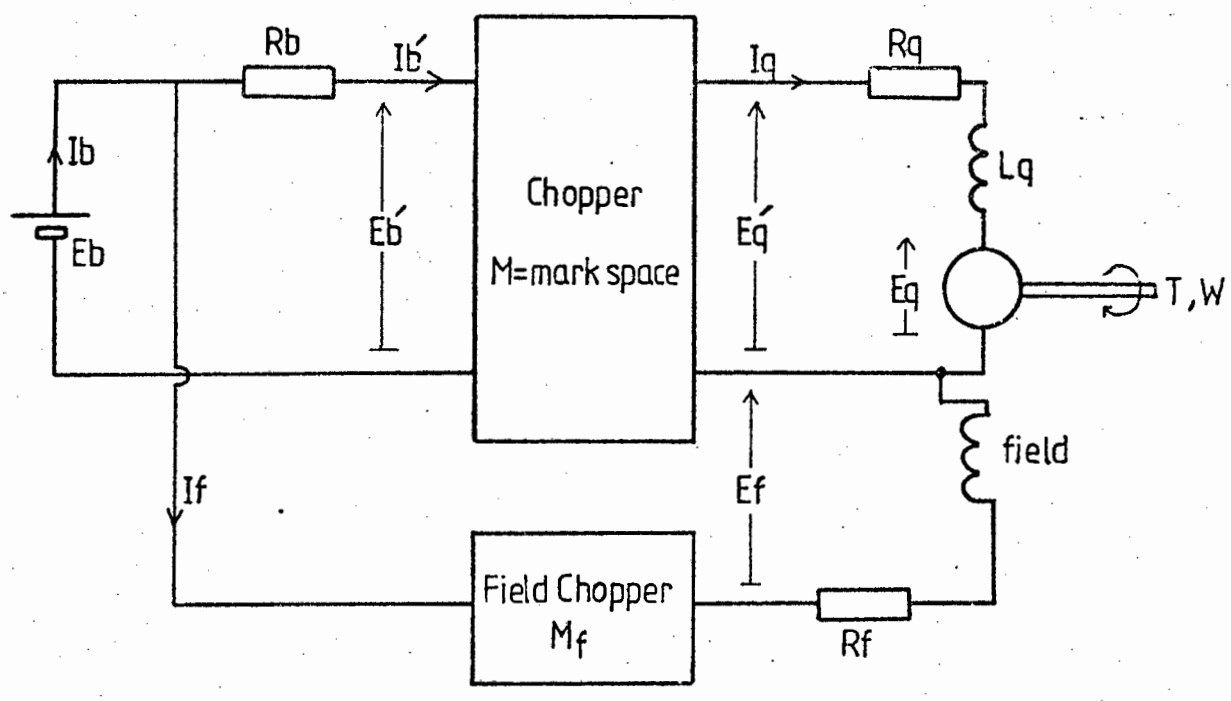

FIGURE 5.11

Motor:

1. $T = K(I_f)I_fI_q - (k_H + k_EW)I_f - (k_{f_1}W + k_{f_2}) - (k_sWI_q^2)$

2. $E_{q'} = K(I_f)I_fW + I_qR_q + S.V_B$

3. $E_f = I_fR_f = M_fE_B$

Chopper;

4. $$I_{B'} = \frac{E_B'}{R_q}\left[(1 - \frac{K(I_f)I_fW + SV_B}{E_B'}.M - \frac{TC}{T}\frac{(1 - e^{-(1-M)\frac{T}{TC}})(1 - e^{-M\frac{T}{TC}})}{(1 - e^{-\frac{T}{TC}})}\right]$$

5. $M = E_{q'}/E_{B'}$

Battery:

6. $E_{B'} = E_B - I_BR_B - \frac{1}{k_{B1}} \sinh^{-1}(\frac{I_B}{2k_{B2}})$

Efficiency: 7. $N = \frac{TW}{I_B E_B}$

Algebraic manipulation with these equations is not possible and in addition a smooth function for $K(I_f)$ is not available. For these two reasons the only way to proceed is to perform a numerical analysis on a computer.

5.3.2.3 The computer program

The program must be able to find the optimum efficiency and the corresponding combination of I_f and I_q for any given torque and speed. The block diagram in Figure 5.12 shows how this may be done using equations (1) to (7) in Section 5.2.3.1. The mark space ratio of the field chopper is repeatedly incremented until the optimum is found.

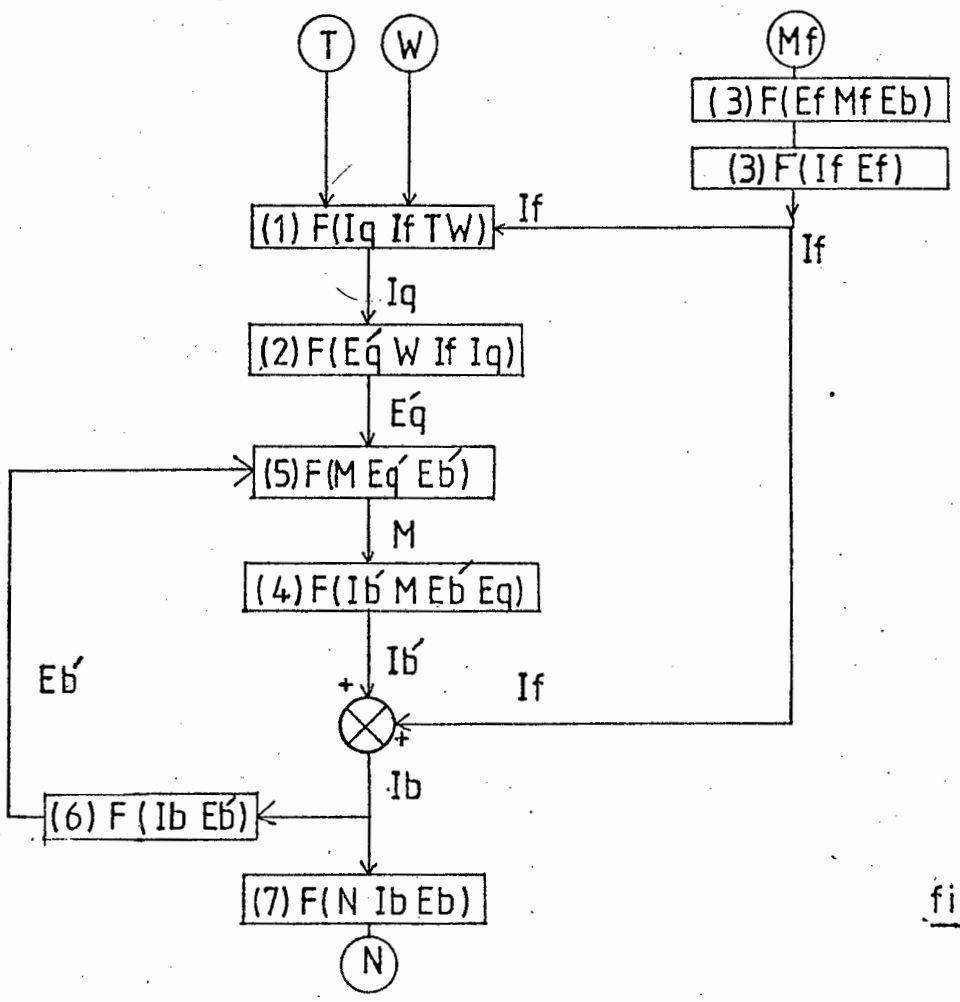

figure 5.12

A flowchart describing the program is shown in Figure 5.13. A full program listing is given in Appendix 8.1. The computer used was a Hewlett Packard HP85[64]:

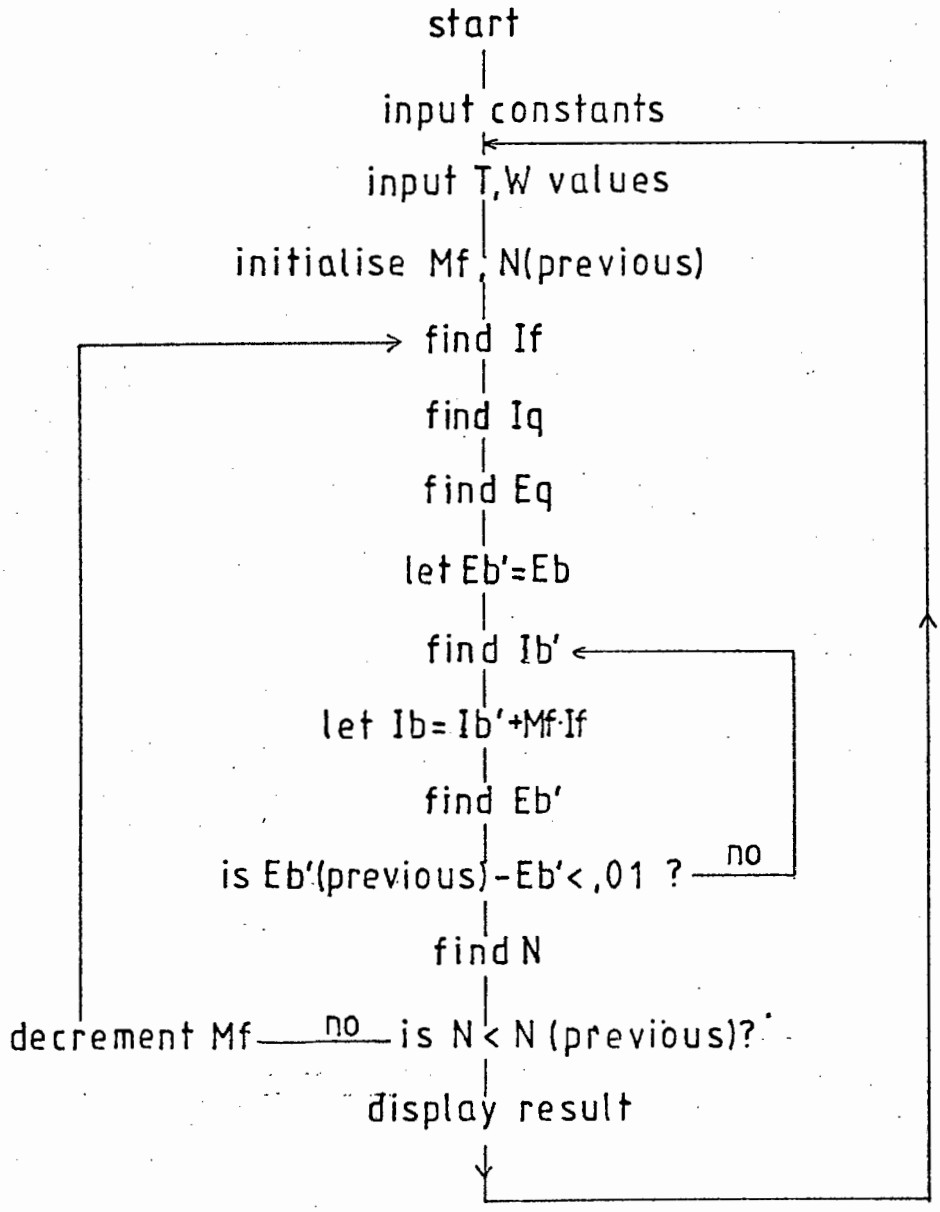

figure 5.13

It should be noted that values of $K(I_f)$ and $\text{Sin}\,h^{-1}x$ are stored in an array with discrete values. To improve accuracy a straight line between points is assumed and the values calculated from this.

5.2.3.3 Results and discussion

The results obtained are shown in the graphs in Figures 5.14 and 5.15. In addition the control equation using the approximation in Section 5.2.1 is plotted as well as the control equation for a normal series motor.

The optimum control equation can be approximated fairly well by the straight line series characteristic. However, the slope is less than that predicted in Sections 5.2.1 and 5.2.2. This is accounted for in the discussion on the effect of the approximations in Section 5.2.2.1.

Therefore, for any given machine, the discontinuous series control equation approximates closely to the optimum. The slope of this equation can be determined by using the program in this section.

5.3 EFFICIENCY COMPARISONS USING VARIOUS CONTROL EQUATIONS

5.3.1 Introduction

The optimum control equation relating field and armature currents has been discussed. This section will investigate

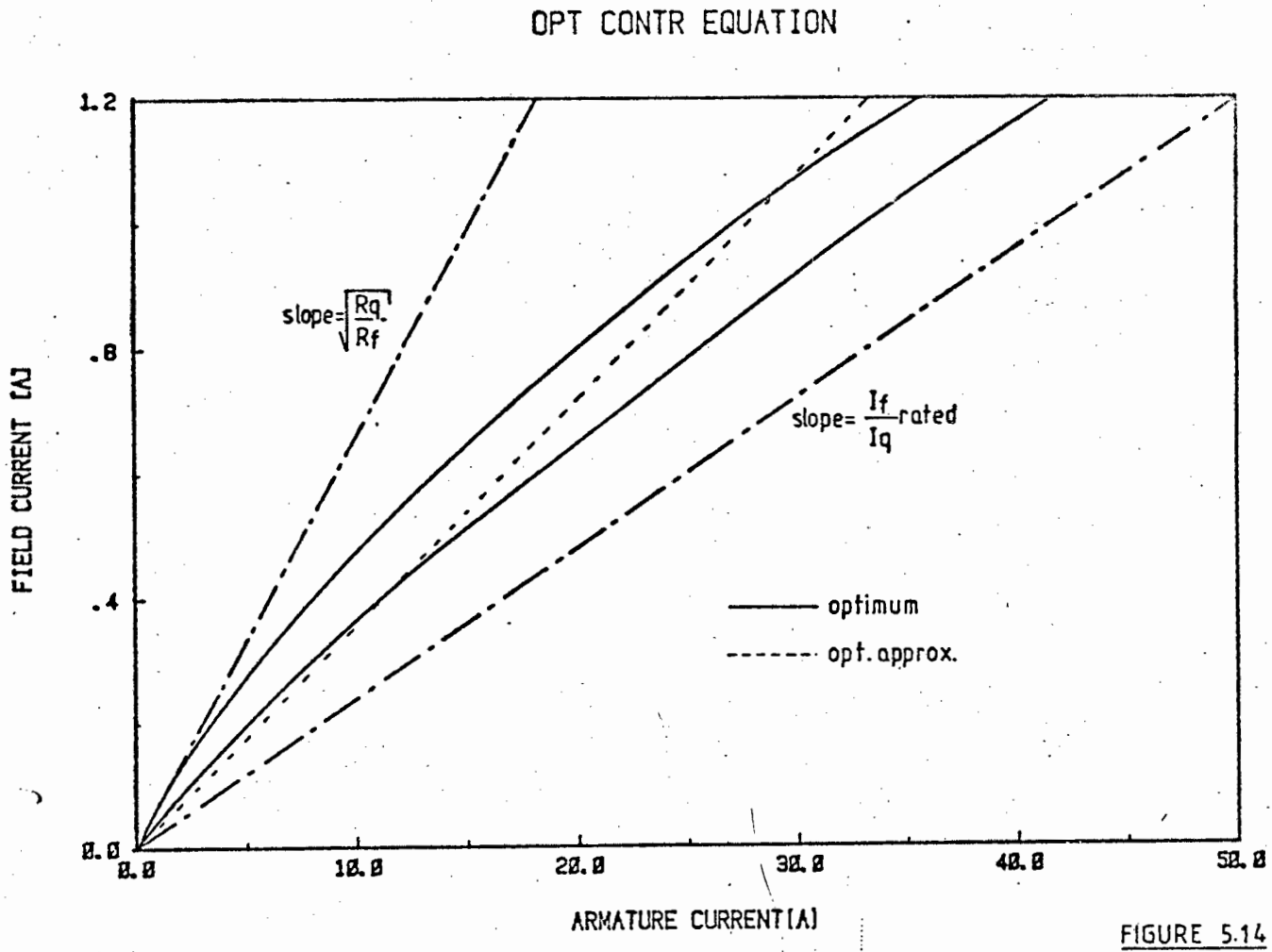

FIGURE 5.14

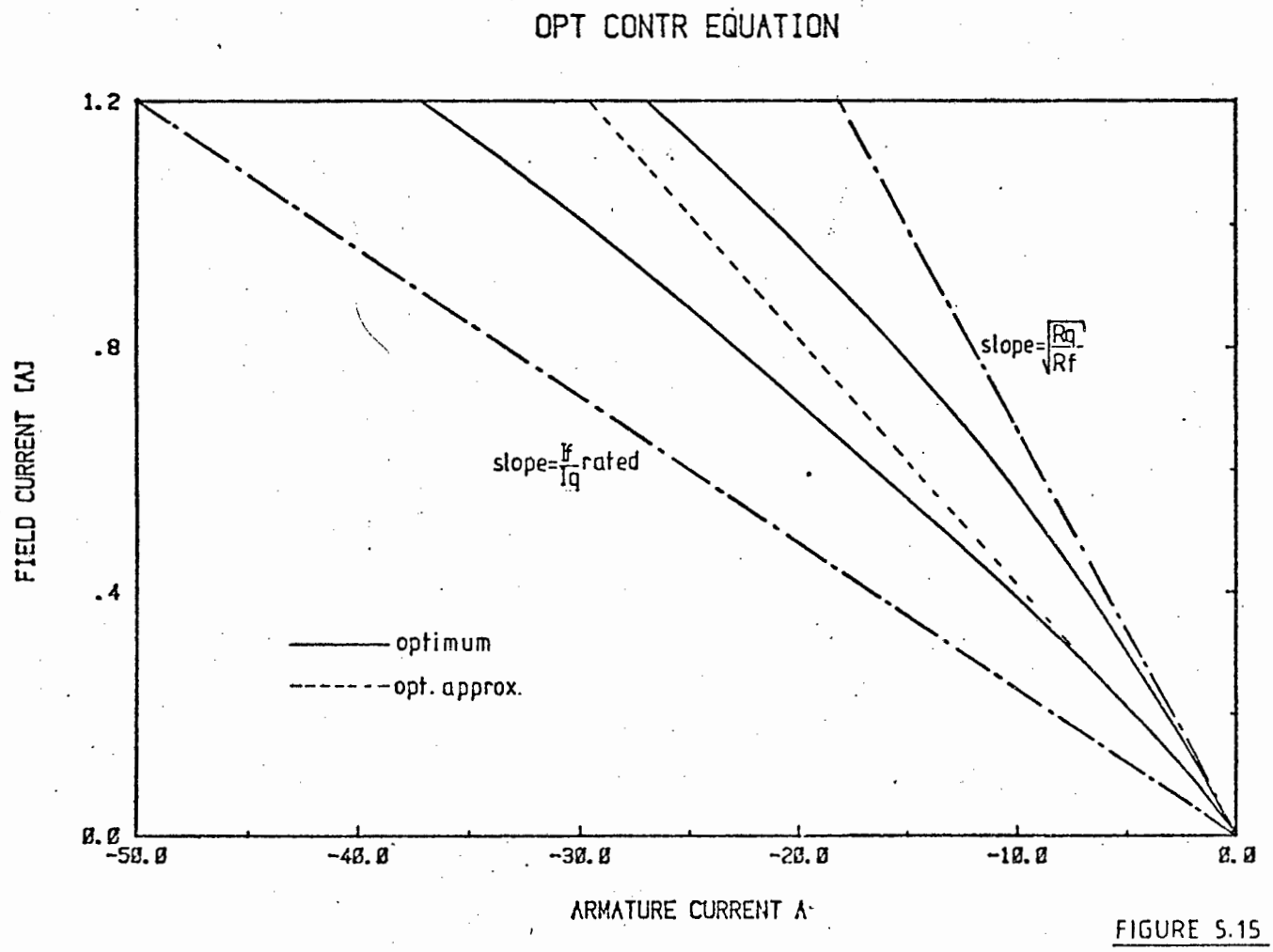

FIGURE 5.15

SHUNT MOTOR

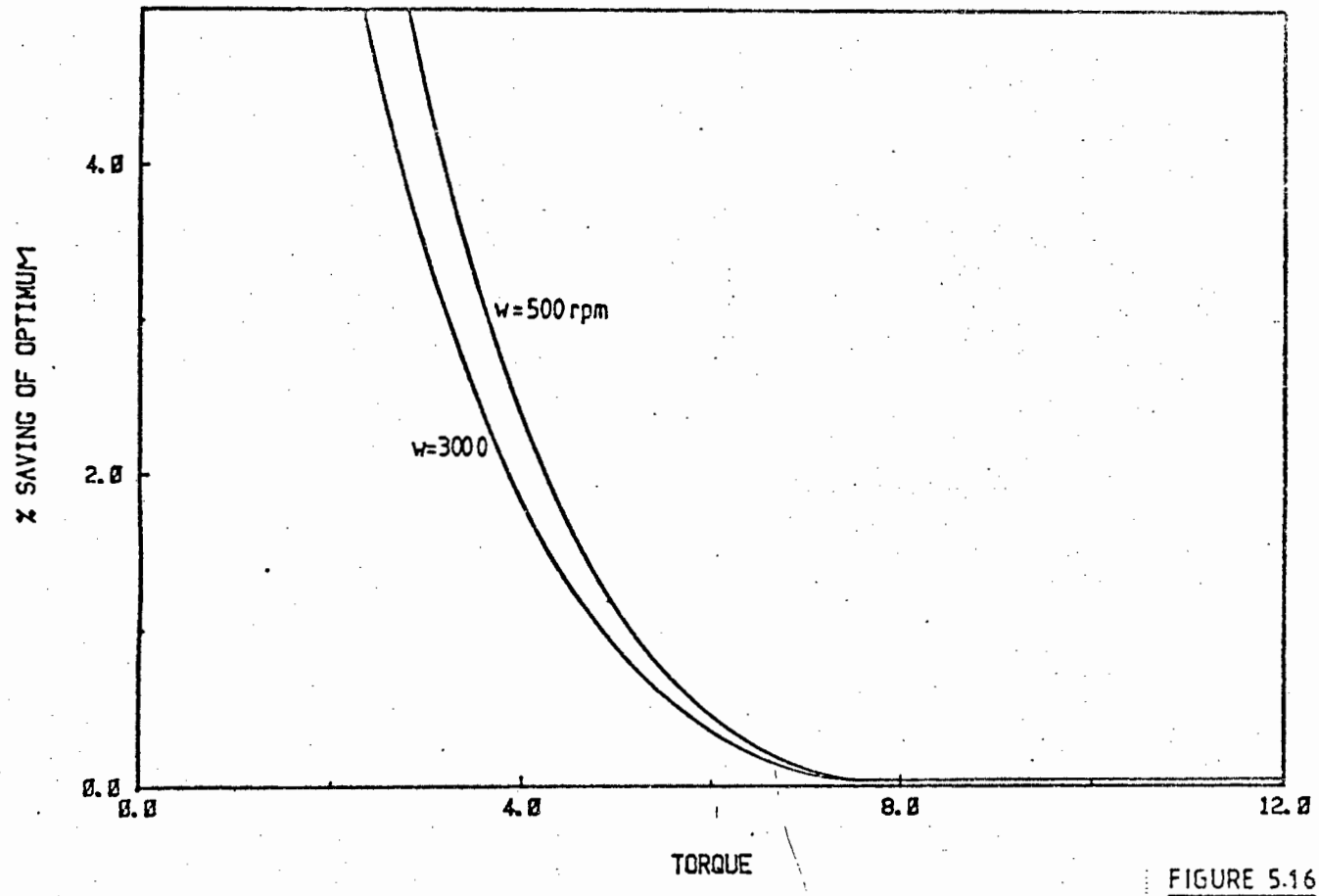

FIGURE 5.16

SHUNT MOTOR

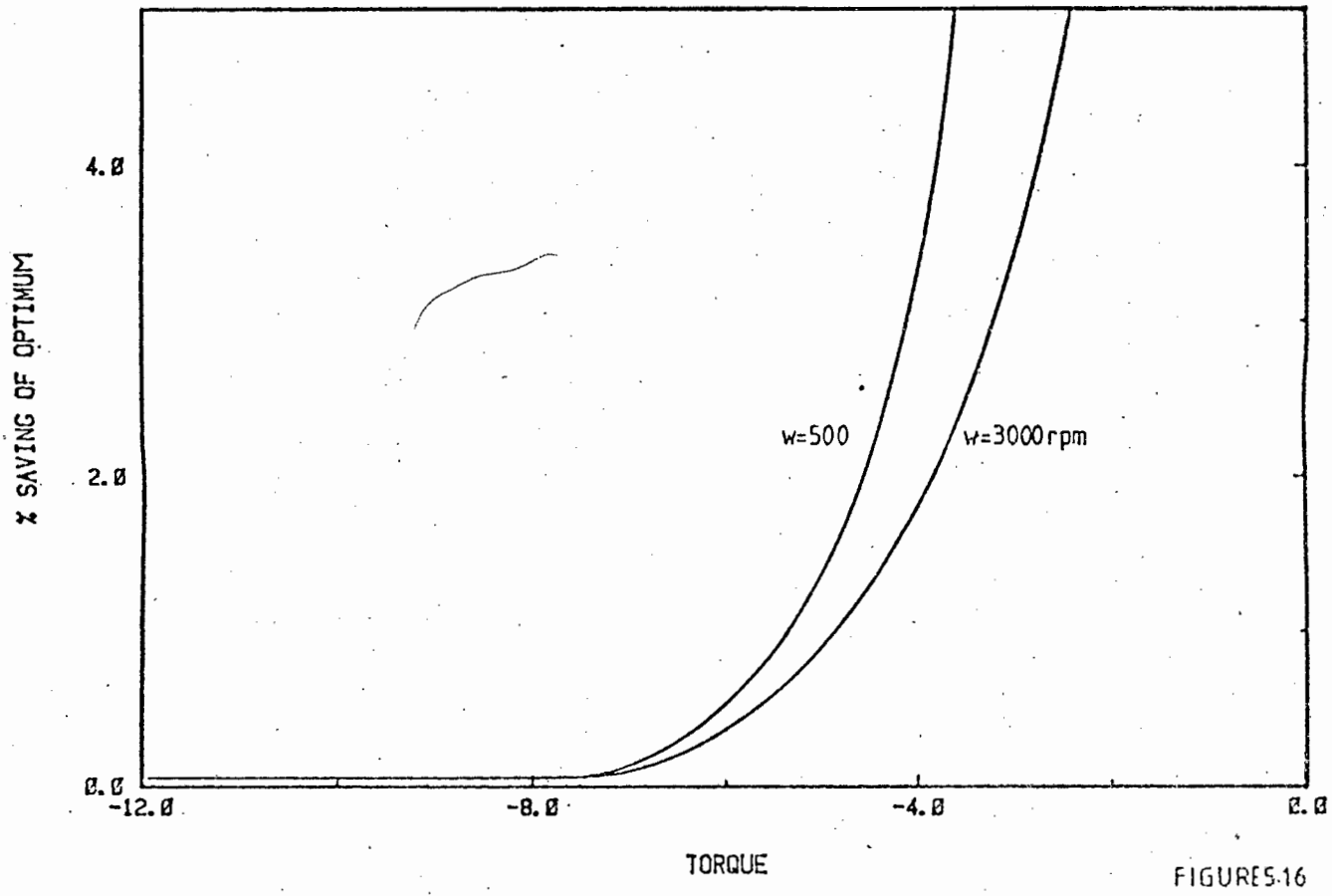

FIGURE 5.16

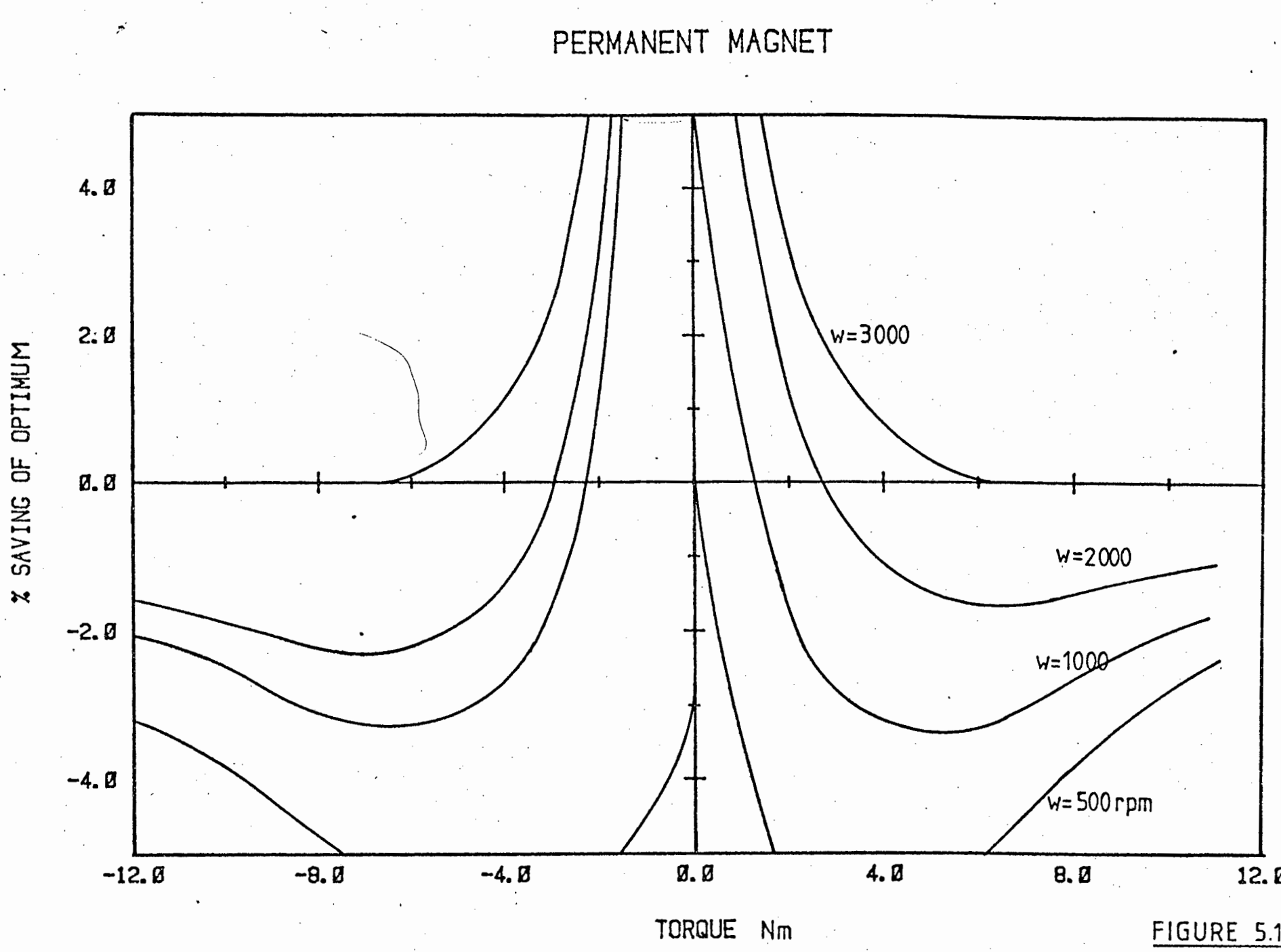
PERMANENT MAGNET
% SAVING OF OPTIMUM
4.0
2.0
0.0
-2.0
-4.0
-12.0
-8.0
-4.0
0.0
4.0
8.0
12.0
TORQUE Nm
w=3000
w=2000
w=1000
w=500 rpm

FIGURE 5.17

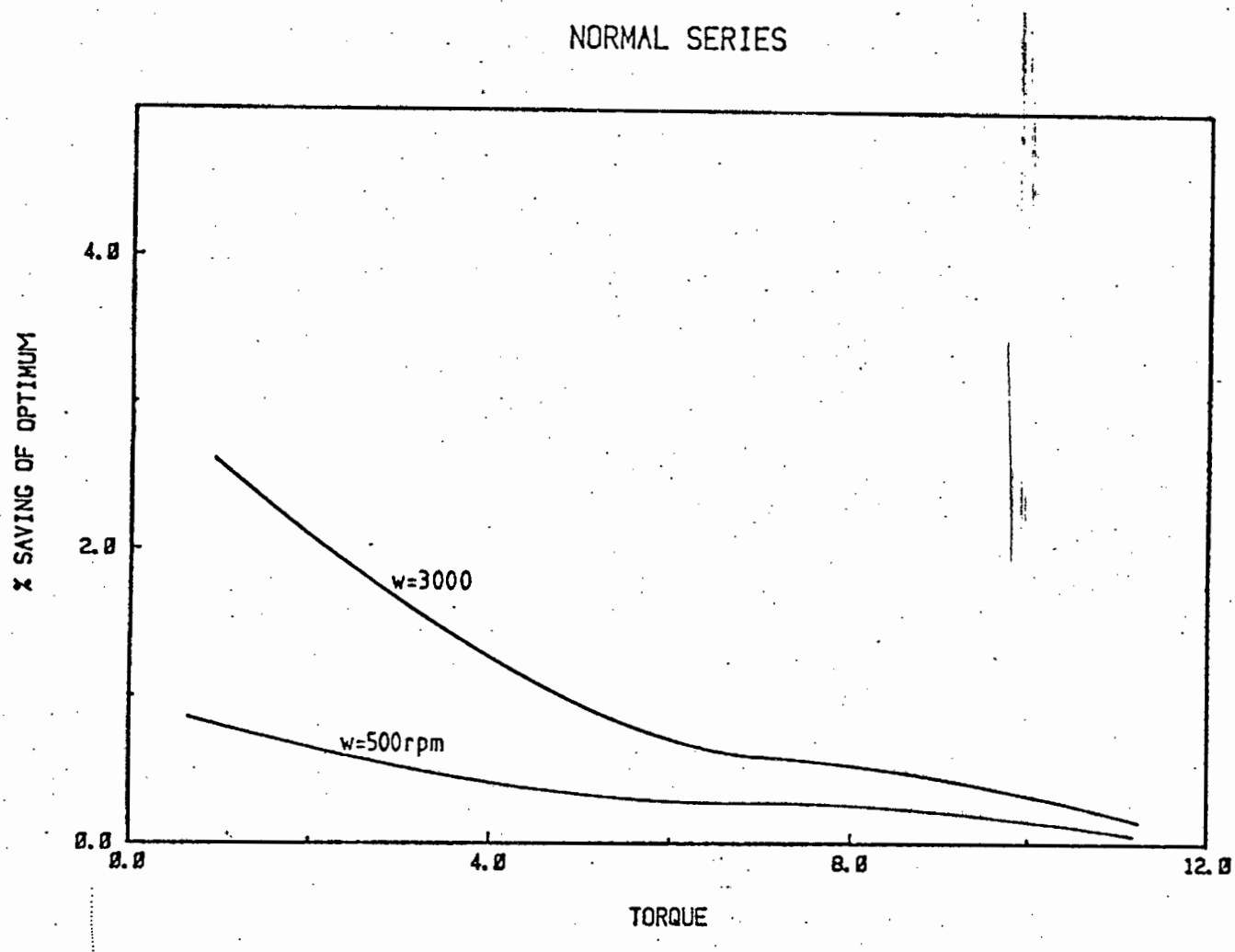
NORMAL SERIES
% SAVING OF OPTIMUM
4.0
2.0
0.0
w=3000
w=500rpm
0.0
4.0
8.0
12.0
TORQUE

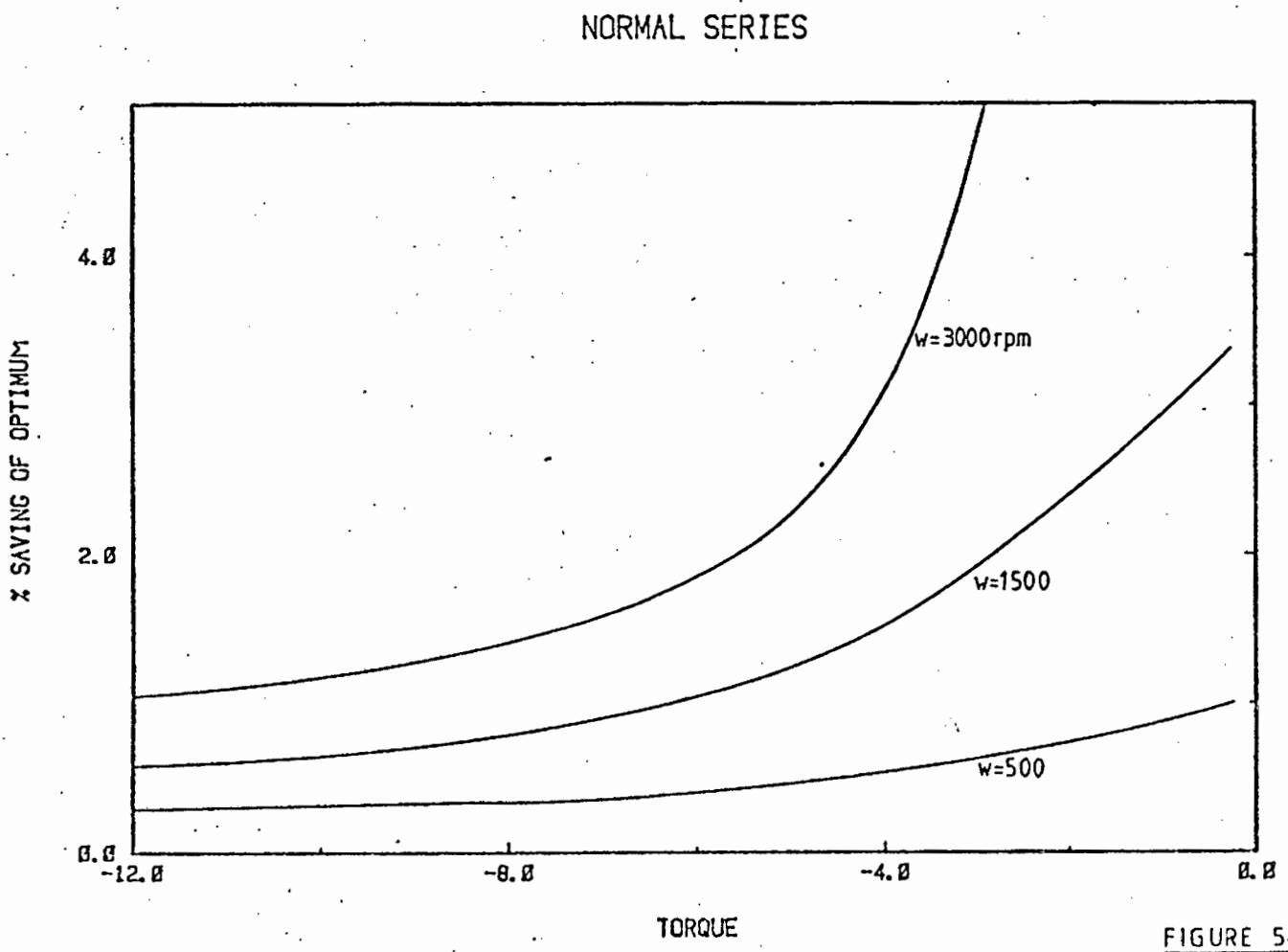
NORMAL SERIES
% SAVING OF OPTIMUM
4.0
2.0
0.0
w=3000rpm
w=1500
w=500
-12.0
-8.0
-4.0
0.0
TORQUE

FIGURE 5.18

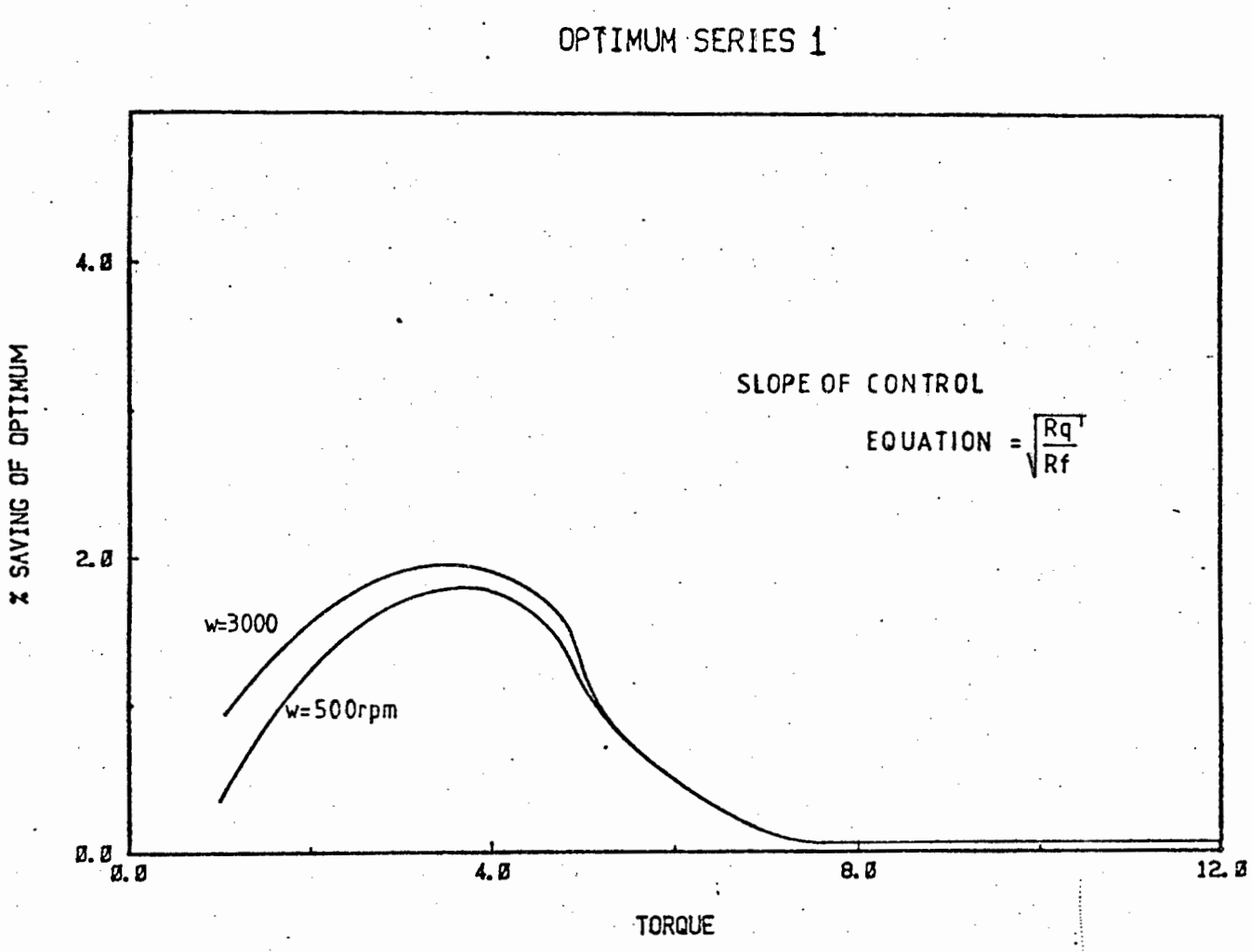
OPTIMUM SERIES 1
% SAVING OF OPTIMUM
4.Ø
2.Ø
Ø.Ø
SLOPE OF CONTROL
EQUATION = √(Rq'/Rf)
w=3000
w=500rpm
Ø.Ø
4.Ø
8.Ø
12.Ø
TORQUE

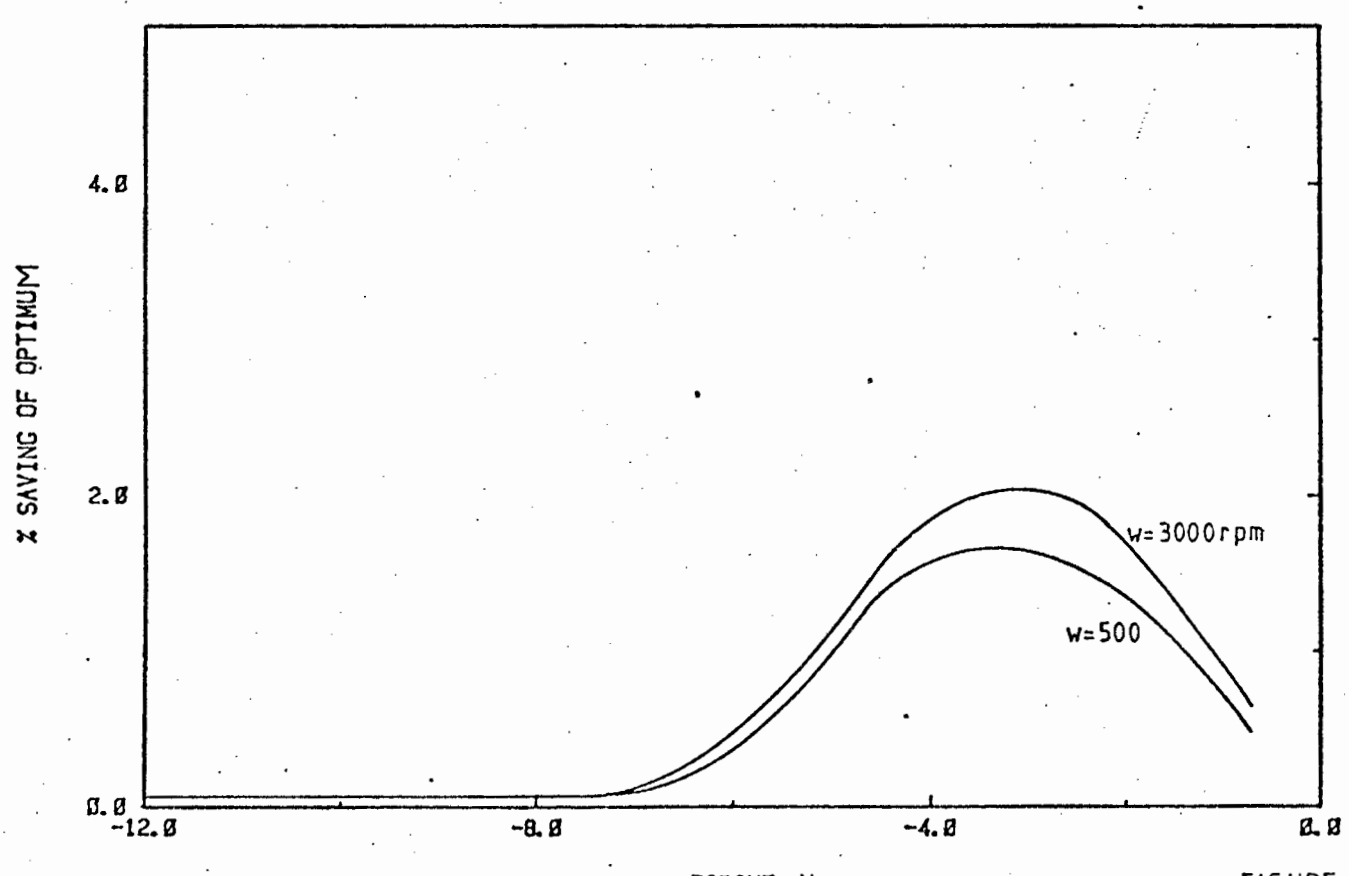
OPTIMUM SERIES 1
% SAVING OF OPTIMUM
4.Ø
2.Ø
Ø.Ø
w=3000rpm
w=500
-12.Ø
-8.Ø
-4.Ø
Ø.Ø
TORQUE Nm

FIGURE 5.1

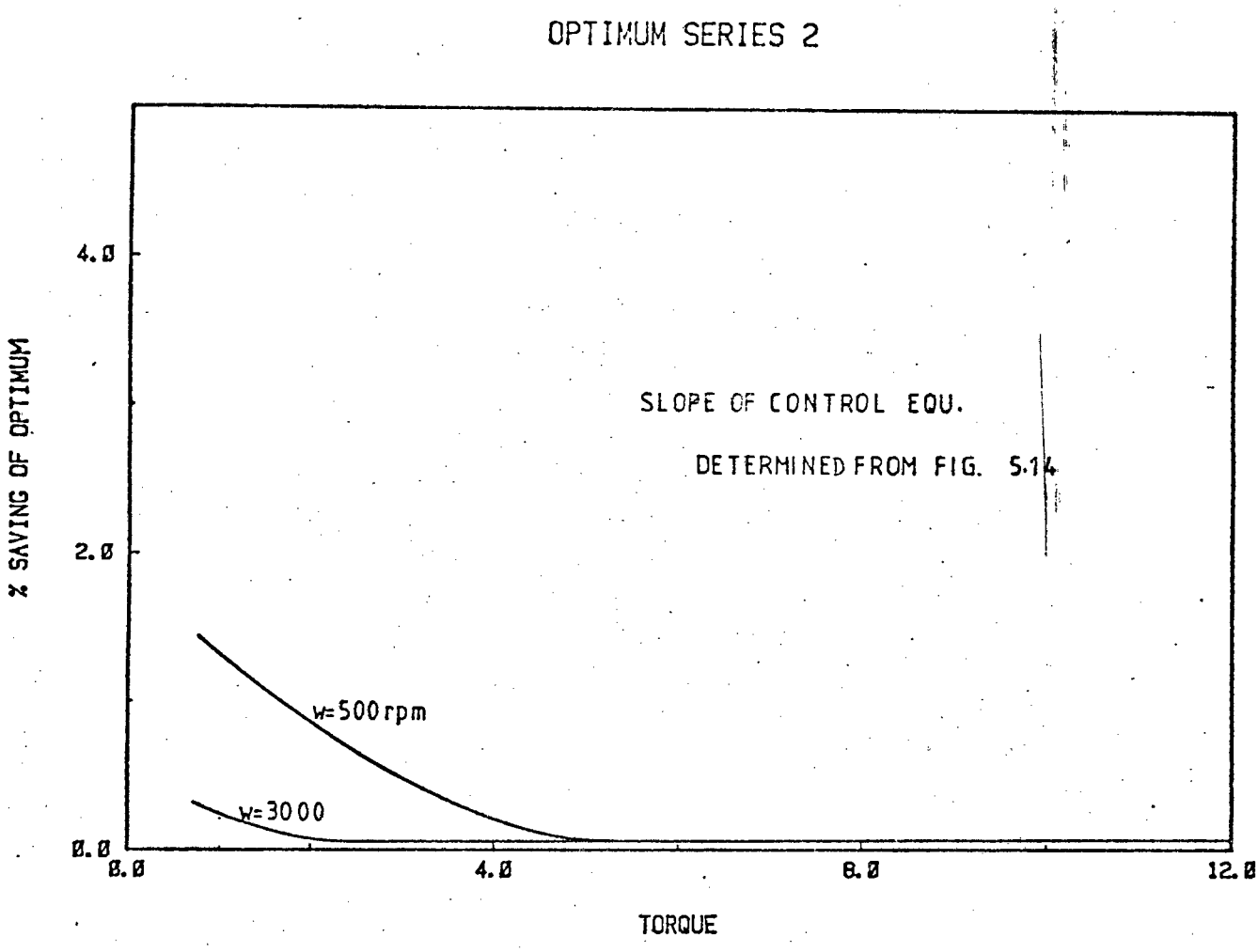
OPTIMUM SERIES 2
% SAVING OF OPTIMUM
4.Ø
2.Ø
Ø.Ø
SLOPE OF CONTROL EQU.
DETERMINED FROM FIG. 5.14
W=500 rpm
W=3000
Ø.Ø
4.Ø
8.Ø
12.Ø
TORQUE

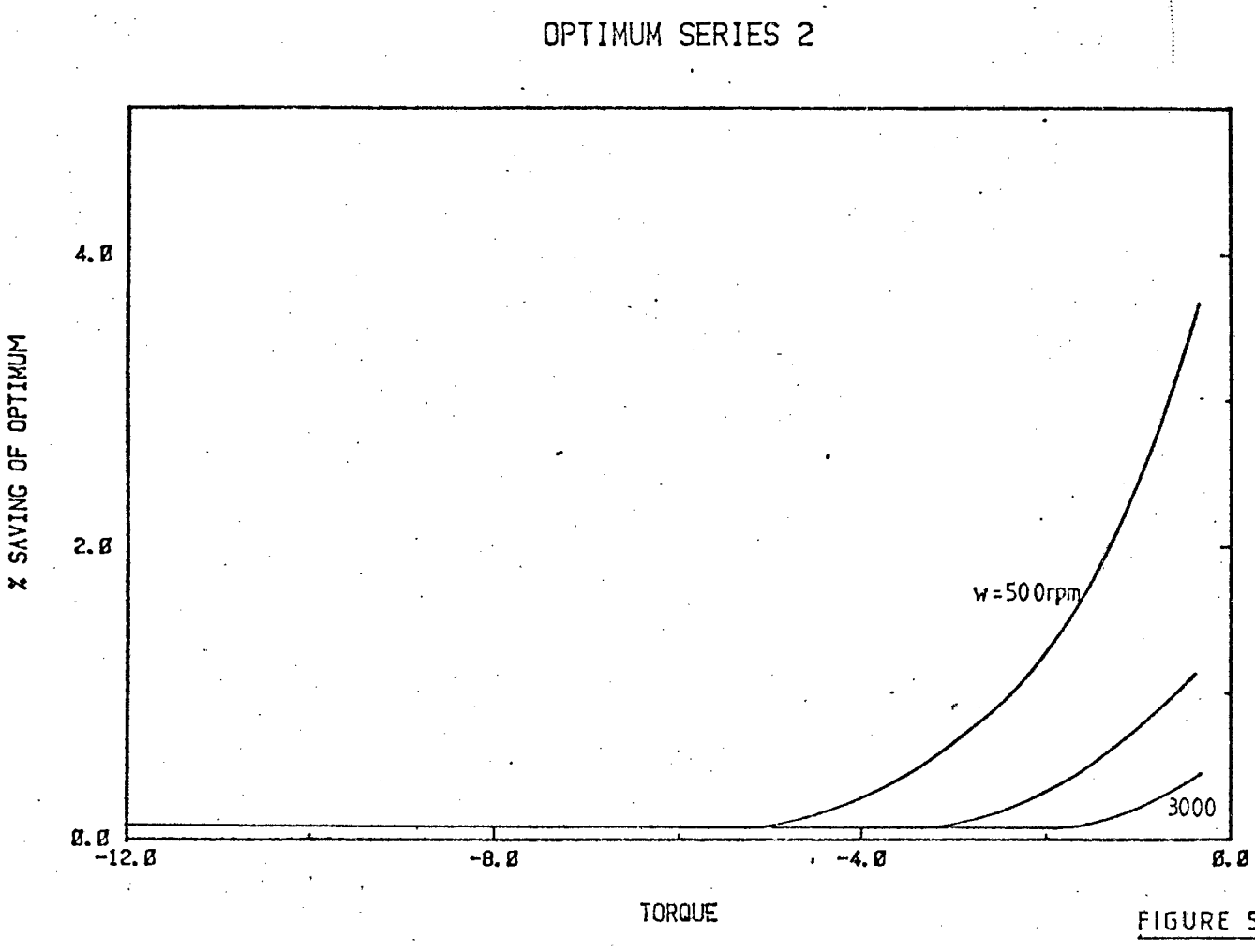
OPTIMUM SERIES 2
% SAVING OF OPTIMUM
4.Ø
2.Ø
Ø.Ø
W=500rpm
3000
-12.Ø
-8.Ø
-4.Ø
Ø.Ø
TORQUE

FIGURE 5.20

the amount by which the control equation affects efficiency and several systems are quantitatively compared with the optimum.

(a) Shunt machine - constant field current

(b) Permanent magnet motor

(c) Normal series motor - slope of control equation

$$= \frac{I_{fmax}}{I_{qmax}}$$

(d) Series characteristic with equation as in Section 5.2.1,

$$\text{slope} = \sqrt{\frac{R_q}{R_f}}$$

(e) Series characteristic with the slope of a straight line through the graph of optimum efficiency in Figure 5.14.

5.3.2 Computer Program

The program listed in Appendix 8.1 is used with several minor changes for the various systems. These changes are listed in Appendix 8.2.

5.3.3 Results

The results obtained are shown in Figures 5.16 to 5.20. The differences between the optimum efficiency and the efficiency of the strategy being considered are plotted against torque for various values of speed. The X-axis may, therefore, be considered to be the optimum efficiency and the graph shows the saving which this optimum control strategy represents.

5.3.4 Discussion on Results

The shunt motor is very inefficient at low torques and the efficiency difference is virtually independent of speed.

The normal series motor is much more efficient than the shunt motor at low torque and slightly less efficient at high torques. The series characteristic with $I_f = \sqrt{R_q/R_f}\, I_q$ keeps the efficiency within 2% of the optimum at all times.

The series control equation with a slope approximating the optimum results in Section 5.2.3 yielded efficiencies within 0.5% of the optimum with the exception of very low torques and speeds.

The permanent magnet motor showed a significant improvement over the optimum field controlled machine under all conditions except low torque and speeds. This result is dependent on the assumption that the field can be directly replaced by a permanent magnet motor with a flux density equivalent to full field current.

5.3.5 Efficiency Comparisons Over a Standard Test Cycle

Figures 5.16 to 5.20 show the efficiency differences for various torque-speed conditions. A more useful comparison would be to compare the energy used by various control strategies over a standard test cycle.

An example of such a standard cycle for an electrical vehicle (SAEJ227a) is shown in Figure 5.21.[65] Other possible standard cycles are mentioned in references (55, 66 and 69).

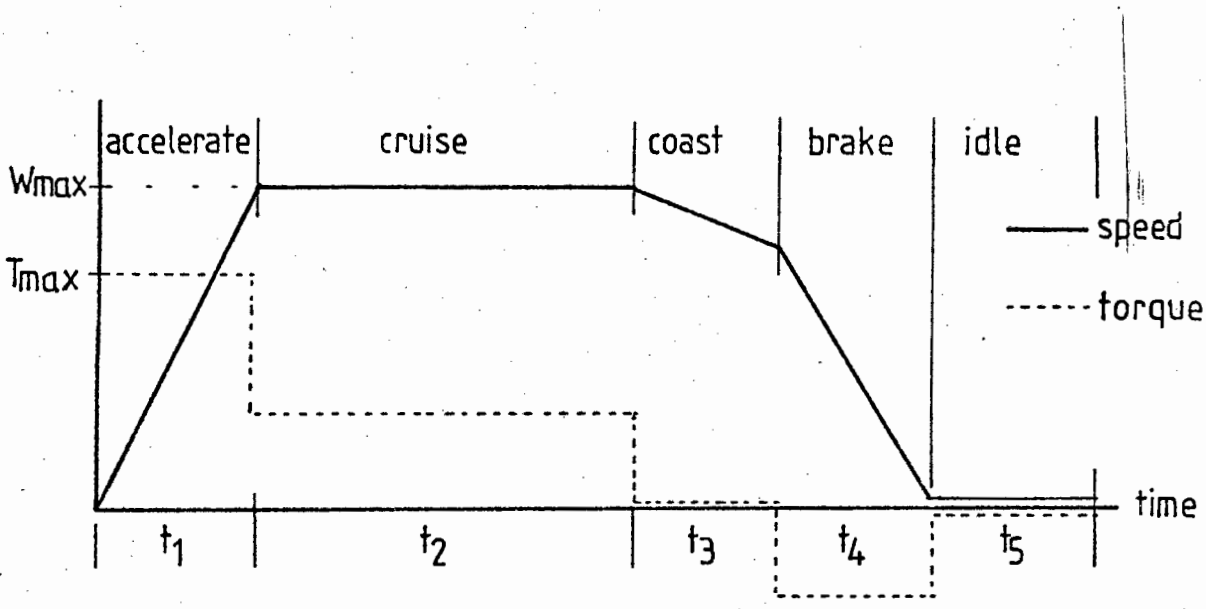

FIGURE 5.21

It is assumed that each stage requires a constant torque (this being an approximation) as shown by the dotted line in Figure 5.21.

It is clear that the choice of test cycle and corresponding constants (e.g. W_{max}, T_{max} and t_1 to t_5) has a large effect on the efficiency comparison of various strategies. For example, a shunt machine, which is inefficient at low torques will be dependent on the choice of T_{max}, T_{cr} and T_{br}. The permanent magnet motor is influenced by the choice of both torque and speed profiles. The times t_1 to t_5 also influence the result. Ideally the torque speed profile of the proposed application should be known to give an accurate comparison.

However, despite these variations, an example of a particular

application is analysed in this thesis. The torque-speed profile in Figures 5.21 is used with the constants listed in Table 5.1. The values of t_1 to t_5 are suggested in reference (65). A description and listing of the computer program is contained in Appendix 8.3 and the results obtained in Table 5.2.

W_{max}	T_{max}	T_{cr}	T_{br}	t_1	t_2	t_3	t_4	t_5
3 000 rpm	11 Nm	4 Nm	-4 Nm	29 sec	51 sec	11 sec	9 sec	26 sec

TABLE 5.1

Strategy	Efficiency saving over optimum strategy
Shunt	-0.75%
Normal Series	-0.25%
Permanent Magnet	+0.78%

TABLE 5.2

From these results it can be seen that the choice of control strategy does not have a very significant effect on a typical electrical vehicle test cycle. However, other applications which require more time at low torque and speed will realise greater efficiency savings.

5.3.6 The Use of a Gearbox

From the graph in Figure 5.22 it can be seen that efficiency is dependent on torque and speed. The torque-speed operating point is determined by the load presented to the machine and the required speed. However, it is possible to alter the

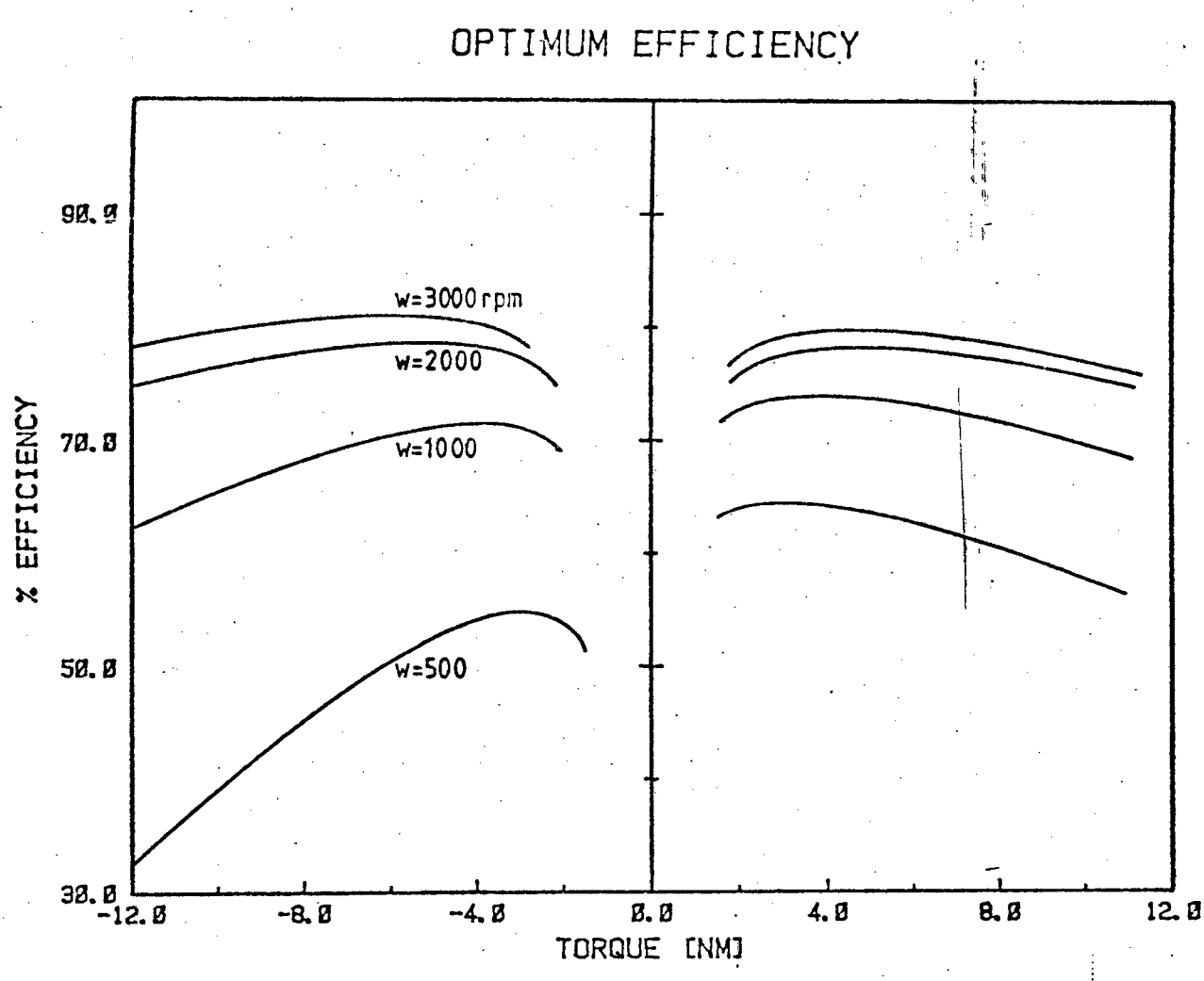
OPTIMUM EFFICIENCY
90.0
70.0
50.0
30.0
% EFFICIENCY
w=3000 rpm
w=2000
w=1000
w=500
-12.0
-8.0
-4.0
0.0
4.0
8.0
12.0
TORQUE [NM]

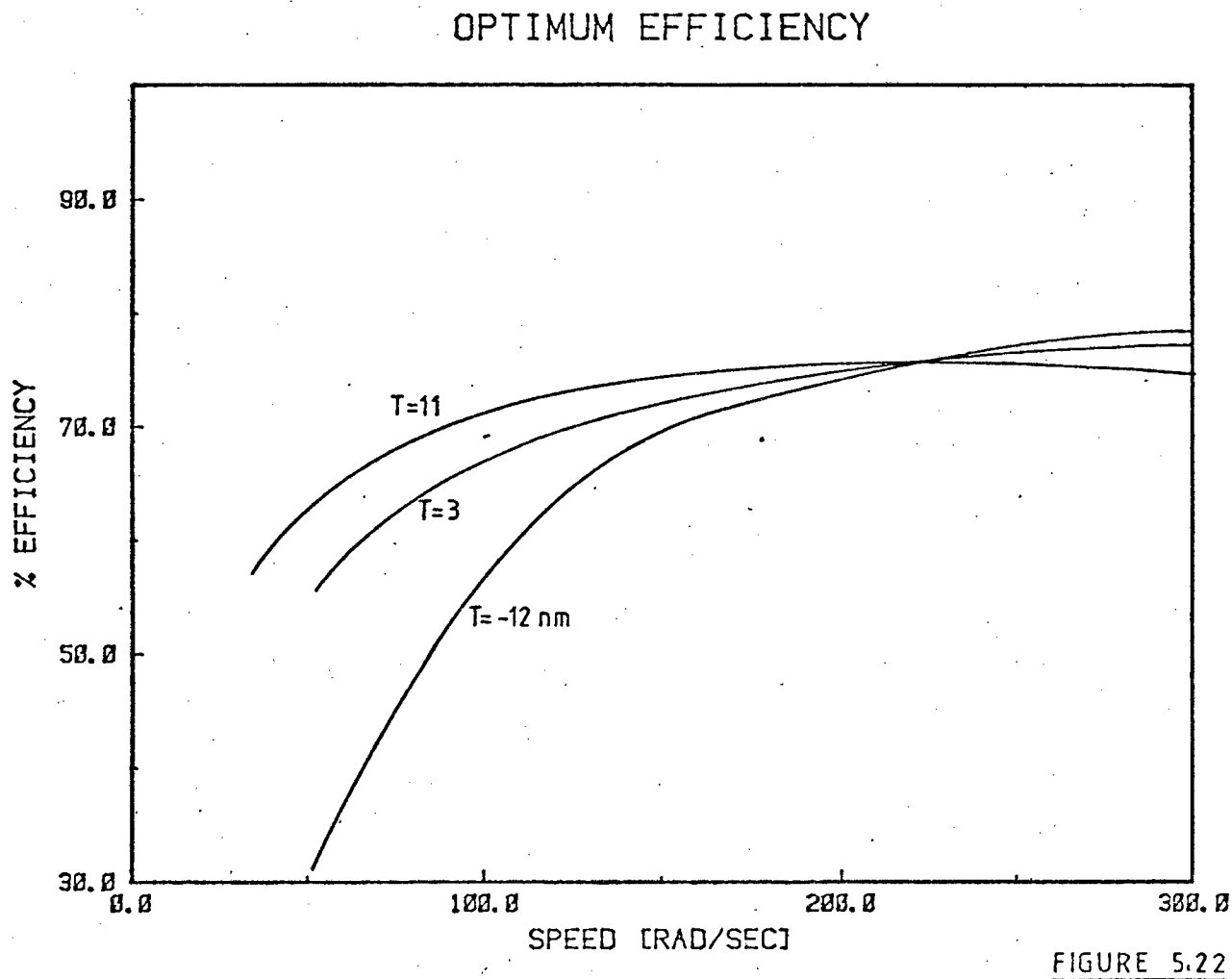
OPTIMUM EFFICIENCY
90.0
70.0
50.0
30.0
% EFFICIENCY
T=11
T=3
T=-12 nm
0.0
100.0
200.0
300.0
SPEED [RAD/SEC]

FIGURE 5.22

torque-speed condition as seen by the motor by the use of a gearbox.

This possibility is extensively investigated in references (20, 66, 67, 70) and has potential for more significant efficiency improvement (about 10%).

5.3.7 Field Control

It is possible to control the motor speed by varying the field while maintaining the armature voltage constant.[68] For this system some form of armature control is required for start-up (e.g. resistance controller). A high motor speed and gearbox may also be necessary.

The motor used in this thesis was not suitable for this type of control and so no direct comparisons could be made. The control equation for this system is mentioned in Section 5.1.1.

CHAPTER 6

PROPOSED CHOPPER AND CONTROLLER

6.1 REQUIREMENTS

It has been shown in Chapter 5 that the control equation shown in Figures 5.14 and 5.15 approximate closely to the optimum. This is the same characteristic as a series motor with the field current being limited at a specific value of armature current.

In addition to providing the optimum control equation, the controller must also implement the desired torque-speed characteristic. It has been suggested in Section 5.1.2 that a combination of constant torque and constant power characteristic is an attractive option.

It is possible for the set-point controlled by the operator to be either torque[3], speed or a combination of both.[43, 78] it was decided in this design to implement torque control.

It should be noted that the permanent magnet motor provides a greater overall efficiency than the optimum field controller and should be considered if at all practical and economical. This would require a straight-forward armature current controller.

The purpose of this chapter is to investigate the practical realisation of an optimum field and armature control system. Several possibilities are described and a design proposed which uses a microprocesor.

6.2 IMPLEMENTATION

6.2.1 Series Motor

An adapted series motor may be used with a chopper across the field as in Figure 6.1 to provide the optimum control equation.

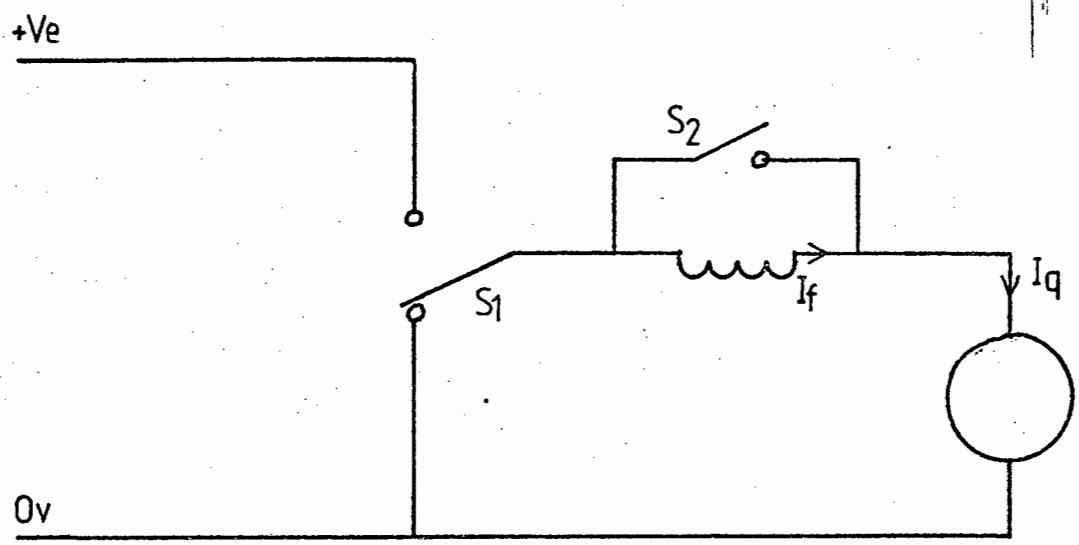

FIGURE 6.1

Switch S_1 represents the operation of a standard bidirectional chopper as described in Section 2.1. Switch S_2 is controlled by a current feedback signal and is closed when the current I_f exceeds a pre-set level. The number of turns on the field winding must be calculated to give the correct slope for the control equation at levels below the field current limit.

This system is easily implemented using either analogue or digital approaches. However, it has one major drawback in that the field winding needs to be reversed for current regeneration. This can be done either using a mechanical or a solid state change-over switch.[8]

6.2.2 Separately Excited Motor

The series characteristic can be simulated on a separately excited machine as in Figure 6.2.

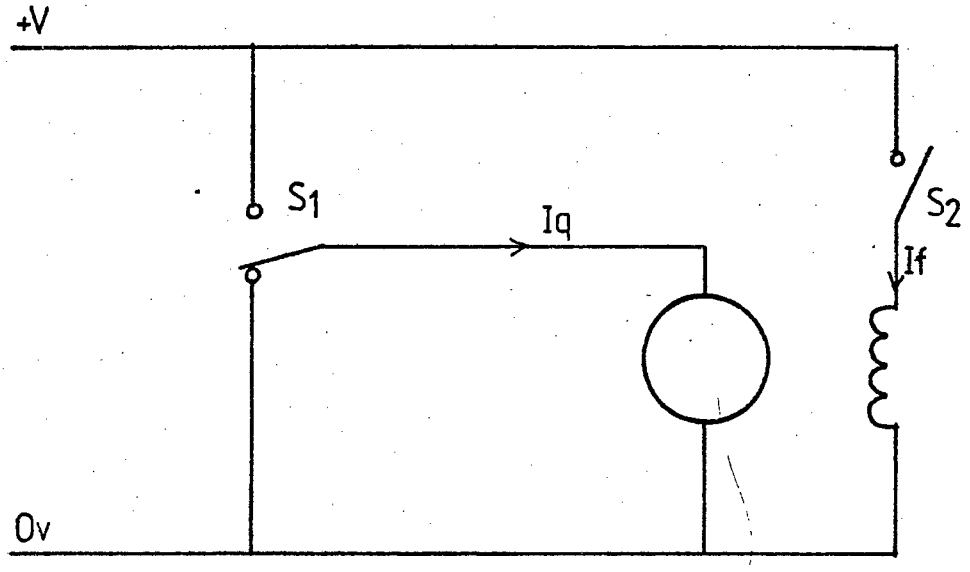

FIGURE 6.2

Both I_f and I_q are monitored and S_2 is switched so as to maintain the correct relationship between field and armature currents.

6.2.3 Microprocessor Based Controller

Both of the above two proposals can be implemented using either analogue or digital circuitry. It was decided to use a microprocessor for the controller in this design.

Using a microprocessor minimises the component count and this increases reliability. Greater flexibility is allowed and

there is potential for a more complex and higher performance control system.

The main limitations of a microprocessor are speed and accuracy (particularly in an 8 bit system). These may be important in applications requiring fast response times and high levels of accuracy, for example, rolling mill or paper machine drive motors.[73]

Since 1980, several papers have been published on the use of microprocessors in dc drives (see references 12 and 70-76). This is likely to become an increasingly attractive option, particularly with developments such as including the A-D converter, RAM and ROM on a single chip.[77]

6.3 HARDWARE

The diagrams of all circuits discussed are listed in Appendix 9. Figure 6.7 gives an overview of the system components. (See Appendix 9.)

6.3.1 The Microprocessor

An SDK 85 microprocessor system design kit[79] was used to develop the controller. This is based on the INTEL 8085 microprocessor.[80] Machine code instructions are entered via a hexidecimal keyboard and stored in RAM for ease of alteration during development. The final software could be stored in an EPROM.

Three I/O ports are available and these are used for the A-D converter and for supplying control signals to the chopper switches.

6.3.2 Analogue to Digital Conversion

The A-D contained an 8 channel multiplexor with decoding addresses listed in Table 6.1 outputed together with a 4-bit address. An end of conversion bit is returned once conversion is complete. Conversion time is about 10 μS. The A-D was adjusted to accept input voltages 0-5 V and to yield a digital output $(00-FF)_h$. Details of operation are described in reference (76).

Multiplexor decoding

Channel	X0	X1	X2	X3	X4	X5	X6	X7
Address	18	19	1A	1B	14	15	16	17

TABLE 6.1

6.3.3 Interface Buffers (Figure 6.8)

The microprocessor ports are buffered and isolated from the chopper using an open collector buffer chip and an opto-isolator. The circuit described in Section 2.4.1.2 is used to enable high speed switching at the correct voltage level. The motoring hexfet requires a power supply with a separate ground reference. All other voltages used are referenced with respect to the microprocessor OV reference.

6.3.4 Feedback Measurement (Figure 6.9)

The armature and field currents need to be measured for both motoring and regenerating. Resistive shunts were used for this purpose. Other possibilities are the Hall effect transducer or the magnetoresistor. These alternatives may be preferred since they consume negligible power. They do, however, require additional circuitry for use.[3]

The circuit for the measurement amplifier is shown in Figure 6.9. A single chip containing four op-amps was used. An inverting amplifier was used for motoring current and a non-inverting configuration for regenerating and field currents.

6.3.5 Chopper Circuit (Figure 6.10)

The chopper was required to switch 80 V at 50 A. The hexfet armature switches consisted of two IRF 150s in parallel. Schottky diodes were used for freewheeling. Protection circuits as described in Section 2.3 were used.

A difficulty is encountered when using two capacitive turn off snubbers in a bidirectional chopper, since the snubber on the non-conducting switch provides a momentary short circuit path across the supply. One solution is simply to use zener diodes for protection. Alternatively a turn-on snubber (see 2.4.3) could be included in the circuit. A further possibility is to insert a fast switching transistor in the snubber circuit. The snubbers could then be interlocked to the controller to ensure that the two are not simultaneously operational.

Two 14 000 uF electrolytic capacitors were used to smooth the battery current.

The circuit layout was carefully designed to minimise circuit inductance. This is shown in Figure 6.3. The heatsink was over-designed and could have been much smaller. (Figure 6.3 is shown overleaf.)

6.4 SOFTWARE

A flowchart for the software is contained in Figure 6.4 and a program listing in Appendix 9.2.

Operator setpoints are required for motoring torque (T_{MO}) and regenerating (braking) torque (T_{RO}). These are read through channels X0 and X1 of the A-D. They are then compared and the greater becomes the current torque setpoint (T_o). At the same time T_{sign} (stored in register C) is set to 1 for motoring or for regenerating.

Since $T = KI_fI_q$, the current setpoint (I_{qo}) is proportional to $\sqrt{T_o}$ in the linear region and proportional to T_o in the cut-off region. A lookup table (locations 8100 - 81FF) is, therefore, used to find the setpoint I_{qo} corresponding to T_o.

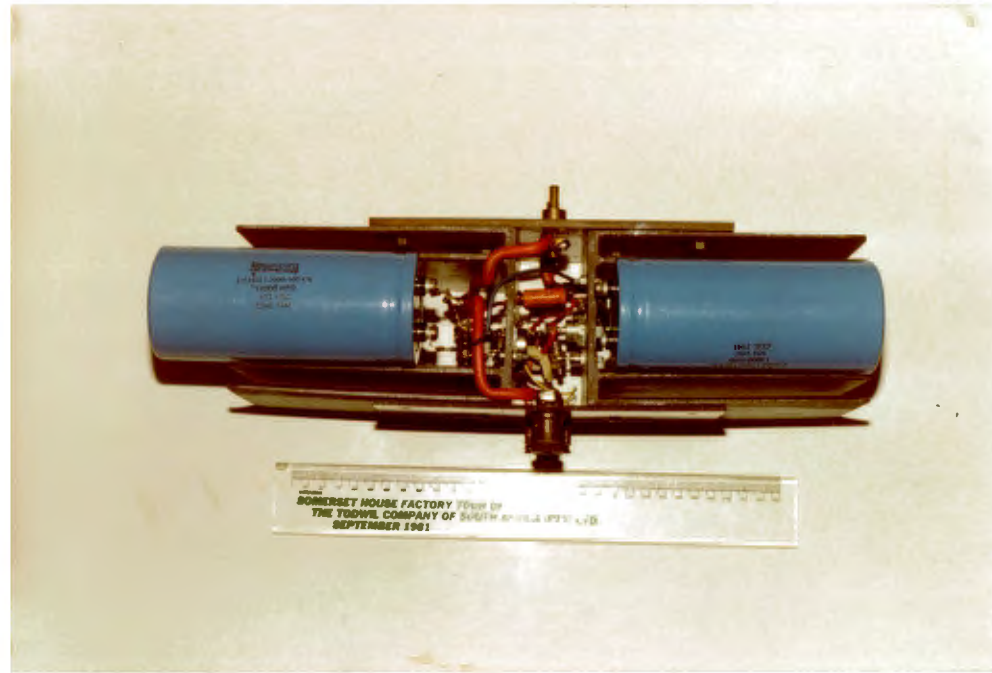
SOMERSET HOUSE FACTORY
THE TOOWOL COMPANY OF
SEPTEMBER 1961

FIGURE 6.3

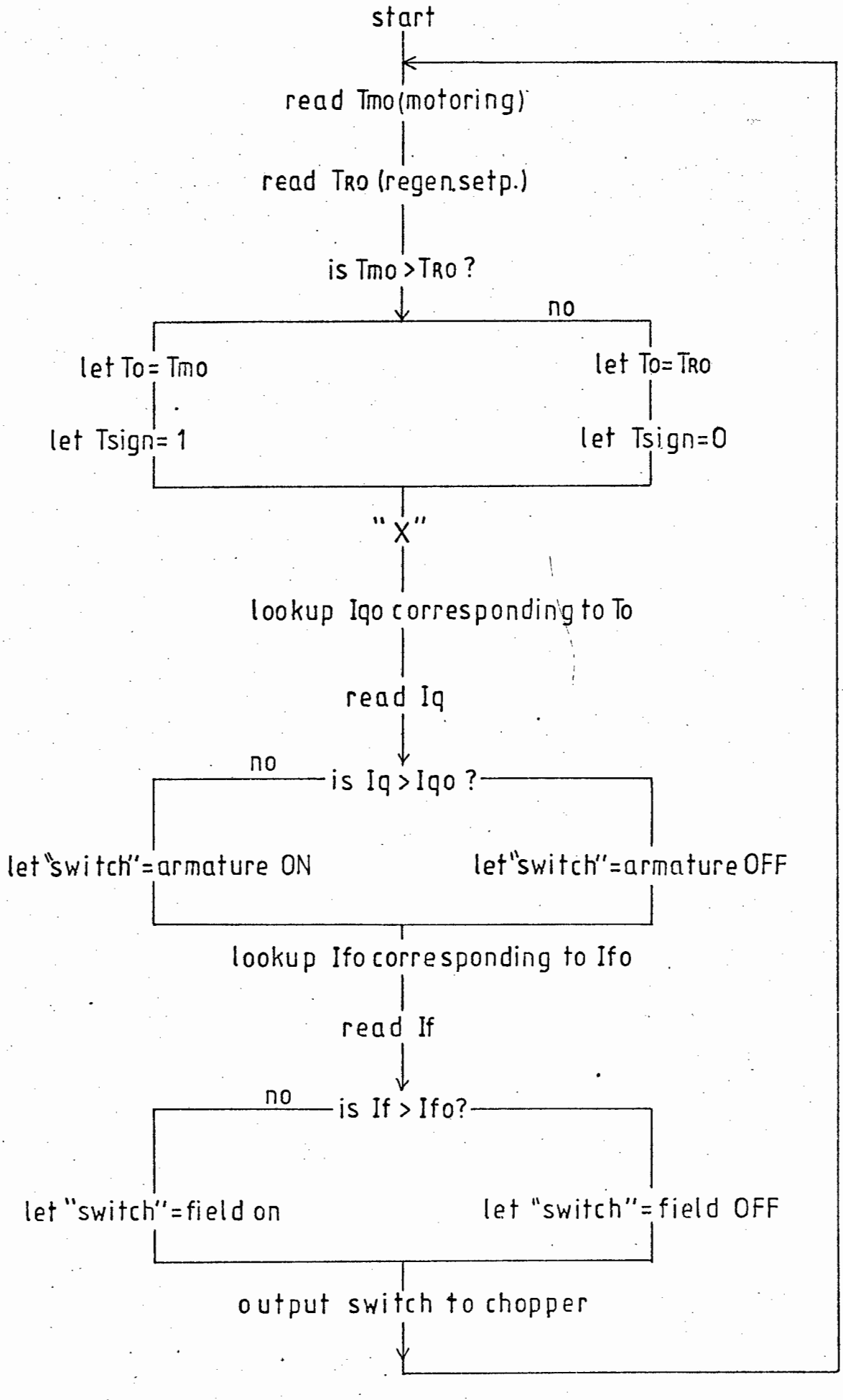
start
read Tmo(motoring)
read TRO (regen.setp.)
is Tmo > TRO ?
no
let To= Tmo
let Tsign= 1
let To= TRO
let Tsign=0
" X"
lookup Iqo corresponding to To
read Iq
no
is Iq > Iqo ?
let "switch"=armature ON
let "switch"=armature OFF
lookup Ifo corresponding to Ifo
read If
no
is If > Ifo?
let "switch"=field on
let "switch"=field OFF
output switch to chopper

figure 6·4

The armature current is read through A-D channel X2 or X3 (motoring or regenerating current depending on T_{sign}). This value is then compared with the setpoint and a decision is made whether to switch the armature chopper switch ON or OFF.

An 8-bit output port is available and the three lowest bits are used for switching the chopper. The variable "SWITCH" (stored in register D) is set according to Figure 6.5. Armature ON is defined as either S_M or S_R ON, depending on T_{sign}.

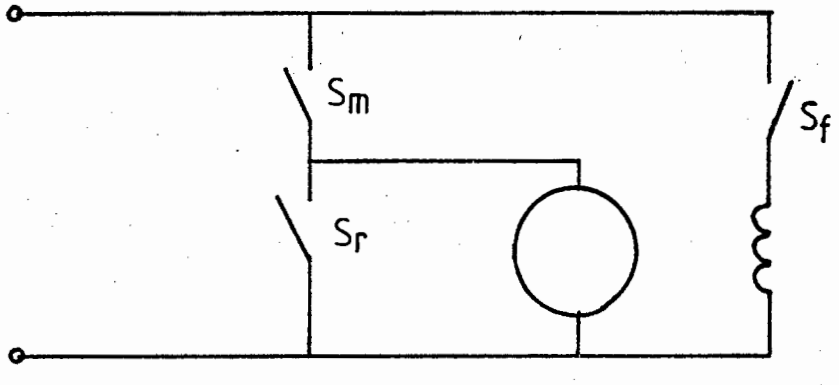

FIGURE 6.5

S_R "ON" bit 0 = 1 switch = $(01)_H$

S_M "ON" bit 1 = 1 switch = $(02)_H$

S_f "ON" bit 2 = 1 switch = $(04)_H$

The optimum control equation is also stored in a lookup table (locations 8200 to 82FF). Thus the field current setpoint (I_{fo}) corresponding to I_{qo} is found. The actual field current is read and compared with the setpoint. The variable "SWITCH", containing the correct control signals is outputed

to the chopper. The inverse logic of the chopper requires that "SWITCH" be first inverted.

6.5 DISCUSSION ON DESIGN

The controller and chopper described were built and tested. The microprocessor was able to switch up to a frequency of 2KHz. The field was shown to track the armature current in a manner described by the control equation. Since the control equation is stored in a lookup table, it should be noted that it is easily adapted for any control equation and, therefore, the exact optimum equation could be used rather than the series approximation.

The controller provided a constant torque characteristic. The constant torque-constant power combination suggested in Section 5.1.2 can be implemented using the flowchart in Figure 6.6, inserted at point "X" in Figure 6.4.

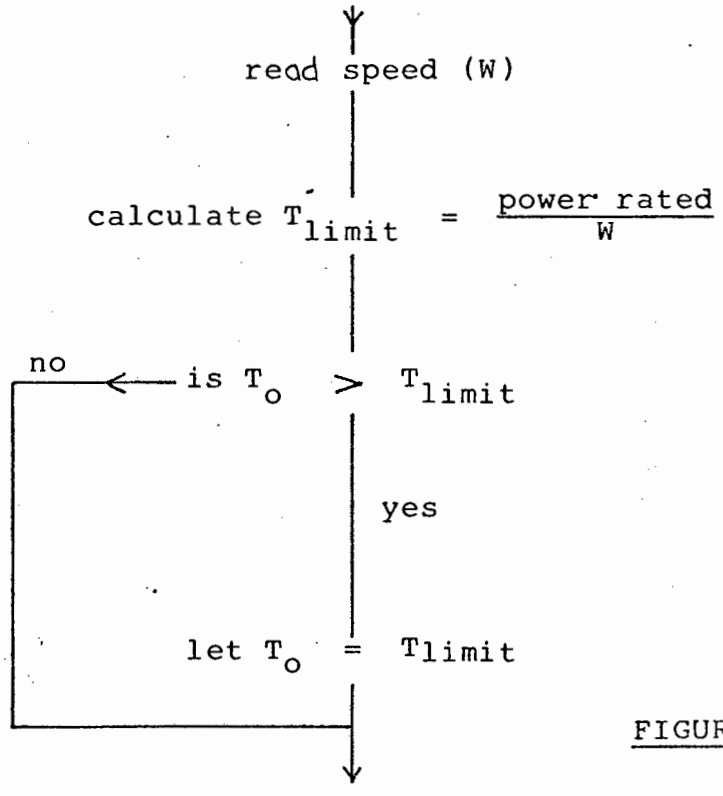

FIGURE 6.6

This would require the measurement of speed and a standard divide routine. Alternatively, the speed could be calculated by the microprocessor from

$$W = (E_q - I_q R_q) / KI_f$$

Another possibility is to have the constant torque controller limited by a temperature feedback signal[11] instead of the rating P_{rated}/W. This would ensure that optimum power is available from the system.

A further adaptation could be the use of a single A-D converter to measure positive and negative armature currents and a single torque setpoint for both motoring and regenerating.[6] This would increase the speed of the program since only one setpoint need be read. The speed could be further increased by only reading the setpoint every 10th cycle for example.

It should be noted that a practical design would require an interrupt signal and corresponding software to stop the program. The reset button on the SDK 85 kit fulfilled this and simultaneously switched all the hexfets OFF.

6.6 ANALOGUE ALTERNATIVE

A block diagram for a possible analogue alternative is shown in Figure 6.11. The absolute value of I_q can be found using the circuit in Figure 6.11b.

The switches S_M and S_R in Figure 6.5 are always switched in a complementary manner. Thus a single armature control signal is required. Regeneration will automatically occur when required (see Section 2.1.2).

It should be noted that this circuit gives optimum current control but does not give the required torque-speed characteristic. A square root transfer function would be required which is difficult to implement. It may be possible to do this using the fact that

$$x = \text{antilog } (\tfrac{1}{2}\log x)$$

and using the diode characteristic as in reference (63).

CHAPTER 7

CONCLUSIONS

7.1 REVIEW

Each element of a dc motor drive system has been investigated in detail with regard to the criteria of efficiency. The goal has been to minimise losses at each stage and also to model each component as accurately as possible in order to analyse the overall system using a computer.

7.1.1 Chopper

The chopper is designed in this thesis and thus has potential for efficiency improvement. A well designed circuit can reduce chopping losses to negligible proportions.

Chopper losses fall into four categories: switching, snubber, on-state and inductor losses. Switching losses are minimised by using hexfets with high speed switching drivers. Careful component choice and circuit layout eliminates the need for snubbers. However, snubbers alter the switching load line characteristic and optimising component values can further reduce switching losses. With these measures, switching and snubber losses are negligible.

The on-state loss is the most significant chopper loss. It is reduced by paralleling hexfets and using a large heatsink since the on-state resistance is reduced if temperature is reduced. Using Schottky diodes reduces the on-state diode loss.

If the inductor is too small an additional loss will be caused

by the increased form factor owing to the output current ripple. In addition hysteresis and eddy current losses will be caused by the high chopping frequency. A higher chopper frequency reduces the ripple and thus reduces all inductor losses.

The choice of chopping strategy affects frequency and ripple. PWM and TLC are shown to be equally good while PFM is seen to be unattractive.

Transfer equations are developed to model the chopper. The on-state loss is modelled by a small resistance which is included with the armature resistance (this being an approximation). Other losses are regarded as negligible in the final model.

7.1.2 Motor

The motor is regarded as a given and its design is not investigated. It is important, however, to use a motor with laminated iron poles.

The copper, brush, no load iron, mechanical and stray load losses are modelled and the constants determined experimentally. The model is able to predict efficiency to within about 2%.

7.1.3 Battery

The battery losses can be reduced by reducing the form factor

of the battery current. Several methods of doing this are described and the method proposed is the use of a large capacitor in parallel with the battery. In addition it is possible to reduce the losses by smoothing the current over the operational cycle. An aproximate model and equivalent circuit is described, a simple resistance and EMF being insufficient.

7.1.4 Field and Armature Current Control

Efficiency can be improved by controlling both armature and field currents. The control equation is defined as the relationship between the two currents at various torque values. The optimum efficiency control equation is similar to a discontinuous series characteristic, where field current is proportional to armature current and field current is limited at its rated value.

This optimum controller can be implemented using a microprocessor.

For a typical electric vehicle speed-torque test cycle, the saving of the optimum controller is not very significant (less than 1%). However, for applications which operate for long periods at low speed and torque this saving will be more significant. The saving in larger motors is also likely to be more significant. It should be noted that a permanent magnet motor is more efficient than the optimum field controlled motor over a standard test cycle.

7.2. CONCLUSION

The overall efficiency of a dc-dc drive system has been investigated in detail and minimisation of losses is discussed. A computer program is described which can be used to find the characteristic optimum control equation for any motor if the machine constants are measured.

The only further possibilities for efficiency improvement lie in the redesign of the motor and battery and also the use of a gearbox or torque converter. The latter possibility is discussed in references (20, 6, 67, 70).

REFERENCES

1. P. Wood, Switching Power Converters, Van Nostrand, New York, 1981.

2. A.B. Plunkett and G.B. Kliman, Electrical Vehicle AC Drive Development, General Electric, New York, December 1979.

3. M.D. Claassen, A DC Chopper Controller for a Battery Electric Vehicle, M.Sc. Thesis, University of Cape Town. 1973.

4. W. McMurray, Stepless Solid-State Controls for Battery-Powered DC Electric Vehicles, Control in Power Electronics and Electrical Drives - IFAC Symposium reprints Vol.2, Düsseldorf, October 1974, pp.421-435.

5. J. Finnell and R. Hoft, Thyristor Step-Up Chopper for Modified Series Motor, IFAC Symposium (as in 4), Oct. 1974, pp.89-101.

6. B. Berman, Battery Powered Regenerative SCR Drive, IEEE transactions on Industrial Applications. Vol.IA-8, No.2, March 1972

7. R. Bailey, D. Williamson and T. Stitt, A Modern Chopper Propulsion System for Rapid Transit Application with High Regeneration Capability, IEEE Trans. Ind. Appl. Vol.IA-14, No.6, December 1978.

8. B.Berman, All Solid-State Method for Implementing a Traction Drive Control, IEEE Trans. Ind. Appl. Vol.IA-8 No.2, March 1972.

9. R. Zeccola and E. Weiser, Thyristor (SCR) Chopper Control System for Transportation Equipment, IEEE Trans. Ind.&Gen. Appl. Vol.IGA-5, July 1969.

10. J. Byrne and J. Lacy, Compatible Controller-Motor System for Battery Electric Vehicle, IEEE Proceedings, Vol.117, No.2, February 1970.

11. B. Bose and R. Steigerwald, A DC Motor Control System for Electric Vehicle Drive, IEEE Trans. Ind. Appl. Vol.IA-14, No.6, November 1978.

12. R. Steigerwald, A Two Quadrant Transistor Chopper for an Electric Vehicle Drive, IEEE Trans. Ind. Appl. Vol.IA-16, No.4, July 1980.

13. J. Garnier, S. Manzoni and P. Vilpert, Electrical Equipment for Chopper Trolleybuses, Brown Boveri Rev. 12-78.

14. J. Brokman, J. King and A. Kusko, Rapid Transit Experience with Chopper Controlled DC Motor Propulsion, IEEE Trans Ind. Appl. Vol.IA-16, No.3, May 1980.

15. J. Garnier and P. Riondel, Solid State Control Systems - A Means of Optimising the Operation of Electric Traction Vehicles, Brown Boveri Rev. July, 1979.

16. B. Berman, Design Considerations Pertaining to a Battery Powered Regenerative System, IEEE Trans Ind. Appl. Vol.IA-8, No.2, March 1972.

17. H. Knöll, High-Current Transistor Chopper, 2nd IFAC Symposium Procedure, Düsseldorf, October 1977.

18. E. Reimers, Design Analysis of Multiphase DC Chopper Motor Drive, IEEE Trans. Ind. Appl. Vol.IA-8, No.2, March 1972.

19. E. Reimers, An Application of Two-Phase DC Chopper Motor Drive, IEEE Trans. Ind. Appl. Vol.IA-9, No.3, May 1973.

20. J. Welz and H. Van Niekerk, The Use of a Gearbox for Efficiency Control in the Drive System of a Battery Vehicle, Symposium on Electric Transport SAIEE Proceedings, 10-11 April, 1979.

21. J.D.N. Van Wyk, A Review of the Current Status and Future Prospects of Battery-Powered Electric Road Vehicles, SAIEE Trans Ind. Appl. February 1978.

22. J.D.N. Van Wyk, Battery-Driven Vehicles, Energy Utilisation Unit of the University of Cape Town, paper 7-7.

23. A. Cupsa, Analysis of Drives for Electric Road Vehicles - Requirements, Basic Design, Properties, Value and Optimisation Criteria, 2nd IFAC Symposium Proc. (Pergamon press), October 1977, pp.835-840.

24. B. Smith, A Simple Bilateral Variable-Ratio dc Pulse Converter, Trans. Ind. Appl. Vol.IECI-15, November 1968.

25. S. Dewan and A. Straughen, Power Semi-conductor Circuits, Wiley-Interscience, New York, 1975.

26. A. Michel and H. Voss, Frequency and Current Ripple of DC-DC Power Converters with Respect to Different Modulation Techniques, IEEE Trans Ind. Appl. Vol.IA-16, No.3, May 1980.

27. T. Barton, The Transfer Characteristics of a Chopper Drive, IEEE Trans Ind. Appl. Vol.IA-16, July 1980.

28. P.W. Franklin, Theory for the DC Motor Controlled by Power Pulses, IEEE Conference Recording of 5th Annual Meeting of Ind.and General Appl. Group, 1970.

29. S. Cúk, Advances in Switched-Mode Power Conversion, IEEE Trans Ind. Appl. Vol.IE-30, No.1, February 1983.

30. B.D. Bedford and R.G. Hoft, Principles of Inverter Circuits, John Wiley and Sons, New York, 1964.

31. I. Takahiko, New DC Chopper Circuits using Fast-Switching

Reverse-Conducting Thyristors for Low-Voltage DC Motor Control, IEEE Trans Ind. Appl. Vol.IA-16, No.1, January 1980.

32. M.W. Smith, Series Switching Regulator Using General Electric Switch-Power™ Power Transistors, General Electric publication 200.83, New York, September 1979.

33. R.J. Walker, Circuit Techniques for Optimising High Power Transistor Switching Efficiency, Proc. POWERCON 5 - Fifth National Solid-State Power Conversion Conference, San Francisco, May 1978.

34. M.J. Case, A Direct AC to AC Regenerative Frequency and Voltage Converter, UCT Ph.D. Thesis, July 1980.

35. Various Authors, Power Transistors in the Switching Mode, Sescosem, Aix on Provence, 1974.

36. Hexfet Data Book, International Rectifier, California, 1981.

37. M.W. Smith, Conduction and Switching Losses in Power Transistors, General Electric publication 200.84, New York, September 1979.

38. J. Chopra and D. Roark, Base Drive and Snubber Circuit Techniques for the Minimisation of Transistor Switching Losses, 2nd IFAC Symposium Proceedings, Düsseldorf, October, pp.148-155.

39. Philips Semiconductor and Integrated Circuits - part 1, Philips, Netherlands, September 1971.

40. J.R. Schwab, Performance of a 14.9 KW Laminated-Frame DC Series Motor with Chopper Controller, US National Aeronautics and Space Administration Publication DOE/NASA/1044-79/2, June 1979.

41. D. Fink and J. Carroll, Standard Handbook for Electrical Engineers, McGraw-Hill, USA, 1968.

42. A.Balestrino, et al., Pulse Ratio Modulation - An Interesting Technique to Implement dc to dc Conversion, IFAC Symposium, 1977, pp.165-172.

43. R.B. Prest, High Performance DC to DC Chopper Using a Microprocessor, UCT B.Sc. Thesis, 1981.

44. A. Laingsdorf, Principles of dc Machines, McGraw-Hill, 1940.

45. C. Carr, Electric Machinery; Wiley, New York, 1958.

46. A. Daniels, Introduction to Electrical Machines, McMillan London, 1976.

47. A. Clayton, Performance and Design of Electrical Machines, Pitman, London, 1938.

48. H. Colton, Design of Electrical Machinery, Oxford University Press, London, 1934.

49. A. Still and C. Siskind, Elements of Electrical Machine Design, McGraw-Hill, New York, 1954.

50. R. Kloeffler et al., DC Machinery, McMillan, New York, 1949.

51. A.A. Middlecote, Service Operation of DC Traction Motors, SAIEE Trans Ind. Appl. Vol.43, part 4, April 1952.

52. O.E. Mainer, Reducing Brush Losses, Electrical Journal, 2 October 1959.

53. Torque Transduces T1 and T2 Operating Manual, Hottinger Baldwin Messtechnik (Manual supplied with transducer).

54. C. Amato, Latent Losses in 'Lectric Lizzies, IEEE Trans Ind. Appl. Vol.IGA-5, No.5 September 1969.

55. H. Van Niekerk, Enkele notas oor algemene vereistes vir die aandryfstelsel van battery-aangedrewe elektriese voertuie, CSIR publication, May 1982.

56. R.C. Shair, Lead Acid Storage Batteries in Telephone Service, AIEE Trans. Part 2 - Applic. and Ind. No.47, March 1960.

57. H.G. Zimmerman and R.G. Peterson, An Electrochemical Cell Equivalent Circuit for Storage Battery/Power System Calculations by Digital Computer, ENERGY 70 Inter-society Conversion Engineering Conference Proceedings Vol.1, Las Vegas, September 1970.

58. G.W. Vinal, Storage Batteries, John Wiley and Sons, New York, 1955.

59. J.J. Welz, Some Aspects of Battery Driven Vehicle Testing, CSIR Special Report ELEK179, July 1980.

60. W. Runge, Untersuchungen an Bleikkumulatoren, Wissenchaftliche Mitteilungen aus dem Institut für Elektrische Antriebe der Rheinisch - Westfälischen Technische Hochschule Aachen. Herausgegeben von T. Wasseraab, 1973.
(This reference is quoted in (59)).

61. G. Kortun and J. Bockris, Textbook of Eletrochemistry, Elsevier Publishing Company, 1951, p.363.

62. G. Wille, A range measuring device for electric vehicles, "Micro-electronics in power electronics" VDE conference proceedings, Darmstadt, October 1982.

63. B.M. Bird and R. Harlen, Variable Characteristic dc machines, Proceedings IEEE, Vol.113, No.11, November 1966.

64. HP-85 Owners Manual and Programming Guide, Hewlett-Packard Company, USA, 1979.

65. Electric Vehicle Test Procedure - SAE Recommended Practice, SAE J227a, February 1976.

66. H.R. Van Niekerk, Comparison of the Energy Consumption During Start/Stop Driving Conditions of Two Types of Battery Vehicle Drive Systems, CSIR Special Report Elek 238, March 1982.

67. H.R. Van Niekerk and J.J. Welz, Automatic gearshift control for an efficient battery vehicle drive system, Paper No.8012 presented at EV Expo 80 Conference, Missouri, May 1980.
(This reference is quoted in (66)).

68. M. Pachter, Speed control of a field controlled DC motor, Technical Report TWISK 120, NRIMS, October 1979.
(This reference is quoted in (66)).

69. Laboratory simulated studies of lead acid traction batteries under duty cycles normal to electric vehicle service, Journal of electro-analytical chemistry, Vol. 118, 1-470, 1981, p.131.

70. B.B. Van Zyl, Microprocessor control applied to an electric vehicle system, Pulse, December 1981, p.12.

71. Y.T. Chan et al., A Microprocessor-based current controller for SCR-DC Motor Drives, IEEE Trans Ind. Appl. Vol.IECI-27, No.3, August 1980, p.223.

72. B. Williams, Microprocessor Control of DC 3-phase Thyristor Inverter Circuits, IEEE Trans on Ind. Electr. and Control Instr., vol.IECI-27, No.3, August 1980, p.223.

73. T. Konishi et al., A performance analysis of micropro-

cessor-based control systems applied to adjustable speed motor drives, IEEE Trans Ind. Appl. Vol.IA-16, No.3, May 1980, p.378.

74. S. Dewan and A. Mirbod, Microprocessor-based optimum control for four-quadrant chopper, IEEE Trans on Industrial Applications, Vol.IA-17, No.1, January 1981.

75. W. Dunford and S. Dewan, The design of a control circuit for a two-quadrant chopper based on the Motorola 6800 Microprocessor, IEEE Trans Ind. Appl., IA-16, No.4, July 1980.

76. P. Kulentic, Microprocessor Control of a Cycloconverter, UCT M.Sc. Thesis, 1980.

77. W. Ittner and J.A. Miller, Microcomputer's on-chip Functions Ease User's Programming Chores, Intel Corp. Article AR-63, August 1978.

78. H. Grotstollen, Comparison of Speed Controlled DC Drives With and Without Subordinate Current Loop, 2nd IFAC Symposium Proceedings, Düsseldorf, October 1977, p.583.

79. SDK-85 User's Manual, Intel Corporation, December 1977.

80. MSC-85 User's Manual, Intel Corporation, September 1978.

81 M.B. Stout, Basic Electrical Measurements, Prentice-hall Incorporation, Englewood Cliffs, N.J., USA, 1960.

APPENDIX 1

CHOPPER TRANSFER EQUATIONS

1.1 EQUATIONS FOR BATTERY AND MOTOR CURRENT

1.1.1 Problem

Derive expressions for average battery and motor currents in terms of mark space ratio M. Constants are inductance L, resistance R, battery voltage E_B and armature voltage E_q.

1.1.2 Assumptions

(i) Continuous current is assumed. This will always be the case when a bidirectional chopper is used.

(ii) It will take several cycles before a steady state is reached. Steady state operation is assumed here.

The circuit is shown in Figure 2.1, the mark space ratio is defined in equation 2.1 and T_A and T_B are defined in Figure 2.2.

1.1.3 Solution

1.1.3.1 Differential equations

(i) **Time interval T_A:**

$$E_B = E_q + Ri(t) + L\frac{di}{dt}$$

solution: $$i_{(t)} = \frac{E_B - E_q}{R} + Ae^{-\frac{R}{L}t} \qquad (a)$$

note: Both time and voltage origins are chosen as the commencement of time interval T_A.

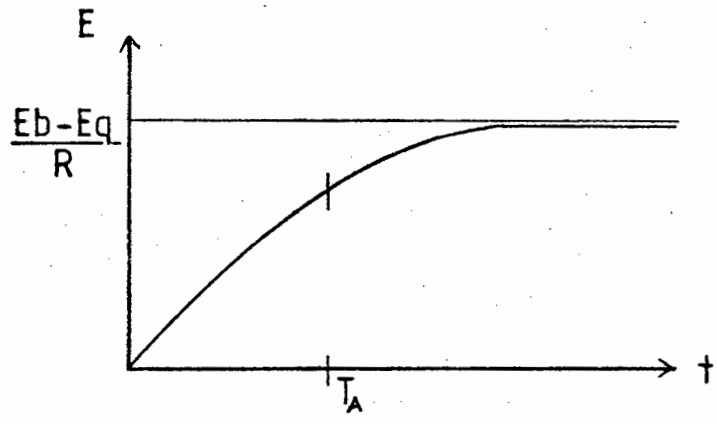

(ii) **Time interval T_B**

$$O = E_q + Ri(t - T_A) + B_e^{-\frac{R}{L}(t - T_A)}$$

solution: $$i_{(t)} = -\frac{E_q}{R} + Be^{-\frac{R}{L}(t - T_A)} \qquad (b).$$

note: The origin of this equation is offset from zero by the time T_A.

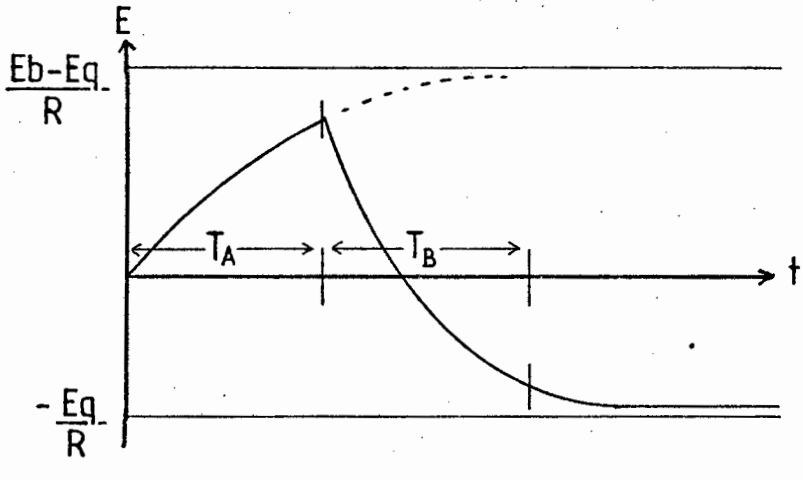

1.1.3.2 Boundary Conditions

(i) Voltage at end of period T_A must equal voltage at beginning of T_B for continuity.

$$\text{therefore} \quad i(t_A) = \frac{E_B - E_q}{R} + Ae^{-\frac{R}{L}T_A}$$

$$= -\frac{E_q}{R} + Be^{-\frac{R}{L}(T_A - T_A)}$$

$$\text{therefore} \quad B = \frac{E_B}{R} + Ae^{-\frac{R}{L}T_A} \qquad (c)$$

(ii) Voltage at beginning of T_A must equal voltage at end T_B for steady state operation.

Therefore i(o) from equation (a) = $i(T_A + T_B)$ from equation (b)

$$\text{Therefore} \quad \frac{E_B - E_q}{R} + A = -\frac{E_q}{R} + Be^{-\frac{R}{L}(T_A + T_B - T_A)}$$

$$\text{Therefore} \quad \frac{E_B - E_q}{R} + A = \frac{-E_q}{R} + \frac{E_B}{R}e^{-\frac{R}{L}T_B} + Ae^{-\frac{R}{L}(T_A + T_B)}$$

(eliminate B using (c))

$$\text{Therefore} \quad A = -\frac{E_B}{R} \frac{e^{-\frac{R}{L}T_B} - 1}{e^{-\frac{R}{L}(T_A + T_B)} - 1} \qquad (d)$$

1.1.3.3 Final equations

Boundary conditions (c) and (d) are substituted in D.E. solutions (a) and (b).

(i) **Time interval T_A**

$$i_{(t)} = \frac{E_B - E_q}{R} - \frac{E_B}{R} \frac{e^{-\frac{R}{L}T_B} - 1}{e^{-\frac{R}{L}(T_A + T_B)} - 1} e^{-\frac{R}{L}t} \qquad (e)$$

(ii) **Time interval T_B**

$$i_{(t)} = -\frac{E_q}{R} + \frac{E_B}{R} e^{-\frac{R}{L}T_A} - \frac{e^{-\frac{R}{L}T_B} - 1}{e^{-\frac{R}{L}(T_A + T_B)} - 1} e^{-\frac{R}{L}t}$$

$$= -\frac{E_q}{R} + \frac{E_B}{R} \frac{e^{-\frac{R}{L}T_A} - 1}{e^{-\frac{R}{L}(T_A + T_B)} - 1} e^{-\frac{R}{L}(t - T_A)} \qquad (f)$$

1.1.3.4 Average value of battery current

Referring to figure (2·2), the battery current is zero during interval T_B and equal to armature current during interval T_A.

$$I_{ave} = \frac{1}{T}\int_o^T i\,(t)dt \quad \text{where } T = \text{period of chopping cycle}$$

Therefore $$I_{Bave} = \frac{1}{T_A + T_B}\int_o^{T_A} \left[\frac{E_B - E_q}{R} - \frac{E_B}{R}\left(\frac{e^{-\frac{R}{L}T_B} - 1}{e^{-\frac{R}{L}(T_A + T_B)} - 1}\right) e^{-\frac{R}{L}t}\right] dt$$

Therefore $$I_{Bave} = \frac{E_B - E_q}{R} \cdot \frac{T_A}{T_A + T_B} + \frac{1}{T_A + T_B} \cdot \frac{E_B L}{R^2} \frac{(e^{-\frac{R}{L}T_B} - 1)}{e^{-\frac{R}{L}(T_A + T_B)} - 1} \quad (g)$$

1.1.3.5 Average value of armature current

$$I_{q\,ave} = \frac{1}{T}\int_0^{T_A} i(t)dt + \frac{1}{T}\int_{T_A}^{T_A + T_B} i(t)dt$$

$$= \frac{E_B - E_q}{R} \frac{T_A}{T_A + T_B} + \frac{E_B L}{R^2 (T_A + T_B)} \frac{(e^{-\frac{R}{L}T_B} - 1)(e^{-\frac{R}{L}T_A} - 1)}{(e^{-\frac{R}{L}(T_A + T_B)} - 1)}$$

$$- \frac{E_q}{R} \cdot \frac{T_B}{(T_A + T_B)} - \frac{E_B}{R^2} \frac{L}{(T_A + T_B)} \frac{(e^{-\frac{R}{L}T_A} - 1)(e^{-\frac{R}{L}T_B} - 1)}{(e^{-\frac{R}{L}(T_A + T_B)} - 1)}$$

$$= \frac{E_B}{R} \cdot \frac{T_A}{T_A + T_B} - \frac{E_q}{R} \quad (h)$$

1.2 CURRENT EQUATIONS ASSUMING INFINITE INDUCTANCE AND FREQUENCY

1.2.1 Problem

Does the equation for average battery current simplify if the inductance (L_q) is very high or if the chopping frequency is very high (i.e. small period T)?

Described mathematically, find Lim as $\frac{T}{TC} \rightarrow 0$ of $I_{Bave}(\frac{T}{TC})$ for any given mark space ratio (M) where T = chopping period and TC = electrical time constant = L_q / R_q.

1.2.2 Solution

Taking part of equation (2.2) let $x = \frac{T}{TC}$

and $$y = \frac{f(x)}{g(x)} = \frac{(e^{-(1-M)x} - 1)(e^{-Mx} - 1)}{x(e^{-x} - 1)}$$

according to the final value theorem, $\lim_{x \to 0} \frac{f(x)}{g(x)} = \lim_{x \to 0} \frac{f'(x)}{g'(x)}$

$$y_1 = \frac{f'(x)}{g'(x)} = \frac{-e^{-x} + Me^{-Mx} + (1 - M)e^{-(1-M)x}}{-X\, e^{-x} + e^{-x} - 1}$$

$$y_2 = \frac{f''(x)}{g''(x)} = \frac{e^{-x} - M^2 e^{-Mx} - (1-M)^2 e^{-(1-M)x}}{xe^{-x} - e^{-x} - e^{-x}}$$

$$\lim_{x \to 0} y_2 = \frac{1 - M^2 - (1 - M)^2}{-2}$$

$$= M(M - 1) \qquad (a)$$

substituting (a) back into equation (2.2)

$$I_{Bave} = \frac{E_B - E_q}{R_q} M + \frac{E_B}{R_q} \cdot M(M - 1)$$

$$= \frac{E_B}{R_q} M^2 - \frac{E_q}{R_q} M \qquad (b)$$

1.3 VERIFICATION OF CURRENT EQUATIONS ASSUMING POWER IN AND OUT ARE EQUAL

1.3.1 Problem

Verify equation 2.3 by using the fact the power in and power out of the chopper are equal.

1.3.2 Assumptions

(i) The chopper is lossless.

(ii) If the time constant $\frac{L}{R}$ is small compared with the chopping period (T), there will be an additional loss in the resistance due to the form factor of the armature current.

Here it is assumed that $\frac{L}{R} \gg T$, so that this loss is negligible.

1.3.3 Solution

The circuit is represented in Figure (a)

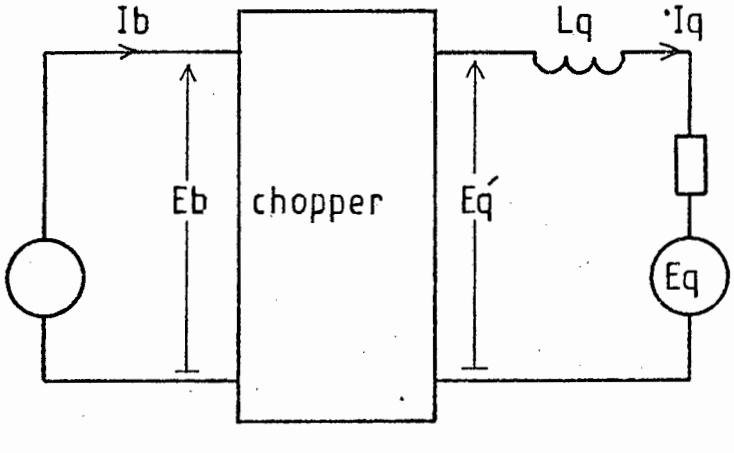

fig. a

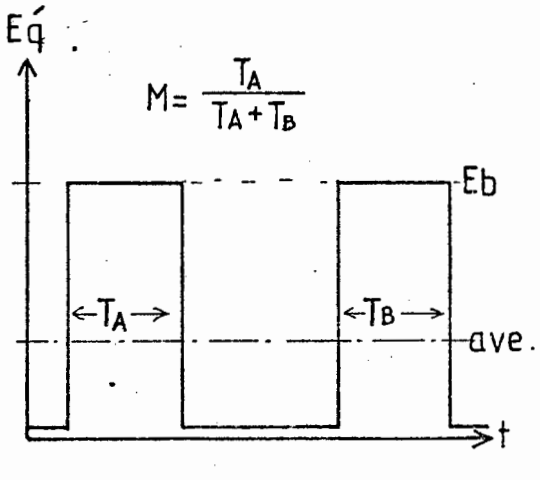

fig. b

From Figure (b) it can be seen that average $E_q' = ME_B$ (a)

(Note: This is true even without assumption ii)

Equating power in and power out:

$$E_B I_B = E_q' I_q$$

therefore $E_B I_B = ME_B I_q$ (eliminate E_q' using (a))

therefore $I_B = MI_q$ (b)

Average current through R

$$I_q = \frac{E_q' - E_q}{R_q}$$

therefore $$\frac{I_B}{M} = \frac{ME_B - E_q}{R_q}$$

therefore $$I_B = \frac{E_B}{R_q} M^2 - \frac{E_q}{R_q} M \quad (c)$$

which is the same as equation (2.3)

APPENDIX 2

CAPACITIVE-SNUBBER LOSSES

2.1 PROBLEM

Determine the losses in the capacitive snubber circuit shown in Figure 2.10.

2.2 ASSUMPTIONS

It is assumed that the current in the hexfet decreases linearly and the capacitor current increases linearly such that the sum of the two currents remain constant during the switching interval.

It is assumed that the switching time is short enough and the capacitor large enough so that it is not charged to the full supply voltage during the switching interval (t_s).

The diode is also assumed to switch instantaneously and stray inductance is neglected.

2.3 SOLUTION

2.3.1 Formula for $V_c(t)$

$$V_c = \frac{1}{C}\int i_c(t)dt \qquad (a)$$

where $V_c = V_{across\ Capacitor}$ and t_s = switching time

and

$$i_c(t) = I_L \frac{t}{t_s} \qquad (b)$$

where I_L is the current being switched and $i_c(t)$ is the capacitor current.

the charge on C at t_c

$$CV_s = I_L(\frac{t_s}{2} + t_c - t_s)$$

therefore, $$C = \frac{I_L}{V_s}(t_c - \frac{t_s}{2}) \qquad (c)$$

substituting (b) and (c) into (a)

$$V_C = \frac{V_s}{t_s(2t_c - t_s)} t^2$$

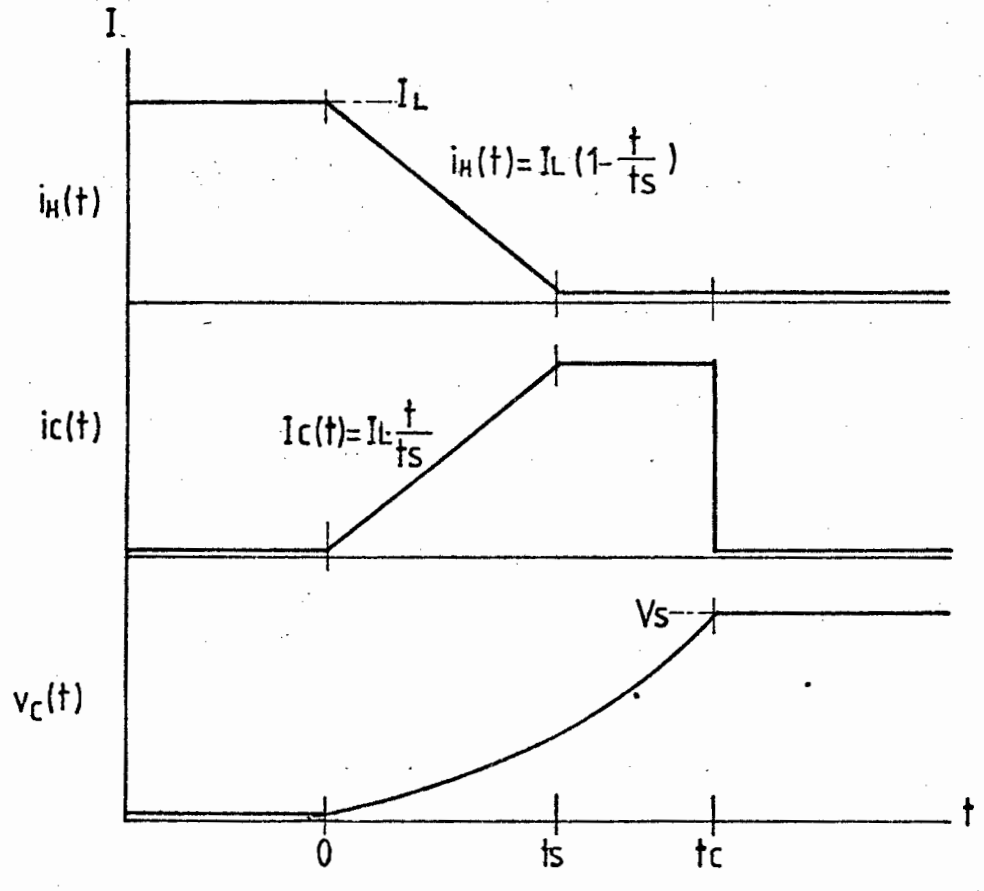

2.3.2 Energy Losses in the Hexfet During Turn-Off

$$E_H = \int_0^{t_s} V_C \cdot i_H dt$$

$$= \frac{V_s I_L}{t_s(2t_c - t_c)} \int_0^{t_s} (1 - \frac{t}{t_s}).t^2 dt$$

$$= \frac{V_s I_L t_s^2}{12(2t_c - t_s)} \qquad (d)$$

2.3.3 Energy Losses in the Snubber

$$E_c = \tfrac{1}{2} C V_s^2$$

eliminate C using equation (c)

therefore $$E_s = \frac{I_L V_s}{2} (t_c - \frac{t_s}{2}) \qquad (e)$$

APPENDIX 3

INDUCTOR LOSSES

3.1 PROBLEM

Find an equation for the loss in the inductor owing to form factor caused by the value of frequency or inductance being too low.

3.2 SOLUTION

The chopper input power is $P_{IN} = E_B I_B$

From the equation 2.2 in Section 2.1 for I_B, an expression for P_{IN} is obtained and normalised with respect to E_B^2 / R_q.

$$P_N = \frac{P_{IN}}{(E_B^2 / R_q)} = (1 - \frac{E_q}{E_B})M + \frac{(e^{-(1-M)\frac{T}{TC}} - 1)(e^{-M\frac{T}{TC}} - 1)}{\frac{T}{TC}(e^{-\frac{T}{TC}} - 1)} \qquad (a)$$

where M is the mark space ratio $M = \frac{T_A}{T_A + T_B}$, T is the chopping period and TC is the time constant L/R_q.

The ideal situation, assuming L is infinite or $\frac{T}{TC} \longrightarrow 0$ if found using equation 2.3

$$P_{N(ideal)} = \frac{P_{ideal}}{(E_{B^2} / R_q)} = M^2 - \frac{E_q}{E_B} M \qquad (b)$$

The power loss due to form factor is, therefore, the difference between equations (a) and (b).

$$P_{N(loss)} = M - M^2 + \frac{(e^{-(1-M)\frac{T}{TC}} - 1)(e^{-M\frac{T}{TC}} - 1)}{\frac{T}{TC}(e^{-\frac{T}{TC}} - 1)} \qquad (c)$$

APPENDIX 4

CONSTANTS

4.1 TEST MOTOR RATINGS

Voltage - 96 V

Current - 50 A

Power - 3.7 KW

Speed - 3 000 rpm

4.2 MACHINE CONSTANT

I_f(A)	$K(I_f)$ (WA^{-1})	I_f(A)	$K(I_f)$ (WA^{-1})
0.02	.2228	0.62	.2731
0.02	.2865	0.64	.2726
0.06	.3077	0.66	.2643
0.08	.3024	0.68	.2640
0.10	.3247	0.70	.2592
0.12	.3236	0.72	.2546
0.14	.3320	0.74	.2503
0.16	.3382	0.76	.2463
0.18	.3395	0.78	.2442
0.20	.3406	0.80	.2387
0.22	.3444	0.82	.2352
0.24	.3448	0.84	.2319
0.26	.3428	0.86	.2280
0.28	.3433	0.88	.2243
0.30	.3417	0.90	.2214
0.32	.3402	0.92	.2180
0.34	.3389	0.94	.2147
0.36	.3360	0.96	.2115
0.38	.3334	0.98	.2085
0.40	.3295	0.00	.2063
0.42	.3259	1.02	.2028
0.44	.3212	1.04	.2002
0.46	.3169	1.06	.1976
0.48	.3130	1.08	.1951
0.50	.3069	1.10	.1927
0.52	.3024	1.12	.1904
0.54	.2983	1.14	.1882
0.56	.2922	1.16	.1860
0.58	.2876	1.18	.1834
0.60	.2822	1.20	.1820

$$K_{remnant} = 0.0232 \ (WA^{-1})$$

The quantity K in the equation $E = K\phi W$ is a dimensionless quantity, therefore, in $E = K(I_f)I_f W$, the units of $K(I_f)$ are Webers per amp. $K_{remnant}$ is the part of the machine constant caused by remnant magnetism.

4.3 OTHER CONSTANTS

friction constants	k_{f1} =	4.577×10^{-4} Nm rad^{-1} sec
	k_{f2} =	0.125 Nm
eddy loss constant	k_E =	3.02×10^{-4} Nm rad^{-1} sec A^{-1}
hysteresis loss constant	k_H =	0.138 Nm A^{-1}
stray load constant	k_s =	7.17×10^{-7} Nm rad^{-1} sec A^{-2}
battery activation potential	k_{B2} =	2.61 A
	k_{B1} =	1.10 V^{-1}
battery resistance	R_B =	0.0217 ohms
armature resistance	R_q =	0.0846 ohms
interpole resistance	R_i =	0.042 ohms
field resistance	R_f =	28.3 ohms
brush voltage drop	V_B =	1.44 V

chopping period	T = 0.2 mS
Time constant	TC = 3 mS

APPENDIX 5

ACCURACY OF THE MODEL

5.1 DETERMINING ERRORS

Given a function of several variables the combined standard deviation can be determined if the standard deviations of the individual components are known.[81]

If the function is

$$X = f(x_1, x_2, x_3, \ldots)$$

then

$$\sigma(X) = \sqrt{(\frac{dX}{dx_1})^2 \sigma(x_1)^2 + (\frac{dX}{d_2})^2 \sigma(x_2)^2 + \ldots}$$

This equation is used to determine the error in calculating each of the motor constants.

5.2 Using the equation in 5.1, the standard deviation of the predicted efficiency from the actual motor efficiency can be estimated.

(a) $I_q = (T + T_f + T_i + T_s) / (K \times I_f)$

therefore, $$\sigma(I_q) = \left[\frac{\sigma(T_f)^2 + \sigma(T_i)^2 + \sigma(T_s)^2}{K^2 I_f^2} + \frac{(T_f + T_i + T_s + T)^2 \cdot \sigma(K)^2}{K^4 I_f^2}\right]^{\frac{1}{2}}$$

(b) $E_q = KI_fW + I_qR_q + V_B$

$$\text{therefore, } \sigma(E_q) = \sqrt{(WI_f\sigma(K))^2 + (R_q.\sigma(I_q))^2 + \sigma(V_B)^2 + (I_q\sigma(R_q))^2}$$

$$\text{(c)} \quad N = \frac{TW}{E_qI_q + I_f^2R_f}$$

$$\text{therefore, } \sigma(N) = \frac{TW}{(E_qI_q + I_f^2R_f)^2}\sqrt{(I_q\sigma(E_q))^2 + (E_q\sigma(I_q))^2 + (I_f^2\sigma(R_f))}$$

A computer program was used to evaluate $\sigma(N)$ for various values T, W and I_f. The standard deviations of the individual components are listed in Table A and the results plotted in Figures a and b.

The probable error in the predicted efficiency can be seen to be dependent mainly on torque and is relatively independent of speed and field current.

The effect of temperature on resistance and the effect of hysteresis on the machine constant have been neglected.

These results describe the absolute error of efficiency. The relative error will be much smaller. For example the point of maximum efficiency will be very close to the predicted value whereas their absolute values may differ by a greater amount. Relative error is more important than absolute error in this investigation.

The rounding off error of the computer in the final model may become significant since the arithmetic involves quantities of greatly differing magnitudes.

Estimated standard deviations
(in corresponding units)

T_f	T_i	T_s	K	R_f	R_q	V_B
2/W	5/W	0.1	0.005 x K	0.5	.005 x R_q	0.3

Table a

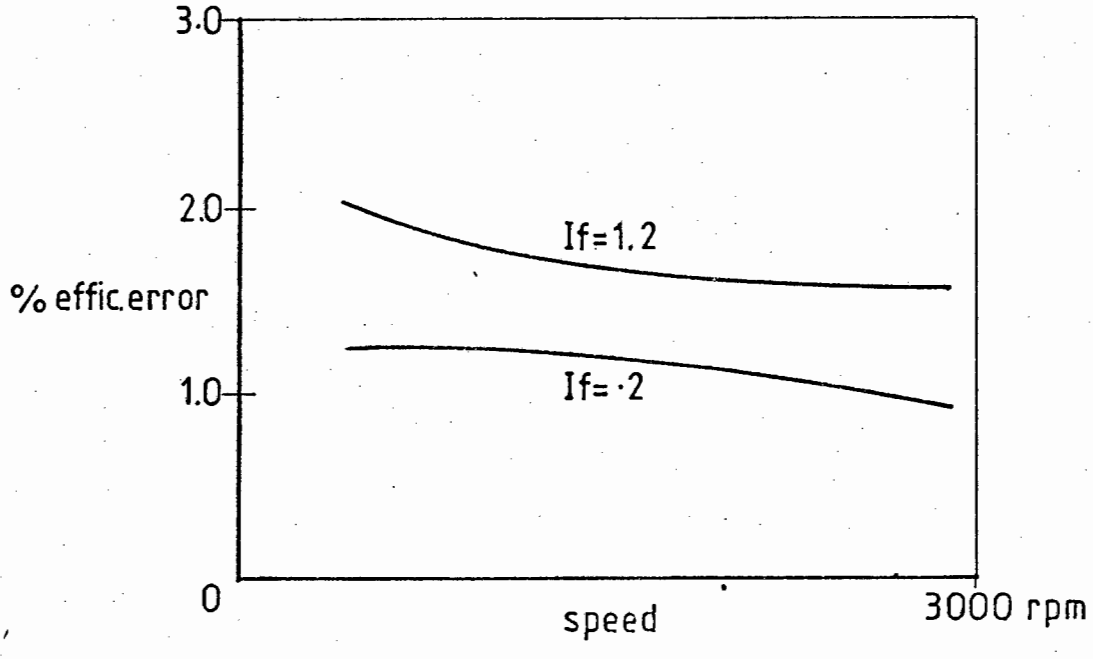

figure a

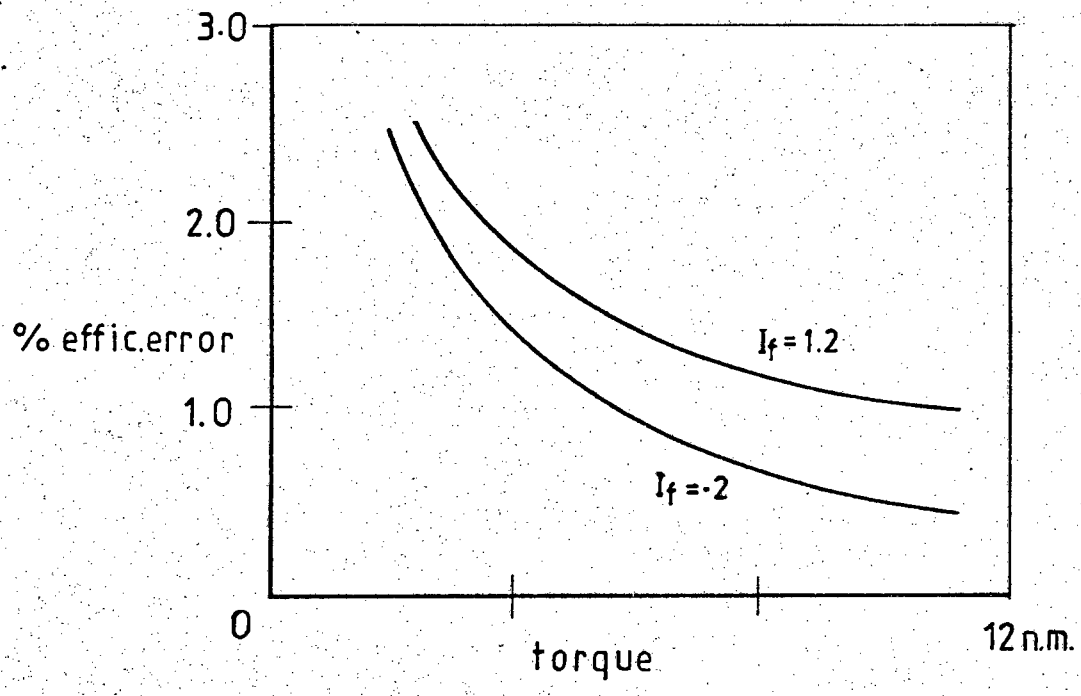

figure b

APPENDIX 6

RMS VALUE OF A CHOPPED WAVEFORM

6.1 PROBLEM

Find the RMS values of the waveforms in Figures (a) and (b).

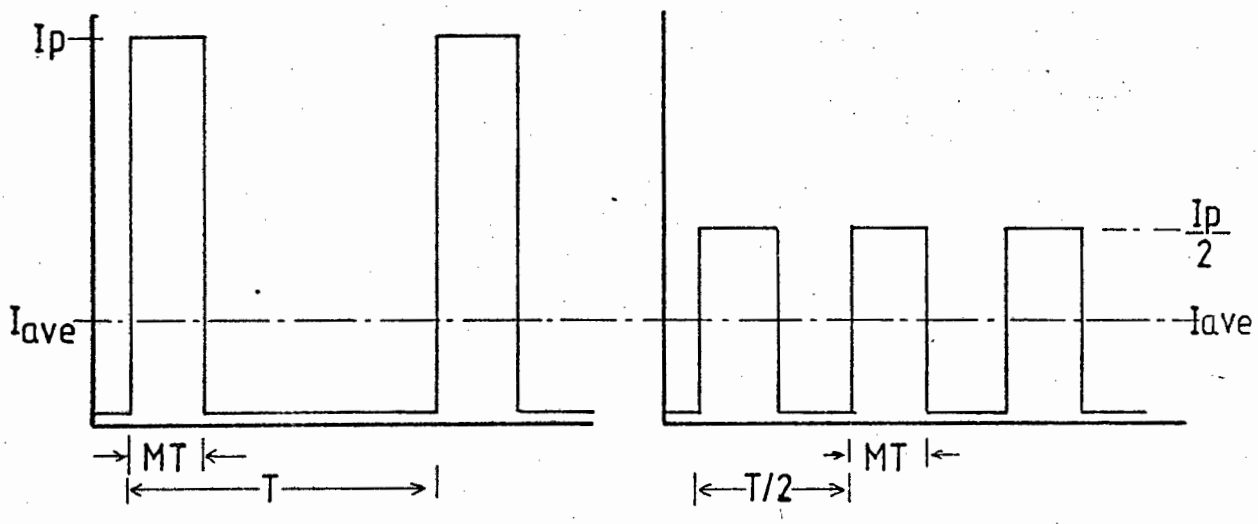

FIGURE (a)

FIGURE (b)

6.1.1 SOLUTION FOR FIGURE (a)

$$I_{average} = \frac{1}{T}\int_{o}^{T} i(t)dt = MI_p \qquad (a)$$

$$I_{rms} = \sqrt{\frac{1}{T}\int_{o}^{T} i(t)^2 dt} = \sqrt{M}\, I_p = \frac{1}{\sqrt{M}} I_{average} \qquad (b)$$

6.1.2 SOLUTION FOR FIGURE (b)

$$I_{average} = \frac{1}{T}\int_{o}^{T} i(t)dt = MI_p \qquad (c)$$

$$I_{rms} = \sqrt{\frac{1}{T}\int_{o}^{T} i^2(t)dt} = \frac{\sqrt{M}}{\sqrt{2}} I_p = \frac{1}{\sqrt{2}\sqrt{M}} I_{average} \qquad (D)$$

6.2 REDUCTION IN BATTERY LOSSES FOR SMOOTHED CURRENT OVER DRIVE CYCLE

This analysis is based on the suggested standard test cycle in Figure 5.21 with the numerical values in Table 5.1.

For an ideal chopper $I_B E_B = I_q E_q$ where $I_q = \frac{T}{KI_f}$

and $E_q = KI_f W + I_q R_q = KI_f W + \frac{TR_q}{KI_f}$

Therefore $I_B = \frac{TW}{E_B} + \frac{T^2 R_q}{(KI_f)^2 E_B}$ where $E_B = 72V$, $R_q = 0.1266\Omega$,

$KI_f = \cdot 2013$ webers

Therefore $I_B = 0.0139\ TW + 0.0434\ T^2$

(a) Accelerate: $T = 11$ Nm, $W = \frac{300}{29}t$

therefore $I_B = 1.582t + 5.251$

(b) Cruise: $T = 4$ Nm, $W = 300$ rad/sec

therefore $I_B = 17.37$

(c) Brake: $T = -4$ Nm, $W = \frac{-225}{9}t + 225$

therefore $I_B = 1.39t - 11.82$

6.2.1 Average Battery Current

$$I_{Bave} = \frac{1}{126}\left[\int_0^{29}(1.582t + 5.25)dt + \int_0^{51} 17.37\,dt + \int_0^{9}(1.39t - 11.82)\,dt\right]$$

$$= 13.12 \text{ A} \qquad \text{(e)}$$

6.2.2 RMS Battery Current

$$I^2_{Brms} = \frac{1}{126}\left[\int_0^{29} (1.582t + 5.251)^2 dt + \int_0^{51} 17.37^2 dt + \int_0^{9} (1.39t - 11.82)^2 dt\right]$$

therefore $I_{Brms} = 18.67$ A (f)

6.2.3 Reduction in Losses

The unsmoothed losses are greater by a factor of

$$\frac{P \text{ unsmoothed}}{P \text{ smoothed}} = \frac{I^2_{B(rms)} \cdot R_B}{I^2_{B(ave)} \cdot R_B} = 2.03 \quad (g)$$

6.3 RMS CURRENT THROUGH SMOOTHING CAPACITOR

If a large capacitor is used as a filter across the battery, the current waveform shown below is obtained

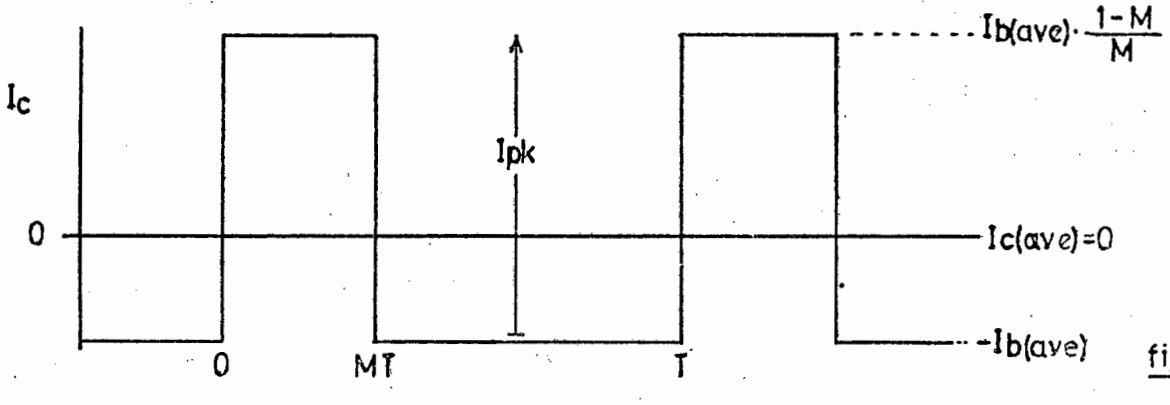

fig.C

The current wave reaches a peak value of,

$$I_{pk} - I_{B(ave)} = I_{B(ave)}\left(\frac{1 - M}{M}\right) \quad \text{since} \quad I_{pk} = \frac{I_{B(ave)}}{M}$$

Therefore $$I^2_{C(rms)} = \frac{1}{T}\int_0^{MT}\left[I_{B(ave)}\cdot\frac{1-M}{M}\right]^2 dt + \frac{1}{T}\int_{MT}^{T} I^2_{B(ave)}\, dt$$

Therefore $$I_{C(rms)} = I_{B(ave)}\cdot\sqrt{\frac{1-M}{M}} \qquad (h)$$

CHAPTER 7

OPTIMUM CONTROL EQUATION

7.1 NEGLECTING SATURATION AND ALL LOSSES EXCEPT COPPER LOSSES

7.1.1 Problem

Neglecting saturation and all losses except armature and field losses, find the relation between I_q and I_f for optimum efficiency.

7.1.2 Solution

For any given torque and speed efficiency is maximised when losses are minimised. The losses are

$$P_L = I_q^2 R_q + I_f^2 R_f$$

therefore $P_L = \frac{T^2 R_q}{K^2 I_f^2} + I_f^2 R_f$ since $I_q = \frac{T}{KI_f}$

therefore $\frac{dP_L}{dI_f} = 0 = \frac{-2T^2 R_q}{K^2 I_f^3} + 2I_f R_f$ for minimum loss

therefore $2I_q^2 R_q = 2I^2{}_f R_f$ since $T = KI_f I_q$

therefore $I_f = \sqrt{\frac{R_q}{R_f}}\, I_q$

7.2 OPTIMUM CONTROL EQUATION ASSUMING $T = K I_f I_q$

7.2.1 Problem

Using the assumptions in Section 5.2.2, find the relation between I_q and I_f for optimum efficiency.

7.2.2 Solution

For any given torque speed, the losses are

$$P_L = aI_f^2 + bI_f + cI_q^2 + dI_q + e + f$$

where $a = R_f$, $b = (k_E W^2 + k_H W)$, $c = (R_q + k_s W^2)$, $d = V_B$,

$e = k_{f1} W^2 + k_{f2} W$ and f = battery losses which are constant.

Therefore $$P_L = \frac{aT^2}{K^2 I_q^2} + \frac{bT}{KI_q} + CI_q^2 + dI_q + e + f \quad \text{since } I_q = \frac{T}{KI_f}$$

therefore $$\frac{dP_L}{dI_q} = 0 = \frac{-2aT^2}{K^2 I_q^3} - \frac{bT}{KI_q^2} + 2cI_q + d \quad \text{for minimum loss}$$

$$= \frac{-2aI_f^2}{I_q} - \frac{bI_f}{I_q} + 2cI_q + d \quad \text{since } T = KI_f I_q$$

therefore $$2cI_q^2 + dI_q = 2aI_f^2 + bI_f$$

therefore $$I_f = -\frac{b}{4a} + \left(\frac{b^2}{16a^2} + \frac{c}{a} I_q^2 + \frac{d}{2a} I_q\right)^{\frac{1}{2}}$$ by changing the subject of the formula (a)

The slope of this function is found by implicit differentiation of equation.

$$4cI_q \frac{dI_q}{dI_f} + d \cdot \frac{dI_q}{dI_f} = 4aI_f + b$$

therefore $\frac{dI_q}{dI_f} = \frac{4aI_f + b}{4cI_q + d}$

therefore $\frac{dI_q}{dI_f} = \left[\frac{16a(cI_q^2 + 8dI_q) + b^2}{16c(cI_q^2 + 8dI_q) + d^2}\right]^{\frac{1}{2}}$

by eliminating I_f with (a) and rearranging.

The initial $\frac{dI_q}{dI_f}$ as $I_q \longrightarrow 0$ is $\frac{b}{d}$

The final $\frac{dI_q}{dI_f}$ as $I_q \longrightarrow \infty$ is $\frac{a}{c}$ since terms b^2 and d^2 become insiginificant.

APPENDIX 8

PROGRAM TO FIND EFFICIENCY

8.1 PROGRAM LISTING

```
  5 !
 10 !
 20 ! PROGRAM TO FIND OPTIMUM
      EFFICIENCY
 40 !
 50 ! ***************************
    *
 60 !
 70 !  MAIN ROUTINE
 80 !
 90 !
100 DISP " FILE NAME"
105 INPUT N$ ! DATA DESTINATION

110 ASSIGN# 1 TO N$
120 !
130 GOSUB 1000 ! READ DATA
135 !
140 FOR W=3000*PI/30 TO 3100*PI/
    30 STEP 500*PI/30
150 FOR T=-12 TO 11
155 !
160 GOSUB 1150 ! INITIALISATIONS
170 GOSUB 1250 !  FIND IF
180 GOSUB 1500 !  FIND IQ
200 GOSUB 2000 !  FIND EQ
210 E2=E3 !       LET EB'=EB
220 GOSUB 2500 !  FIND IB'
230 I3=I2+D1*I4 ! FIND IB
240 GOSUB 3000 !  FIND EB'
250 IF ABS(X-E2)>.005 THEN GOTO
    220 ! IS EB' ACCURATE ENOUGH
260 GOSUB 3500 ! FIND EFFICIENCY
270 IF N1-N>.5 THEN GOTO 300
275 IF N>N1 THEN GOSUB 4000 !
    STORE VALUES FOR THIS IF,IQ
280 D1=D1-.0125*1.2*R1/E3 !
      DECREMENT FIELD M/S RATIO
290 GOTO 170
300 GOSUB 5000 ! DISPLAY RESULT
305 !
310 NEXT T
320 NEXT W
330 !
340 ASSIGN# 1 TO *
350 END
360 !
370 ! ***************************

1000 !
1010 ! READ DATA
1020 !
1030 READ K1,K2,K3,K4,K5,K6,K7,K
     8,K9,R1,R2,R3,T1,T2,V,E3,R
1040 DIM K(70)
1050 FOR Z=0 TO 61
1060 READ K(Z) ! K VALUES
1070 NEXT Z
1080 DIM S(100)
1090 FOR Z=0 TO 100 ! ASIHN VALU
     ES
1100 READ S(Z)
1110 NEXT Z
1120 RETURN
1130 ! ***************************

1150 !
1160 ! INITIALISATIONS
1170 !
1180 N1=-50 @ D1=1.2*R1/E3
1190 IF T<0 THEN S=-1 ELSE S=1
1200 IF T=0 THEN LET T=1
1230 RETURN
1240 ! ***************************
1250 !
1260 ! SHUNT FIELD CURRENT
1270 !
1280 I4=D1*E3/R1
1290 RETURN
1295 ! ***************************

1300 !
1310 ! SERIES FIELD CURRENT + Iq
1320 !
1330 J1=0 @ J2=1.2
1335 I4=(J1+J2)/2
1336 DISP J1;J2
1340 GOSUB 1500 ! FIND IQ
1350 J3=I1 @ I4=J2
1360 GOSUB 1500 ! FIND IQ
1370 J4=I1
1380 IF (R*J3*S-(J1+J2)/2)*(S*R*
     J4-J2)<0 THEN J1=(J1+J2)/2
     ELSE J2=(J1+J2)/2
1390 IF ABS(J2-J1)<.001 THEN I4=
     (J1+J2)/2 ELSE GOTO 1335
1400 I1=(J3+J4)/2
1405 IF ABS(I1)<50 THEN 1410
1407 I4=1.2 @ GOSUB 1500
1410 D1=I4*R1/E3
1420 RETURN
1430 ! ***************************
1500 !
1510 ! ARMATURE CURRENT IQ
1520 !
1540 LET Z=INT(50*I4)
1550 K=(K(Z+1)-K(Z))*50*I4+K(Z)-
     (K(Z+1)-K(Z))*Z
1560 K=K+K9/I4
1570 A=K5*W
1580 B=-(K*I4)
1590 C=T+(K1*W+K2)+(K3+K4*W)*I4
1595 IF B^2-4*A*C>0 THEN 1600
1597 DISP I4 @ I1=50 @ GOTO 1610
1600 I1=(-B-SQR(B^2-4*A*C))/(2*A
     )
1610 RETURN
1620 ! ***************************
2000 !
2010 ! ARMATURE VOLTAGE EQ'
2020 !

2040 LET E1=K*I4*W+I1*R2+S*V
2050 RETURN
```

```
2060 ! ************************
2500 !
2510 ! BATTERY CURRENT IB'
2520 !
2540 LET D=E1/E2
2550 LET Y=T2/T1*(1-EXP(-((1-D)*
     T1/T2)))*(1-EXP(-(D*T1/T2))
     )/(1-EXP(-(T1/T2)))
2560 LET I2=E2/R2*((1-(K*I4*W+S*
     V)/E2)*D-Y)
2570 RETURN
2580 ! ************************
3000 !
3010 ! BATTERY VOLTAGE EB'
3020 !
3040 X=E2
3045 IF I3>50 THEN LET I=50 ELSE
      LET I=I3
3050 Z=INT(ABS(10*I)/(2*K7))
3055 Q=(S(Z+1)-S(Z))*(ABS(5*I/K7
     )-Z)+S(Z)
3060 E5=S*1/K6*Q
3065 E2=E3-I3*R3-E5
3070 RETURN
3080 ! ************************
3500 !
3510 ! FIND EFFICIENCY N
3520 !
3540 LET N=(T*W/(I3*E3))^S*100
3550 RETURN
3560 ! ************************
4000 !
4010 ! STORE OPTIMUM VALUES
4020 !
4030 J4=I4 @ J2=I2 @ J1=I1
4040 G1=E1 @ G2=E2 @ J3=I3
4050 D3=D @ N1=N @ Y1=K @ G5=E5
4070 RETURN
4080 ! ************************
5000 !
5010 ! DISPLAY RESULTS
5020 !
5030 PRINT USING 5040 ; T,W,N1,J
     1,J4
5040 IMAGE 3D.D,4D.2D,3D.3D,4D.2
     D,2D.3D
5050 PRINT# 1 ; T,W,N1,J1,J4
5060 RETURN
5090 ! ************************
6000 !
6010 ! DISPLAY LOSSES
6020 !
6030 PRINT USING 6040 ; K1*W*W+K
     2*W,(K3+K4*W)*J4*W,K5*W*W*J
     1^2,G2*J2-G1*J1
6040 IMAGE /," FRIC  IRON  STRAY
      CHOPPER",/,3D.D,4D.D,4D.D,
     4D.D
6050 PRINT USING 6060 ; J1^2*R2,
     J4^2*R1,J3^2*R3,G5*J3,J1*V*
     S
6060 IMAGE " QCU   FCU   IRB   V
     DP   VBR",/,3D.D,4D.D,4D.D,
     4D.D,4D.D
6070 RETURN
6080 ! ************************
9000 !
9010 ! DATA
9020 !
9030 DATA .000457678,.125,.13819
     56,.0003022,.0000007166,1.1
     ,2.607,0,.0232,28.3,.1266,.
     04232
9040 DATA .0002,.003,1.44,72,.06
     6881694
9100 DATA 0,.228,.2865,.3077,.30
     24,.3247,.3236,.332,.3382,.
     3395,.3406,.3444,.3448,.342
     8
9110 DATA .3433,.3417,.3402,.338
     9,.336,.3334,.3295,.3259,.3
     212,.3169,.313,.3069,.3024
9120 DATA .2983,.2922,.2876,.282
     2,.2731,.2726,.2643,.264,.2
     592,.2546,.2503,.2463,.2442
     ,.2387
9130 DATA .2352,.2319,.228,.2243
     ,.2214,.218,.2147,.2115
9140 DATA .2085,.2063,.2028,.200
     2,.1976,.1951,.1927,.1904,.
     1882,.186,.1834,.182,.1805
9200 DATA 0,.1,.199,.296,.39,.48
     1,.569,.653,.733,.809
9210 DATA .881,.95,1.016,1.078,1
     .138,1.195,1.249,1.301,1.35
     ,1.398
9220 DATA 1.444,1.487,1.53,1.57,
     1.609,1.647,1.684,1.719,1.7
     53,1.786
9230 DATA 1.818,1.85,1.88,1.909,
     1.938,1.966,1.993,2.019,2.0
     45,2.07
9240 DATA 2.095,2.119,2.142,2.16
     5,2.187,2.209,2.231,2.252,2
     .272,2.293
9250 DATA 2.312,2.332,2.351,2.37
     ,2.388,2.406,2.424,2.441,2.
     458,2.475
9260 DATA 2.492,2.508,2.524,2.54
     ,2.555,2.571,2.586,2.601,2.
     615,2.63
9270 DATA 2.644,2.658,2.672,2.68
     6,2.699,2.712,2.726,2.739,2
     .751,2.764
9280 DATA 2.776,2.789,2.801,2.81
     3,2.825,2.837,2.848,2.86,2.
     871,2.882
9290 DATA 2.893,2.904,2.915,2.92
     6,2.937,2.947,2.958,2.968,2
     .978,2.988,2.998
9300 !
9999 END
```

8.2 CHANGES FOR DIFFERENT CONTROL EQUATIONS

8.2.1 **Shunt characteristic** - add 265 GOTO 300

255 GOSUB 4000

8.2.2 **Permanent magnet motor** - same as shunt

change 230 I3 = I2

8.2.3 **Series Characteristic** - same as shunt

- eliminate line 180
- change 170 GOSUB 1300
- the slope of the characteristic is entered as variable R.

8.3 COMPUTER PROGRAM FOR STANDARD TEST CYCLE

8.3.1 Introduction

A computer program is required, which will compare the energy supplied by the source for various control strategies with the optimum strategy.

8.3.2 General

The torque-speed profile in Figure 5.21 can be reduced to that in Figure (a) since no energy is required during coasting and idling. (See Figure a overleaf.)

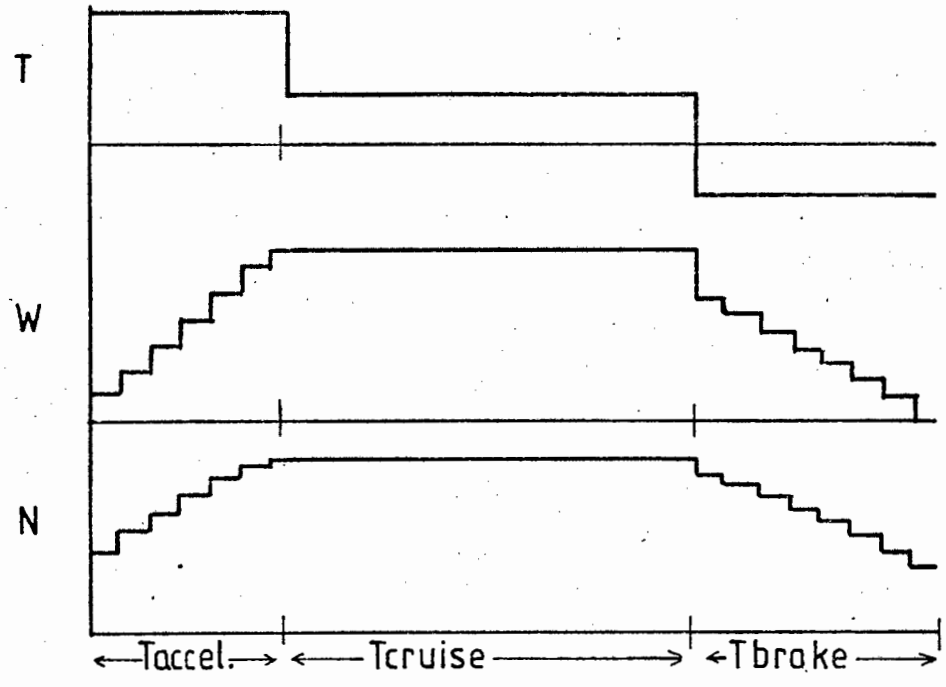

FIGURE a

The speed curve is approximated by a stepped function, the stepped shape of the efficiency equation follows from this. This approximation is valid, particularly when time t_{cr} is dominant.

The energy supplied by the source is

$$E = \int \frac{TW}{N} dt = \sum \frac{TW}{N} \cdot \Delta t$$

Since regeneration efficiency is defined as

$$N_{regen.} = \frac{\text{power from shaft}}{\text{power to source}}$$

the values of n must be inverted during braking.

8.3.3 Program

The values of efficiency for various strategies were read from a data file and then the energy used was calculated.

8.3.3.1 Listing

```
120 ! TEST CYCLE
130 !
140 !
150 ! READ EFFICIENCY VALUES
160 !
165 DIM N1(150),N2(150)
170 ASSIGN# 1 TO "OPTN"
180 FOR I=1 TO 23*6
190 READ# 1 ; T,W,N1(I),J1,J2
195 N1(I)=N1(I)/100
200 NEXT I
235 !
240 READ N$
250 ASSIGN# 1 TO N$
260 FOR I=1 TO 23*6
270 READ# 1 ; T,W,N2(I),J1,J2
280 N2(I)=N2(I)/100
290 NEXT I
300 ASSIGN# 1 TO *
500 !
510 ! CALCULATE ENERGY USED
520 !
530 I1=0 @ I2=0 ! INITIALISE
540 READ T1,T2,T3,A,B,C
550 !
555 ! ACCELERATE
560 !
565 FOR Y=1 TO 6
570 I1=I1+A*Y*500*PI/30*T1/6/N1(
    (Y-1)*23+A+12)
580 I2=I2+A*Y*500*PI/30*T1/6/N2(
    (Y-1)*23+A+12)
610 NEXT Y
620 !
630 ! CRUISE
640 !
650 I1=I1+B*3000*PI/30*T2/N1(5*2
    3+12+A)
660 I2=I2+B*3000*PI/30*T2/N2(5*2
    3+12+A)
680 !
690 ! BRAKING
700 !
720 FOR Y=5 TO 1 STEP -1
730 I1=I1+C*Y*500*PI/30*T3/5*N1(
    (Y-1)*23+13+C)
740 I2=I2+C*Y*500*PI/30*T3/5*N2(
    (Y-1)*23+13+C)
760 NEXT Y
770 !
780 ! DISPLAY ENERGY SAVING
790 !
800 PRINT 1-I1/I2
900 END
5000 !
5010 ! DATA
5020 !
5030 DATA "HPERM"
5040 DATA 29,51,9,11,4,-4
```

APPENDIX 9

DESIGN DETAILS

OVERALL BLOCK DIAGRAM

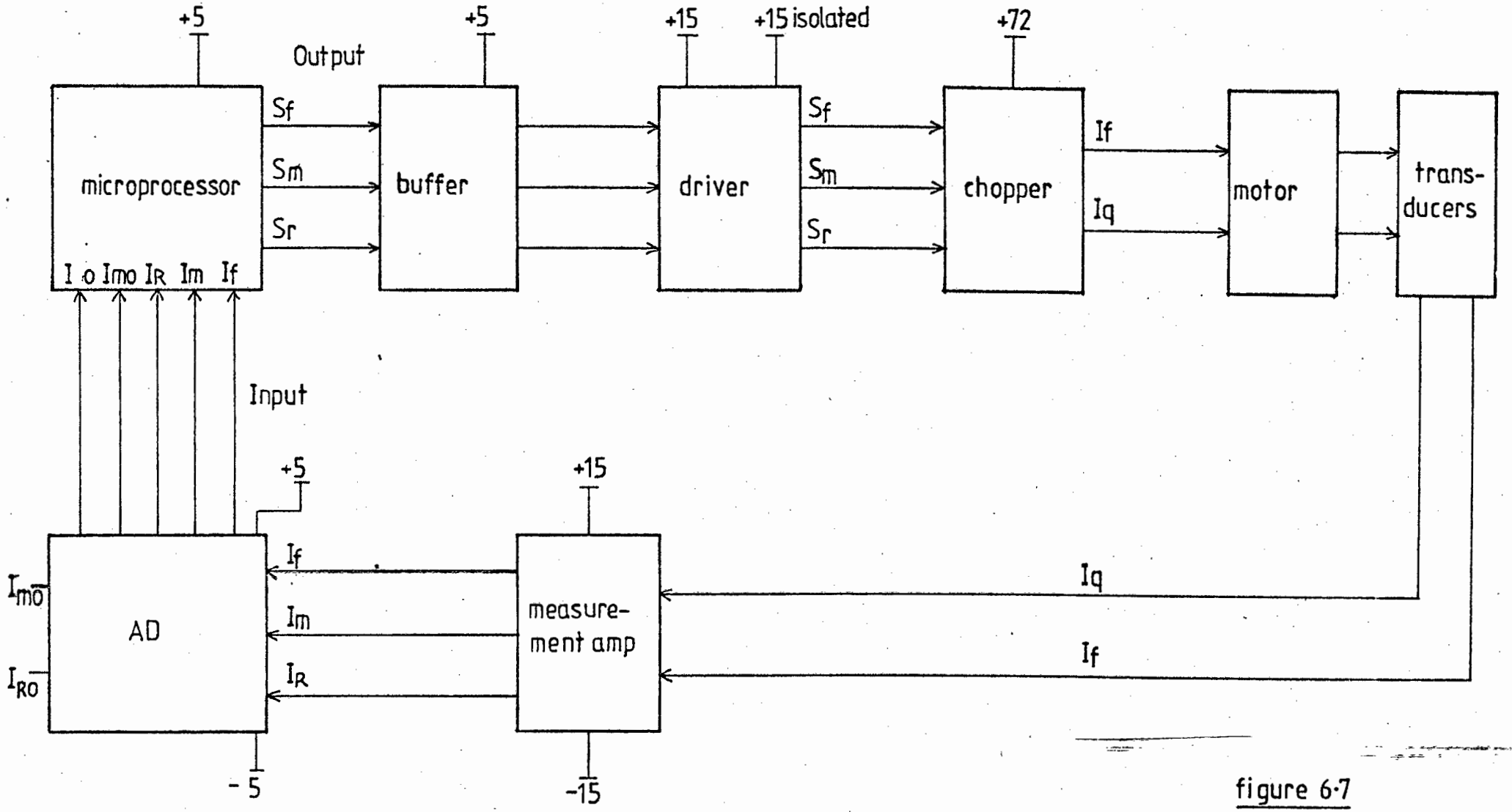

figure 6·7

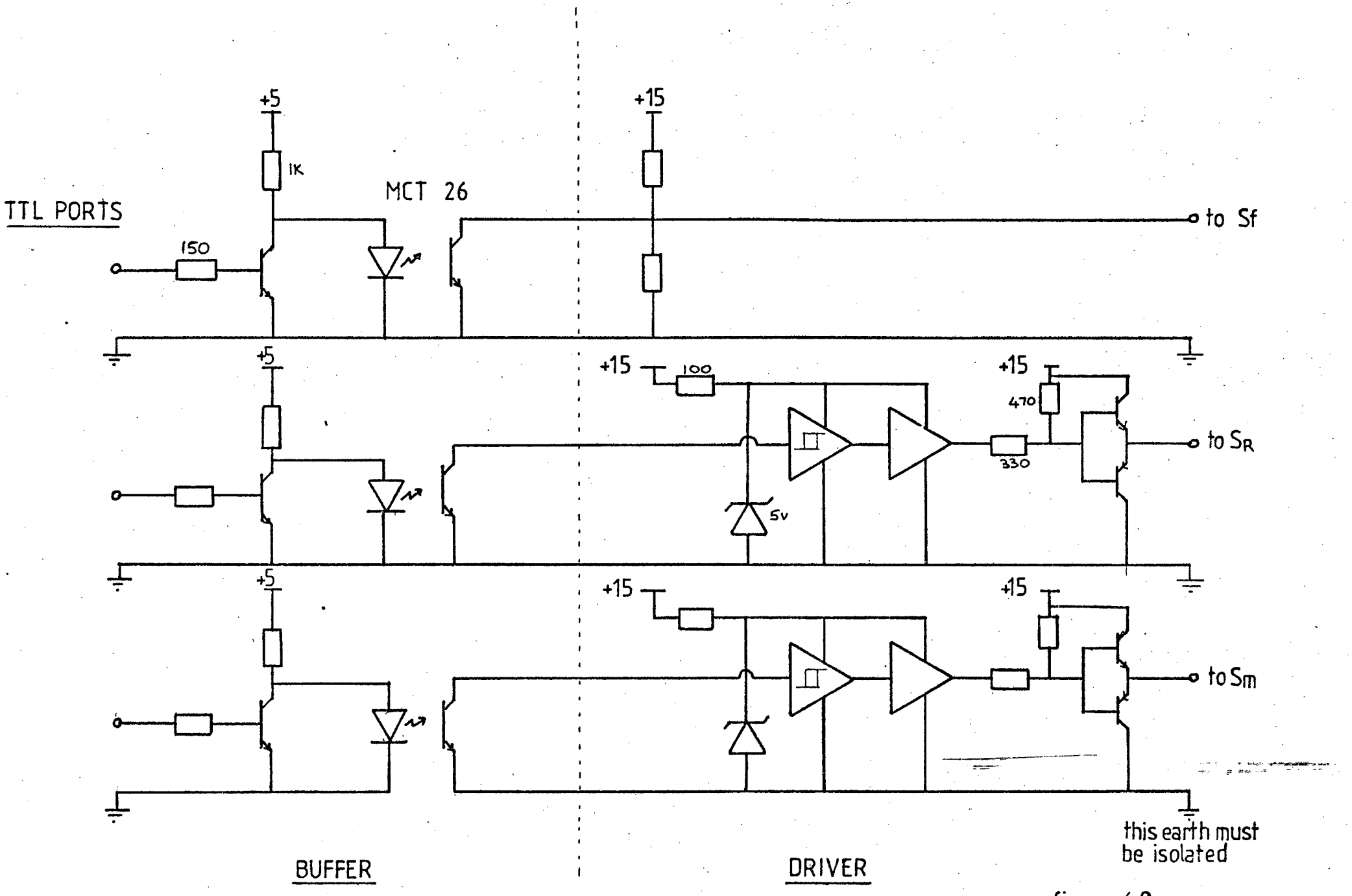
TTL PORTS
+5
1K
MCT 26
+15
150
to Sf
100
470
330
5v
to SR
to Sm
this earth must
be isolated
BUFFER
DRIVER

figure 6.8

MEASUREMENT AMPLIFIER

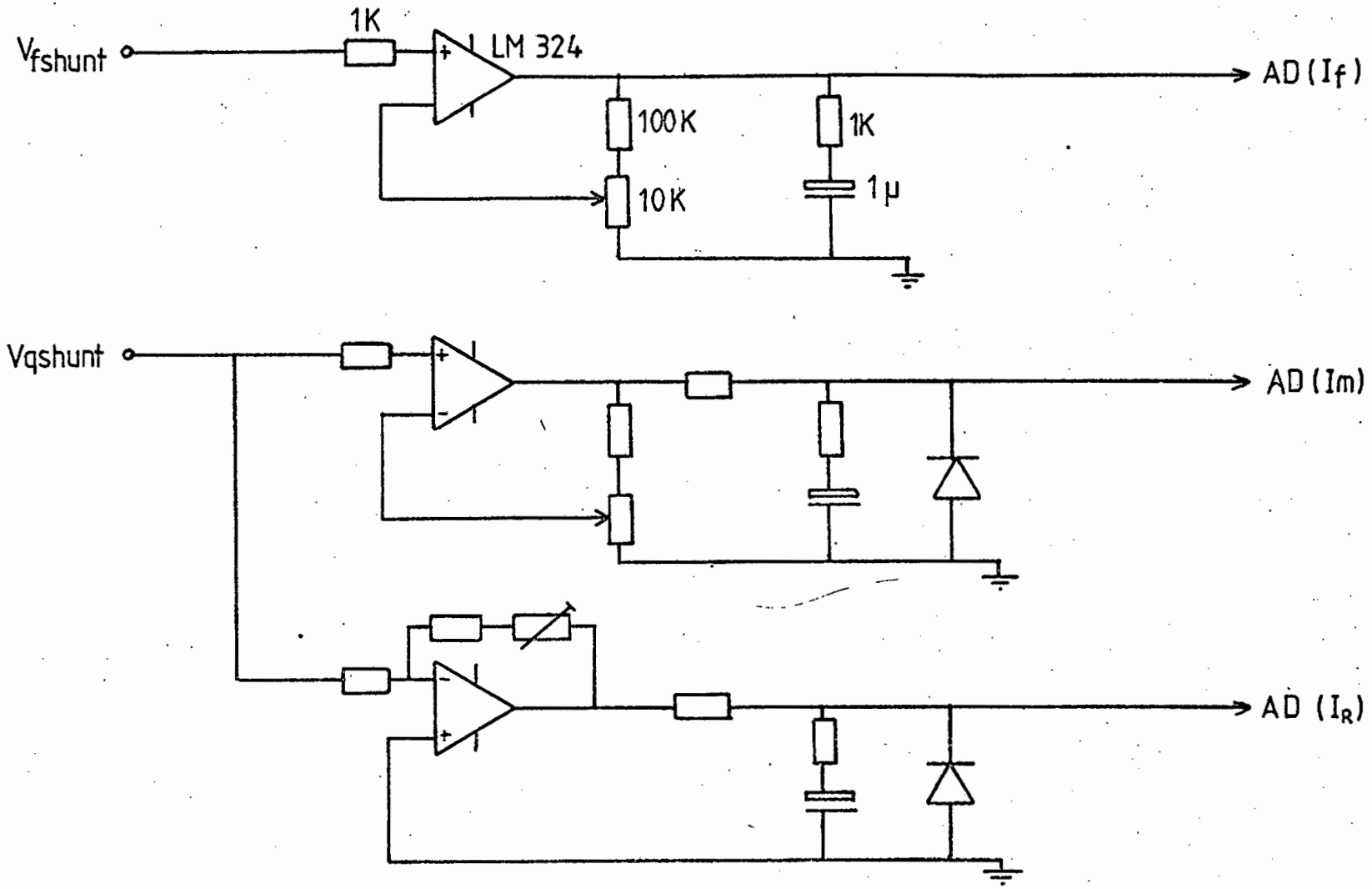

figure 6·9

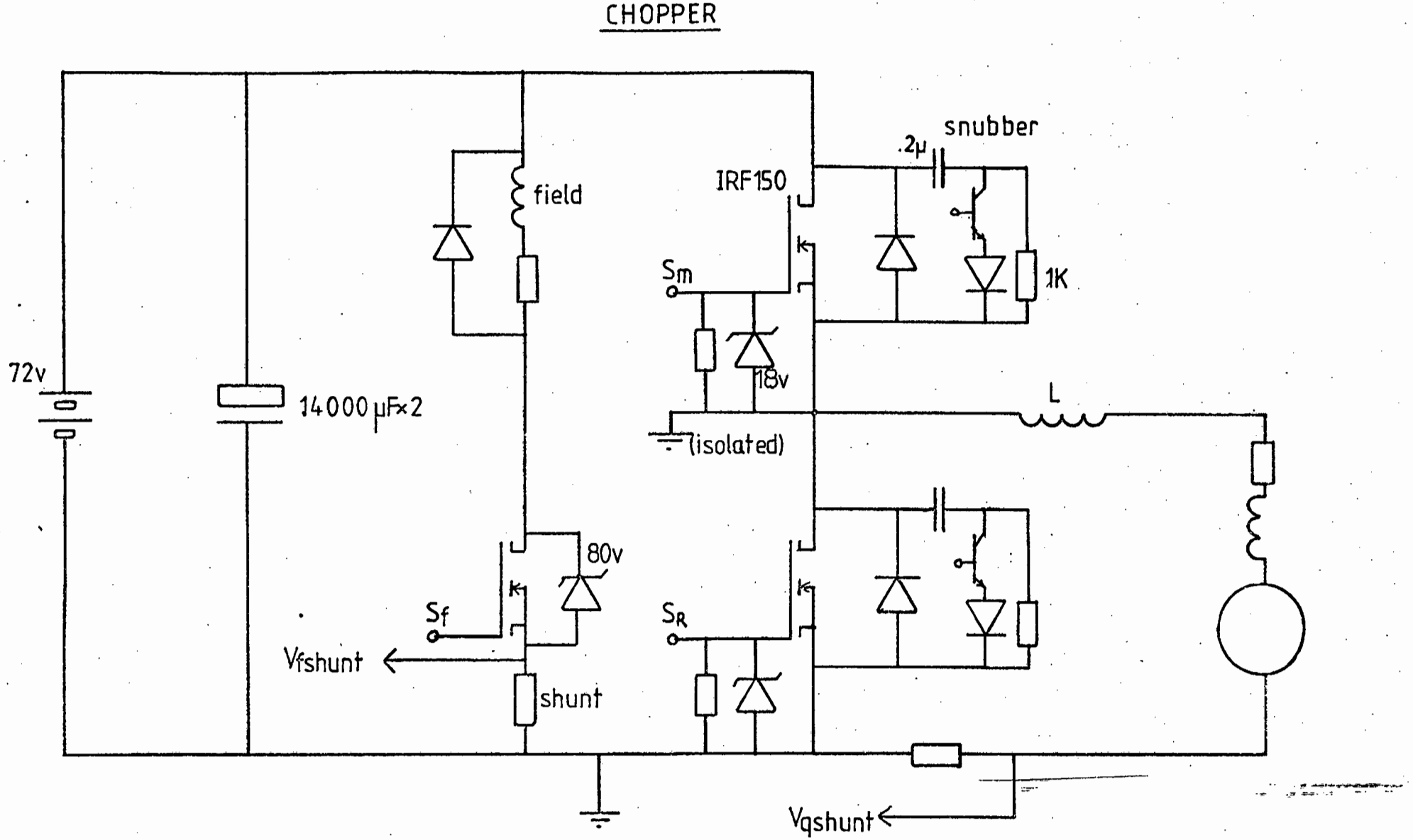
CHOPPER
72v
14000 μF×2
field
IRF150
snubber
.2μ
1K
Sm
18v
(isolated)
L
80v
Sf
Vfshunt
shunt
SR
Vqshunt

figure 6.10

ANALOG IMPLEMENTATION

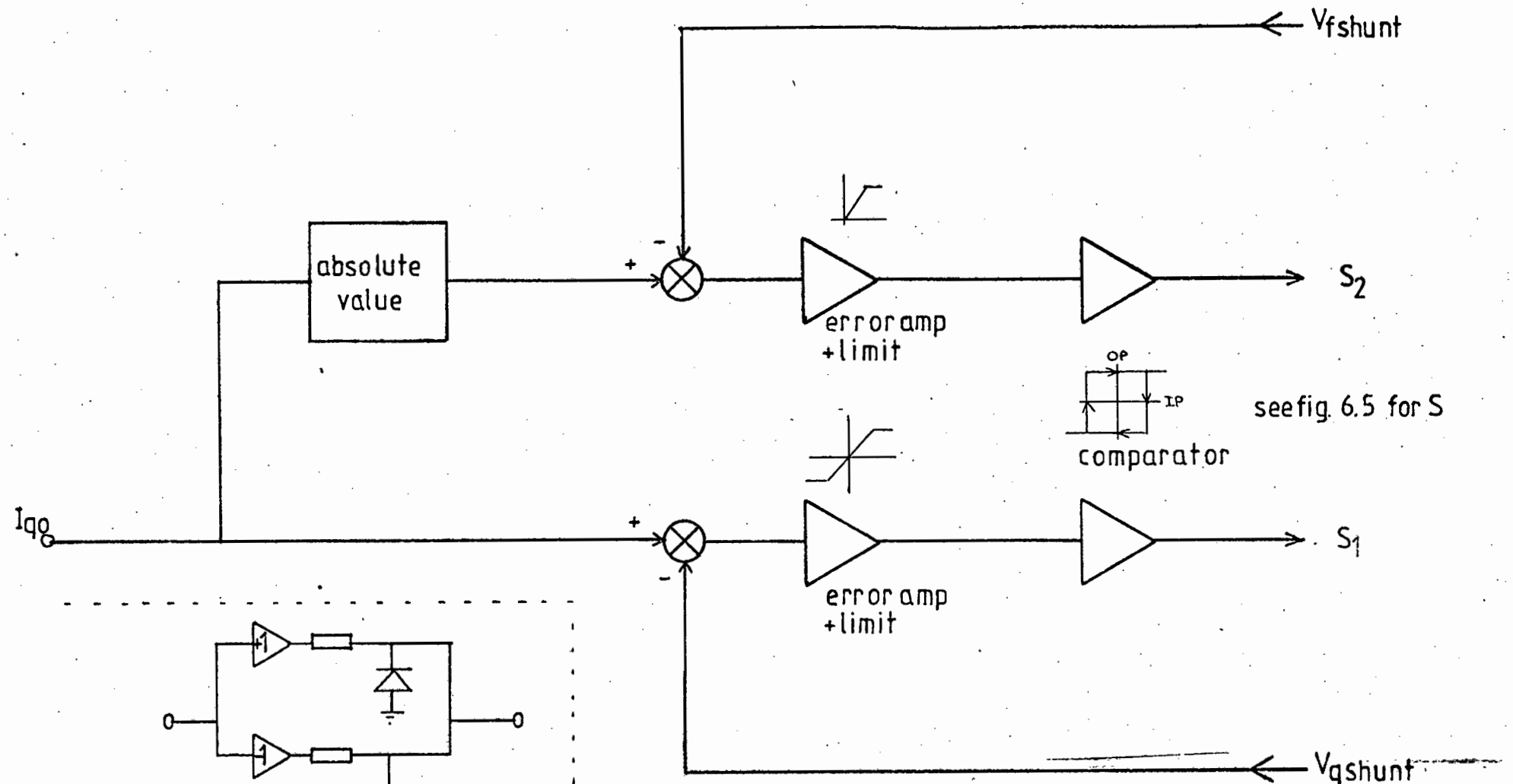

absolute value - figure 6·11b

figure 6·11

9.2 SOFTWARE LISTING

Label	Address	Code	Mnemonic	Description
Start	80 00	F3	DI	initialise stack and command/status register
	01	31 00 83	LXI SP	
	04	3E 0D	MVI A, 0D	
	06	D3 20	OUT PORT 20	
	08	3E OD	MVI A, OD	set interrupt mask for A-D end of conversion
	0A	30	SIM	
Setpoints	0B	3E 18	MVI A, 18	read T_{RO} and store in register B
	0D	CD 4E 80	CALL read	
	10	47	MOV B, A	
	11	3E 19	MVI A, 19	read TMO and store in register C
	13	CD 4E 80	CALL read	
	16	4F	MOV C, A	
MOT./REGEN:	17	90	SBB B	compare T_{RO} and T_{MO}
	18	D2 21 80	JNC A	
	1B	68	MOV L, B	if $T_{RO} < T_{MO}$ then move memory pointer (H_L pair) to T_{RO} on the look up table and let T_{sign} (C) = 0 else let HL = T_{MO} and C = +1
	1C	0E 00	MVI C, 00	
	1E	C3 24 80	JMP B	
A	21	69	MOV L, C	
	22	OE 01	MVI C, 01	
B	24	26 81	MVI H, 81	store setpoint I_D in reg. B
	26	46	MOV B, M	
Read IQ	27	3E 1A	MVI A, 1A	read either I_{Rq} or I_{Mq} depending on value of T_{sign} (register C)
	29	81	ADD C	
	2A	CD 4E 80	CALL read	
Q switch	80 2D	16 00	MVI D,00	If $I_q > I_{qo}$ then let switch (D) = 00 else let switch = 01 for regeneration or switch = 10 for motor
	2F	90	SBB B	
	30	D2 37 80	JNC (IF SETP)	
	33	3E 01	MVI A, 01	

	35	81	ADD C	
	36	57	MOV D, A	
If setpoint	37	26 82	MVI H, 82	lookup I_{fo} corresponding to I_{qo}
	39	68	MOV L, B	
Read If	3A	3E 14	MVI A, 14	read field current
	3C	CD 4E 80	CALL read	
F switch	3F	90	SBB M	If $I_f < I_{fo}$ then let switch = switch + 04
	40	D2 47 80	JNC (output)	
	43	7A	MOV A, D	
	44	C6 04	ADI, 04	
	46	57	MOV D, A	
output	47	7A	MOV A, D	Output chopper control signal
	48	2F	CMA	
	49	D3 21	OUT PORT A	
	4B	C3 0B 80	JMP setpoints	return to beginning
Read	80 4E	D3 23	OUT PORT C	output channel address and start conversion bit
	50	FB	EI	
C	51	00	00	idle for end of conversion interrupt
	52	C3 51 80	JMP C	
	20 C8	C3 55 80	JMP D	
D	55	F3	DI	
	56	F1	POP PSW	restore stack pointer
	57	3E 00	MVI A, 00	reset start conversion bit
	59	D3 23	OUT PORT C	
	5B	DB 22	IN PORT B	read digital result
	5D	C9	RET	
I_{qo} Table	81 00 to 81 FF			a table of values relating setpoints T_o and I_{qo}

I_{fo} Table	82 00 to 82 FF	A table of values relating setpoint I_{fo} to I_{qo}